IMMOBILISATION OF DNA USING THE FLUOROUS EFFECT

Gabriella Flynn MChem, MRes

Supervisors: Dr. Alasdair Clark & Prof. Jonathan Cooper

This thesis is submitted in the fulfilment for the degree of Doctor of Philosophy

School of Engineering

College of Science and Engineering

University of Glasgow

October 2018

This thesis is dedicated to my mum.

DECLARATION

'I declare than, except where explicit reference is made to the contribution of others, this thesis is the result of my own work and has not been submitted for any other degree at the University of Glasgow or any other institution.'

Signed:_____

Date: _____

Gabriella Flynn MChem, MRes
University of Glasgow

ABSTRACT

Reversible biomolecule attachment onto solid supports is of importance to many distinct research fields ranging from microarray development to the synthesis of metamaterials. One method used to immobilise biomolecules in a reversible fashion relies on non-covalent fluorous-fluorous interactions.

The primary focus of this thesis was to investigate the immobilisation characteristics of DNA, tagged with a range of perfluorinated carbon chains, onto fluorinated solid supports. This work showed that the fluorous effect could be used to immobilise single stranded DNA onto patterned arrays permitting hybridisation to its complementary sequence. This duplex could then be removed via the fluorous tag, completely regenerating the surface and allowing for the immobilisation procedure to be repeated.

This was then built upon by varying the fluorine content of the fluorinated carbon chain, allowing for comparison to be made between the fluorine content of the tag and the stringency of the washes required to remove the duplex from the surface. It was further noted that the effect of the linker group had a significant impact on the immobilisation densities of the DNA strands, with longer linkers showing higher hybridisation densities.

Finally, DNA strands modified with fluorinated carbon chains were incorporated into DNA nanostructures. It was found that the inclusion of fluorous tags had a profound effect on the facial immobilisation orientation of the DNA nanostructures

onto mica. It was found that the inclusion of one perfluorinated tag influenced the face on which the nanostructures were immobilised, with around 80 % of the structures immobilising on the face opposite to that modified with a fluorous tag. Therefore, it is thought that this work has potential applications in reusable microarray development and as a means to control the deposition of nanostructures onto solid supports to aid in bottom-up self-assembly.

ACKNOWLEDGEMENTS

I would like to begin by thanking my supervisors, Dr Alasdair Clark and Professor Jon Cooper. I am very appreciative of the opportunity given to me to work with them.

I would also like to thank Dr Sarah Henry and Dr Andrew Glidle for their input and guidance on the work. I truly believe that without them, this thesis would not have been possible. Sarah, thank you for being around in the lab and always being up for a good chat.

To Dr Glenn Burley, Dr Jamie Withers and Dr Andrea Sender, it was fantastic to work with you all and great to get to know you over the years. Thank you for your invaluable scientific input, resources and time that you put into this project.

I would also like to extend my thanks to Dr Gerard Macias and Justin for their assistance in this work. Arslan, Jason, and Laura, thank you for being in the lab with me during unsociable hours. And for the coffee.

I would like to thank my parents for the support they have given me through my PhD. Dad, if you hadn't kept me to a strict timeline and read my thesis chapter by chapter, I may never have submitted. Mum, words can't describe how amazing you have been throughout my life. Nana, thank you for asking me what I have been doing for the last four years on a regular basis. Without you, I may have never have thought about the bigger picture. Xavier, you're not such a bad brother to have around.

Lastly, I would like to thank my best friend.

TABLE OF CONTENTS

List of Figures

List of Tables

List of Abbreviations and Acronyms

D	Dissipation
f	Frequency
A	Adenine
AFM	Atomic Force Microscopy
APS	Ammonium Persulphate
APTES	3-aminopropyl(trimethoxy) silane
ATR	Attenuated Total Reflectance
AuNP	Gold Nanopacticles
Bis	Numecular Prefix - Two
Bp	Base Pair
BSPP	bis(p-sulfonatophenyl)phenylphosphine dehydrate dipotassium salt
C	Cytosine
CCD	Charge-coupled device
DI	Deionised water

DMF	Dimethylformamide
DMSO	Dimethyl Sulfoxide
DNA	Deoxyribonucleic Acid
DNS	DNA Nanostructure
Ebeam	Electron Beam Lithography
EDTA	Ethylenediamenetetraacetic acid
F-HPLC	Fluorous- Higher Performance Liquid Chromatography
FDTS	(Heptadecafluoro-1, 1, 2, 2-tetrahydrodecyl) trimethoxysilane)
FSPE	Fluorous Solid Phase Extraction
FT-IR	Fourier Transform Infrared
G	Guanine
HEG	Hexaethyleneglycol
HPLC	High Performance Liquid Chromatography
IPA	Isopropanol
MeCN	Acetonitrile
MeOH	Methanol
MIBK	methyl isobutyl ketone
Mono	Numecular Prefix - One
n-DTS	n-decyltrichlorosilane
ODN	Oligodeoxynucleotides
PAGE	Poly Acrylamide Gel Electrophoresis
PBS	Phosphate Buffered Saline
PEG	2- methoxy (polyethyleneoxy) propyl trimethoxysilane
PFC	Perfluorocarbon
PMMA	Poly-methyl-methacrylate
QCM	Quartz Crystal Microbalance

QCM-D	Quartz Crystal Microbalance Dissipation
QCM-I	Quartz Crystal Microbalance Impedance
RE	Restriction Enzyme
R_f	Perfluorocarbon Group
RO	Reverse Osmosis
RT	Room Temperature
SEM	Scanning Electron Microscopy
SPR	Surface Plasmon Resonance
T	Thymine
TAE	Tris Acetate-EDTA
TAE.Mg	Tris Acetate-EDTA Magnesium
TAMRA	5-Carboxytetramethylrhodamine
TBE	Tris Borate-EDTA
TCEP	Tris[2-carboxyethyl] phosphine
TEMED	Tetramethylethylenediamine
Tetra	Numercular Prefix- Four
TRIS	Trisaminomethane
UV	Ultra Violet

1 INTRODUCTION

1.1 General Introduction

The primary aim of this project was to investigate fluorous-fluorous interactions as a method to immobilise DNA in a reversible manner. Due to the non-covalent nature of fluorous-fluorous interactions, it was postulated that by tagging DNA with fluorous "ponytails", they could be captured onto fluorinated solid supports. As such, the research objectives were categorised into three sections:

- The utility of fluorous-fluorous interactions for immobilising single stranded DNA (ssDNA), for reusable DNA microarray applications.
- Modulation of the fluorine content of fluorous "ponytails" and its effect on the immobilisation/removal properties.
- The utility of fluorous-fluorous interactions in directing the immobilisation of DNA nanostructures.

Each of these objectives forms a result chapter containing an introduction that provides an explanation on why the project objectives align with prominent issues identified in the literature.

As such, this introduction hopes to give a broader sense of the field of nucleic acid-based technologies and reversible attachment of biomolecules onto solid supports.

1.2 Deoxyribonucleic Acid

1.2.1 Structure & Function of Deoxyribonucleic acid (DNA)

As the blueprint of life, DNA has attracted much attention: the pivotal moment in its history being the elucidation of its structure by Watson and Crick in 1953. (1)

As a molecule, DNA consists of two polynucleotide chains, or DNA strands, composed of four unique subunits called nucleotides. These nucleotides impart chemical diversity and the DNAs information-coding properties. They are composed of a five-carbon sugar attached to one or more phosphate groups and a nitrogen-containing base: adenine (A), cytosine (C), guanine (G) or thymine (T). The nucleotides form the DNA chain by covalently binding through the sugars and phosphates, which make up the sugar-phosphate backbone, and the two ends can be distinguished by either a phosphate group (5'-end) or a hydroxyl group (3'-end). As such, the formation of the double stranded DNA (dsDNA) helix is directional and can be used as a means to control reactions at interfaces, Figure 1.1.

The double helical structure of DNA arises from hydrogen bonding between complementary base pairs on two different strands. The bonding always occurs between a bulkier two-ring base (A and G) and a single-ring base (T and C). This allows the base pairs to be packed in the most energetically favourable arrangement in the interior of the helix, and it holds the sugar-phosphate backbones at equal distances apart along the length of the DNA molecule. In order to maximise the packing efficiency, the two antiparallel sugar-phosphate backbones wind around each other to form the well-known double helical structure with one complete turn every 10.5 base pairs at a distance of 3.4 - 3.6 nm.(2)

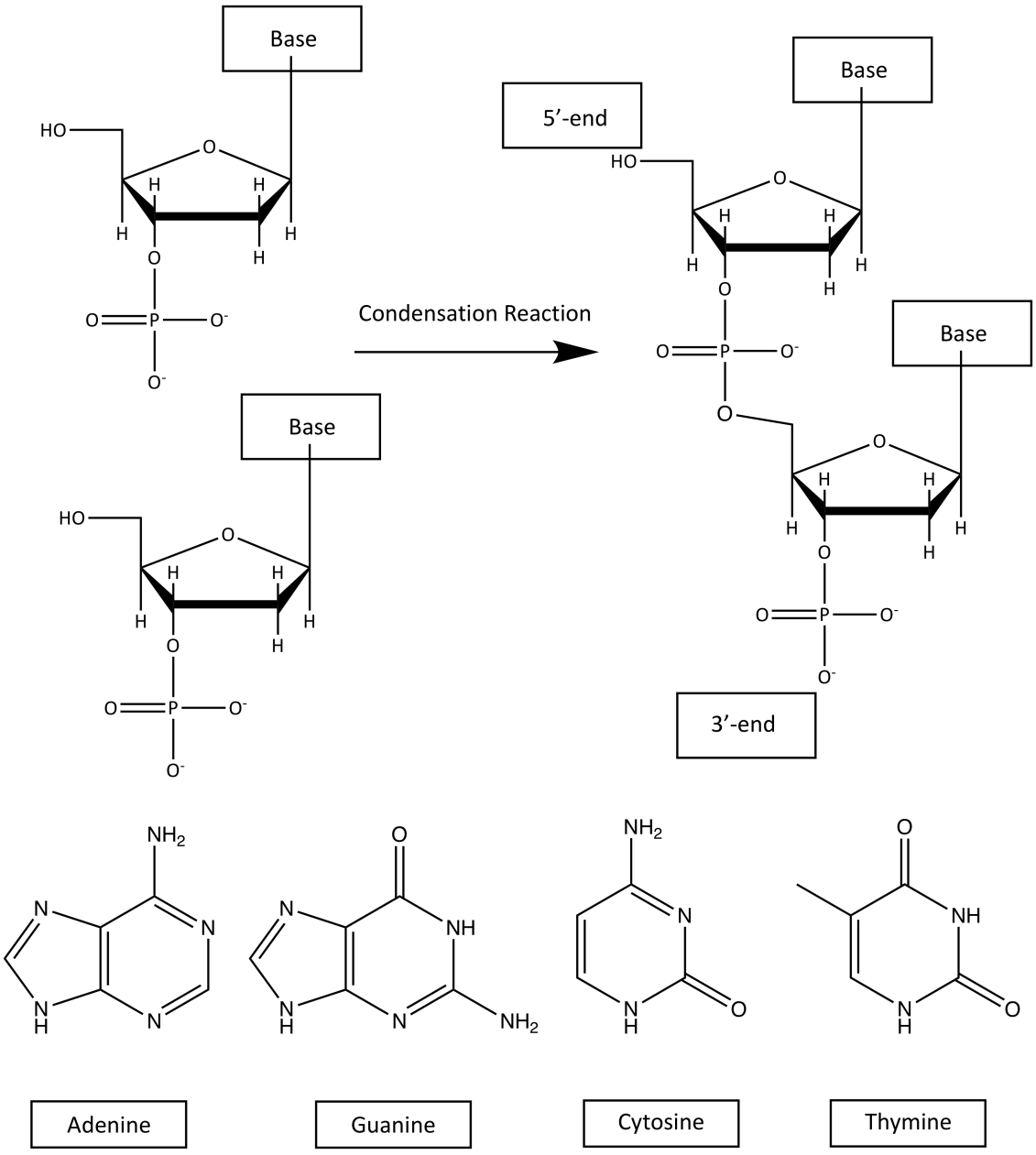

Figure 1-1 The Primary Structure of DNA. DNA molecules are made up of subunits known as nucleotides. These nucleotides differ in the base (either adenine, guanine, cytosine or thymine) that they contain and covalently link to form the sugar-phosphate backbone.

1.3 DNA as a "Smart" Material

Recognizing DNA as a nanomaterial, and not as a biological material, has expanded its utility beyond the realms of biology to exciting applications in nucleic acid-based technologies. This can be attributed to its many appealing properties: it has

a short structural repeat (helical pitch) of 3.4-3.6 nm; it has a persistence length of around 50 nm (single stranded DNA (ssDNA) has a persistence length of 1 nm); it can be a good conductor, insulator or semiconductor with a large band gap depending on the DNA sequence and experimental conditions; there is an added complexity due to a molecular recognition element; and it can self-assemble. (3, 4)

1.3.1 DNA Hybridisation & Branched DNA Formation

The self-recognition property of DNA is important for all aspects of nucleic acid-based technologies. It is the process by which single stranded DNA anneals to its complementary sequence and it occurs through the Watson-Crick model for double helical DNA formation. An interesting application of DNA hybridisation is the formation of long linear duplex DNA from smaller segments of DNA, Figure 1.2. This method relies on sticky ends present on two shorter DNA strands which can overlap and join to form longer strands.(5) As such, it has been used extensively in genetic engineering but is now being applied, and is fundamental, to the synthesis of DNA nanostructures. This allows for programmability in the synthesis of DNA nanostructures, as due to the strict base-pairing rule, we know which two sticky-ends will combine to each other to form the Watson Crick double helix.

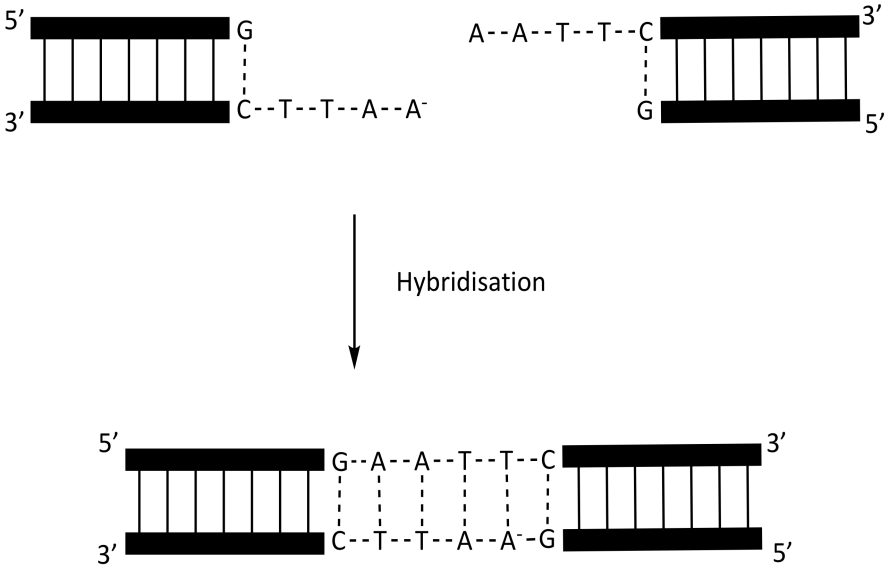

Figure 1-2 Formation of Longer Duplexed DNA via Sticky Ends. Overhangs of unpaired single stranded DNA are known as sticky ends and can be used to form longer duplex DNA.

However, the formation of solely helical structures would inhibit the vast majority of biological reactions taking place. Therefore, nature has allowed for several other branched structures to be formed. For example, during genetic recombination, four-arm branched Holliday junctions are required as an intermediate step.(6)

1.3.2 Application of DNA as a Structural Material

The combination of *in vitro* hybridisation with the formation of branched DNA junctions allows for the synthesis of DNA nanostructures. In brief, the combination of four Holliday branched junctions, with protruding complementary sticky ends, allows for the self-assembly of large arrangements of DNA, Figure 1.3. This is the fundamental principle behind DNA nanostructure assembly via the tile-based method.(7) Another route to the synthesis of DNA nanostructures is known as the origami method and is the method used in this project.

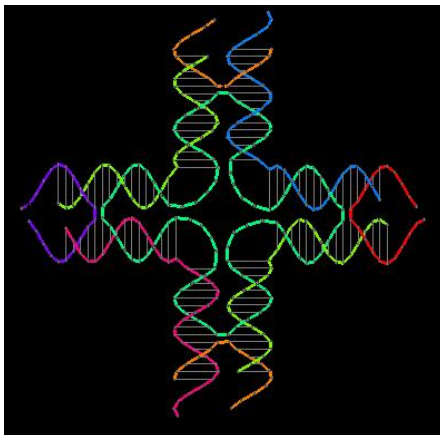

Figure 1-3 Model of a DNA Tile with Sticky Ends. The combination of two or more tiles allows for the fabrication of larger 2D lattices. Model was created using Tiamat.(8)

In 2006, Paul Rothemund introduced a technique, known as DNA origami, to fold DNA into pre-designed shapes. This method relies on hybridisation reactions taking place between a long circular strand of genomic DNA, known as the scaffold strand, and shorter single strands, known as staples. In this method, the self-assembly property of DNA is taken advantage of and all of the components are mixed together in a one-pot reaction step. The DNA solution is then heated and cooled slowly allowing the formation of the designed nanostructures, Figure 1.4. This is a simplified description of a very complex designing procedure, which is often carried out using software, as the design must take into consideration the

incorporation of crossovers and the shape within one turn of the helix in the x-direction and roughly two helical widths in the y-direction. Nevertheless, this method surpasses the tile-based method owing to the ease of synthesis and yields obtained.(9)

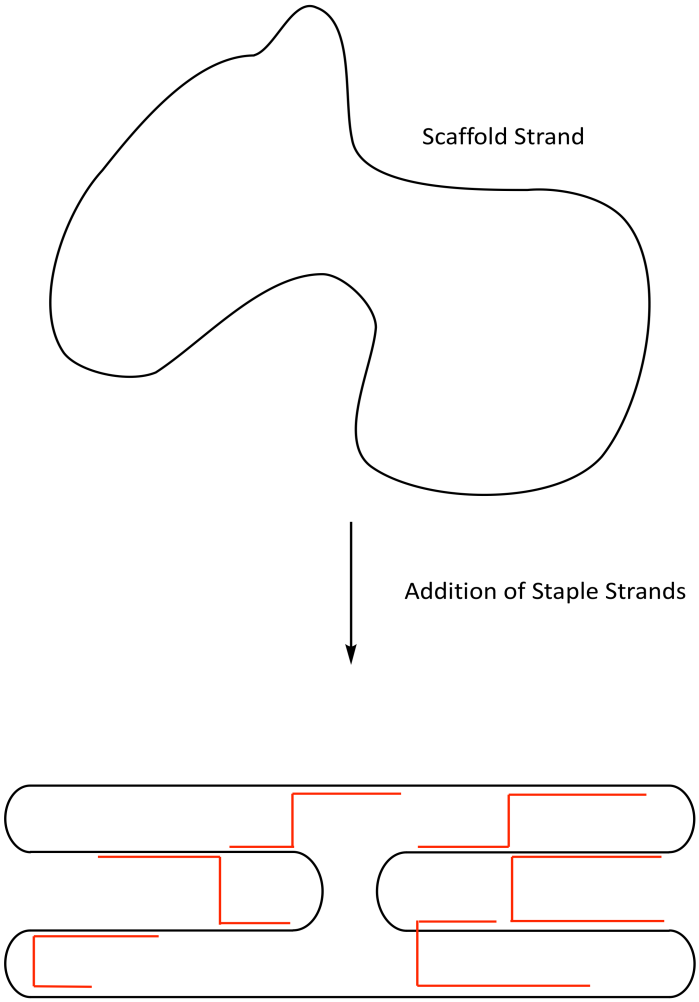

Figure 1-4. The DNA Origami Strategy. Schematic shows the folding of the scaffold strand using shorter staple strands.

1.4 Immobilisation of DNA and DNA Nanostructures

Realising the potential applications of DNA in fields ranging from diagnostics and sensing to materials assembly often requires it to be attached to a solid support, allowing its many unique properties to be taken advantage of. (10, 11) Therefore, the immobilisation of DNA onto surfaces is critical to the realisation of many applications and allows for access to spatially addressable manipulation. For example, in microarray technologies, arrayed DNA can be used to capture their complementary sequences from solution, allowing for highly parallel and

quantitative detection of targets. The foundation of high quality microarray data lies in the surfaces and immobilisation chemistries used.(12) To reduce the high cost and enhance the consistency of microarray experiments, an increasingly popular area of research is in the fabrication of reusable platforms for microarray development. Stripping the surface, by immersing the slides in boiling or near-boiling sodium dodecyl sulphate solution, is often the method of choice. However, this can be detrimental to slide integrity, the effect on the probe is often not considered and the same set of genetic information is probed.(13) Furthermore, due to the directionality of DNA, it can be immobilised to allow or inhibit DNA polymerases that only recognise either the 5' or 3' terminus. Therefore one can selectively modify the desired end of the hybridized target for detection or amplification. (14) As a result, there is an abundance of chemistries and surfaces available to graft DNA.(15)

However, most of the techniques used to date lead to permanent surface immobilisation limiting the possible applications of these surfaces in the formation of materials with dynamic and responsive properties, in particular, reusable functionalities.(16) Therefore, the ability to reversibly attach or modify DNA on surfaces would allow for the introduction, exchange and removal of specific functionalities on surfaces; could be implemented in "write and erase" procedures for DNA microarray development; and be used in *in situ* manipulation of local environments in cell studies or removal of cells from the surfaces for more thorough down stream analysis. (17-19) Therefore, the exploration of new and dynamic immobilisation chemistries is pivotal to the advancement of many different fields. Furthermore, the cost of assays can be reduced and multiple assays can be performed on the same device if the surface can be regenerated reproducibly. (20)

1.5 Reversible Substrate Attachment and Reusable Surfaces

In order to cleave substrates from surfaces, several strategies have been devised. The majority of these methods are based on photocleavable linkers, as they provide external regulation with the highest accuracy in space and time, it is a non-invasive procedure, and it can be used to pattern a variety of shapes. (21) One such extensively used photoliable linker is nitrobenzyl, which undergoes selective bond

cleavage upon irradiation with UV-light.(17, 18, 22-24) However, this group demonstrates slow reaction kinetics, low photochemical efficiency and the irradiation of biomolecules with UV light can be damaging.(21, 25, 26) Another common method used to make covalent bonds reversible include disulphide exchange. (27),(28) However, these methods do not regenerate the surface and therefore once the substrate has been cleaved, the functional group is no longer present in order to immobilise another molecule.

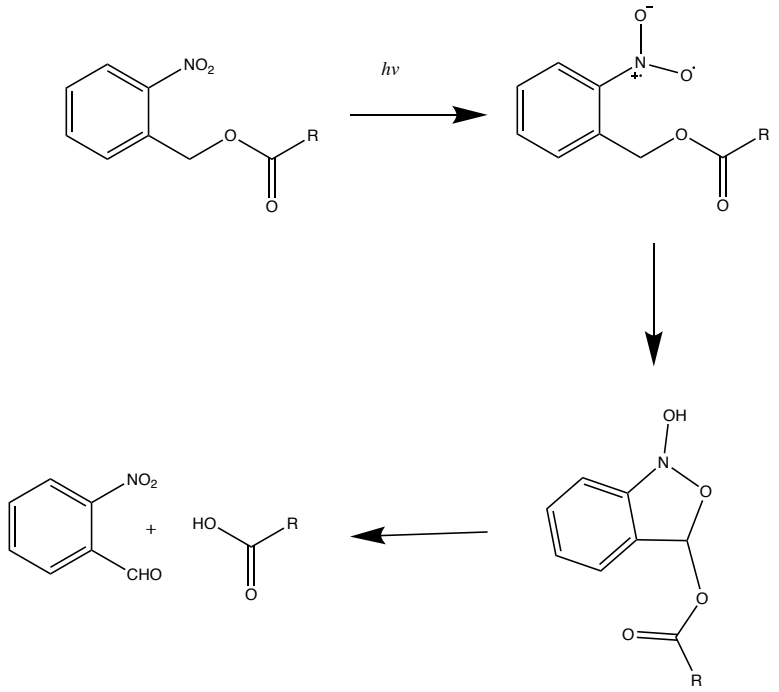

Figure 1-5 Selective cleavage of the photoliable nitrobenzyl upon UV irradiation. (17, 18, 22-24)

Methods used to create reusable surfaces include reactive o-naphthoquinone methindes produced under UV light from 3-(hydroxymethyl)-2-naphthol, which can react with surface thiol groups to yield thioether conjugates. These can then be cleaved using a secondary UV irradiation to regenerate the surface thiol groups. (29) Allyl sulphides incorporated into a hydrogel have also been used to achieve reversible modification with thiol-containing biomolecules while simultaneously regenerating the reactive functionality. (30) Another method to regenerate the thiol group following a reversible photopatterning strategy is based on dynamic exchange reactions resulting from homolytic photocleavage to form sulfenyl radicals.(31) A recent publication showed that the immobilisation of a biomolecule, with an amine functionality, onto a substrate, with a benzoquinone

acid, could be removed using a reducing agent. This results in a dihydocoumarin group on the surface which can be then converted back to the benzoquinone group by oxidation.(32)

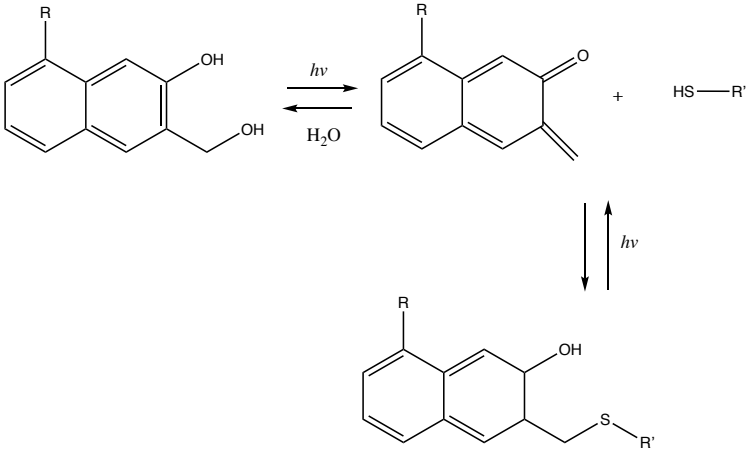

Figure 1-6 Reversible Surface Derivatization Using Thiol– oNQM Photoclick Chemistry. (29)

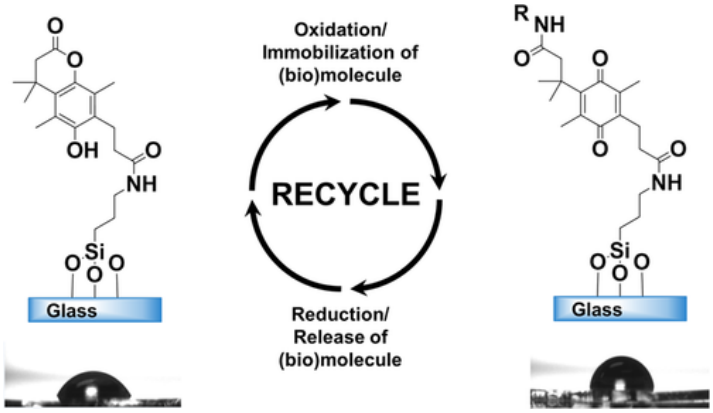

Figure 1-7 Recyclable quinone- presenting substrates. Image taken from Reference 32.(32)

Bio-specific interactions have also been used to create reusable surfaces. For example, a benefit of using protein A/G is that antibodies can be detached by acid treatment and the surface is made reusable allowing for the subsequent immobilisation of more antibodies.(33) Another method to make the surface reusable is through utilising His-tags and chelating agents. The nature of the forces involved in non-covalent interactions have also allowed for a process that can be reversed by changing the conditions that influence the strength of the interaction such as pH, ionic strength, temperature or the polarity of the solvent.(34) For example, increasing the salt concentration can reverse the physisorption of

molecules onto solid supports, especially those arising from electrostatic interactions. (35) Another example of a non-covalent method used to immobilise biomolecules in a reversible method, allowing for the reuse of the surface, is through fluorous-fluorous interactions. (36, 37)

1.6 A Brief History of "Fluorous" Chemistry

Horváth and Rabai first coined the word 'fluorous' over 20 years ago. It was envisaged that it would be used analogously to aqueous.(38) However, usage dictates meaning, and early researchers in this field rapidly expanded its definition to include fluoroalkyl-labelled species. As such, the revised and simplified meaning of this adjective is "rich in fluorine and based upon sp^3-hybridized carbon." (39) Nevertheless, not all compounds that contain fluorine atoms are automatically "fluorous", and in many cases the classification of fluorine-containing species is at the discretion of the researcher.

Molecules termed "fluorous" are often done so due to their ability to partion out of an organic/aqueous phase and into a perfluorinated (or highly fluorinated) phase. This phenomenon is the product of reduced London dispersion forces between per-fluorinated compounds due to the extremely low polarizability of the C-F bond. Simply put, it is due to the avoidance of unfavourable interactions of the fluorine atoms with other atoms and is termed the "fluorous effect". (40)

As such, expanding on the early work of Horváth and Rabai, Curran introduced "fluorous synthesis". This method entailed tagging a molecule (or library of molecules) with a highly fluorinated tag allowing for ease of product purification by drawing the fluorous-tagged compounds into the fluorous layers during liquid-liquid extraction.(41-44) Therefore, owing to the selectivity of fluorous-fluorous interactions, Curran soon expanded the fluorous liquid-liquid biphasic concept to fluorous solid phase extraction and fluorous chromatography using fluorous silica for the separation of fluorous-tagged molecules.(45, 46) To date, fluorous-tags have been employed for the recycling and reuse of catalysts, co-purification of parallel synthesis products, as an enrichment method for mass spectrometry, and for microarray development.(47, 48) (36, 49)

1.7 Motivations

DNA microarrays, which rely on the hybridisation of a probe strand arrayed on a surface and a target strand in solution, were traditionally designed to measure the transcriptional levels of RNA transcripts derived from thousands of genes within a genome in a single experiment.(50) However, to date the uses of DNA microarrays have expanded past gene expression from being used to detect single nucleotide polymorphisms (SNPs) in our genome to pathogen detection. (51, 52) As such, it is a powerful tool used in various biological applications. However, the molecular diagnostic market has not embraced it as much as was expected in the early years of its creation.(53) This is predominantly due to quantification limitations (the signal is only linear over a certain range), specificity issues (it is difficult to design arrays in which multiple related DNA/RNA sequences will not bind to the same probe on the array), and finally, a DNA array can only detect sequences that the array was initially designed to detect. (54) Therefore, this work hopes to alleviate these issues by fabricating platforms that are completely reusable. It is postulated that by using the fluorous effect to immobilise DNA onto solid supports, the DNA, once it has been used to detect one set of genetic information, can be completely removed from the surface allowing a completely different set of genetic information to be screened for. This method would best current methods of DNA microarray regeneration in the fact that it is not stripping the surface of the target DNA, but it is hoped that by washing the substrate in a fluorophilic solvent, which can disrupt the fluorous-fluorous interactions, the DNA duplex would be removed from the surface allowing a completely different probe strand to be immobilised. Furthermore, it is not envisioned that harsh conditions, that limit downstream applications due to deterioration of the samples during release, will be required.(55) Finally, it hopes to best other methods of DNA microarray fabrication in the simplicity of the DNA immobilisation and removal steps as this method relies on a simple wash on wash off method, it is simple enough to allow non-technical individuals to carry out.

2 MATERIALS & METHODS

MATERIALS

General chemicals and kits were obtained from Sigma Aldrich unless otherwise stated in the text. Oligonucleotide (ODN) strands were purchased purified via high performance liquid chromatography (HPLC) or polyacrylamide gel electrophoresis (PAGE) from IDT Technologies (USA). Fluorous-tagged DNA strands were obtained from Dr Glenn Burley's group (University of Strathclyde, UK) purified via HPLC. Borosilicate wafers were obtained from University Wafers (USA) and ultra flat silicon wafers, with a 200 nm layer of thermally grown SiO_2, were obtained from Ted Pella (USA). Single-Stranded M13mp18 DNA (scaffold strand) was purchased from New England Biolabs and the mica was purchased from Agar Scientific. Chips used for the Quartz Crystal Microbalance (QCM) were obtained from (MicroVacuum, Hungary). Restriction enzymes (RE) were obtained from Promega (USA).

2.1 Buffer Solutions

All stock solutions and subsequent buffers can be found in Table 2.1 and were made using deionised (DI) water and autoclaved before use.

Table 2.1 Composition of Stock Solutions used in Materials Sections.

Buffer Name	Composition
0.5 M EDTA Stock Solution	186.1 g disodium ethylenediamenetetraacetic acid (EDTA).$_2H_20$ was added to 800 mL of H_2O and the pH was adjusted to 8.0 with NaOH. Stock soltuion was made up to a final volume of 1 L with H_2O.
4 M NaCl	233.76 g of NaCl was added to 800 mL of H_2O, volume brought up to 1 L.
1 M TRIS-HCl	121.14 g Tris was added to 800 mL of H_2O and the pH was adjusted to 7.0 with HCl. Stock solution was made up to a final volume of 1 L with H_2O.
1 X Phosphate Buffered Saline (PBS)	137 mM NaCl; 2.7 mM KCl; 10 mM Na_2HPO_4; and 1.8 mM KH_2PO_4 (pH 7.4). Obtained from Thermo Fisher Scientific.
10 X Tris Borate-EDTA (TBE)	890 mM Tris-borate; and 20 mM EDTA (pH 8.3). Obtained from Sigma.
50 X Tris Acetate-EDTA (TAE)	2 M Tris; 1M Acetate; and 50 mM EDTA (pH 8.6). Obtained from Sigma.
Annealing Buffer	10 mM Tris-HCl; and 1 mM EDTA (pH 8.0)
Hybridsation Buffer	300 mM NaCl; and PBS (pH 7.0)
10 X TAE.Mg	24.6 g of Magnesium acetate added to 10 X TAE buffer (pH 8.3)
5 X Agarose Gel Loading Buffer	30 % Glycerol, 10 mM TRIS-HCl and 1 mM EDTA
5 X DNA loading dye	30 % glycerol; 0.00125 % w/v bromophenol blue and 0.00125 % w/v xylene cyanol.

2.2 Oligonucleotide Methods

2.2.1 Photometric Determination of Concentration of ODNs

The absorbance of the single stranded ODNs at 260 nm was ascertained using a Nanodrop ND-1000 Spectrophotometer (Thermo, USA) and the concentration was determined using the Beer-Lambert Equation:

$$A = \varepsilon c l$$

Where A is the measured absorbance, ε is the molar extinction coefficient, c is the concentration, and l is the light path length. Each measurement was carried out on 1.5 µL of sample.

2.2.2 Annealing of ODNs in Solution

Single stranded ODNs were mixed in a 1:1.5 ratio, with the strand containing a modification at a slightly higher concentration. This was carried out to ensure that the modified ODN was not the limiting factor during the experiment, for example the strand containing the fluorescent tag was present in a higher concentration to allow for detection. The annealing procedure was carried out in annealing buffer, at 94 °C for 5 minutes in a heating block. The samples were then left to cool to room temperature (RT) with natural heat dispersion from the heating block. This took between 4-6 hours.

2.2.3 Hybridisation of ODNs on Surfaces

ODNs complementary to the sequence immobilised on a surface were diluted to 1 µM in hybridisation buffer, spotted on the surface (typical volume of 20 µL), and left at RT for 2 hours. Surfaces were then rinsed with hybridisation buffer, DI water and dried using a nitrogen gun.

2.3 Nanoparticle Attachment to ODNs

2.3.1.1 Complexation of Nanoparticles with Phosphine Ligands

In order to minimise the salt effects on particle stability, complexation of the gold nanoparticles (AuNPs) was carried out using bis (p-sulfonatophenyl)phenylphosphine dehydrate dipotassium salt (BSPP).(56)

To a 20 mL solution of AuNPs stabilised in citrate buffer (OD 1.0), 4 mg of BSPP was added and the solution was left overnight at RT with gentle agitation. This allowed the phosphine ligands to replace the citrate ligands. Solid NaCl was then added sequentially until the nanoparticle solution turned from a red to a deep purple colour. The particle solution was then centrifuged for 30 minutes at 1600 g at RT to pellet the AuNPs. The supernatant was discarded and the particles were re-suspended in 2.5 mM BSPP (400 µL, in 0.5 X TBE solution) and an equal volume of MeOH was added. The sample was again centrifuged at 1600 g for 30 minutes at RT and finally the supernatant was discarded and the particles were re-suspended in 400 µL of 2.5 mM BSPP (in 0.5 X TBE).

AuNP concentration was determined using a Nanodrop ND-1000 Spectrophotometer (Thermo, USA). The estimated extinction coefficients for the AuNPs at 515-524 nm can be found in Table 2.2.

Table 2.2 Nanoparticle Size and the Extinction Coefficients used to Determine their Concentration.

Nanoparticle Size (nm)	Extinction Coefficient (M^{-1} cm^{-1})
5	1.01×10^7 at 515-520 nm
10	1.01×10^8 at 515-520 nm
20	9.21×10^8 at 524 nm

2.3.1.2 Reduction of Disulphide bond on ODN

Thiol bearing ODNs were delivered in their oxidised form, with the sulphur atoms protected by an S-S bond. In order to reduce the disulphide bond, the ODNs were incubated with Tris[2-carboxyethyl] phosphine (TCEP) in 100 X excess (i.e. 50 mM TCEP to 500 µM ODN) for 2 hours, at RT, prior to conjugation to the nanoparticles.

2.3.1.3 Conjugation of AuNPs to DNA

A solution containing 500 X excess of ODN to nanoparticles in 1 X TBE was made up and left overnight at 50 °C. Six additions of 4 M NaCl were made over a 36 hour time period (final NaCl concentration of 0.1 M) in a process known as "salt-ageing". This process was carried out to screen the negative charges of the ODN, thus increasing the DNA loading on the AuNPs. It was carried out in a step-wise manner in order to reduce the chances of AuNP aggregation: increasing the NaCl concentration slowly increases ODN loading onto the AuNP allowing it to become more stable at higher ionic strengths.(57)

2.3.1.4 Purification of Nanoparticle conjugated DNA.

In order to remove free DNA from the DNA-AuNP solution, it was put through a 30 KDa Amicon filter and washed 3 times with hybridisation buffer. Free nanoparticles were then removed on a 1 % Agarose Gel as per the procedure outlined in Section 2.5.3.2, Figure 2.1. Finally, the DNA and nanoparticle concentrations were calculated using a Nanodrop ND-1000 Spectrophotometer (Thermo, USA) and the solutions were stored in the dark at 4 °C for up to a month before use.

Figure 2-1 1 % Agarose Gel Loaded with DNA-Nanoparticle Conjugates. Bands relating to the DNA-AuNPs, free AuNPs and free DNA are indicated on the gel. After imaging, the top band was chopped out and the conjugated DNA-AuNPs were purified. Conditions used for electrophoresis can be found in Section 2.5.3.2.

2.3.2 Restriction Enzyme Digest of ODNs in Solution

The protocol for DNA conjugation to nanoparticles (Section 2.3) was modified for restriction enzyme digest in solution. This was due to the observation of the formation of concatimers when the ODNs, conjugated to nanoparticles, were allowed to hybridise in solution. Therefore, before the reduction of the disulphide bond, ODNs were annealed according to Section 2.2.2.

Restriction enzyme (RE) digest was carried on the ODNs (Table 2.4) out using several restriction enzymes (Table 2.3). In a sterile tube, 1 uM solution of double stranded ODN (dsODN) conjugated to AuNPs in RE buffer was mixed gently with pipetting. 100 units of the RE was added to a total volume of 60 uL. The tube was then closed and the digest was allowed to proceed overnight at 37 °C. After the incubation step, the enzyme was denatured by addition of 50 mM EDTA.(58) O.5 M DTT was then added to detach the DNA from the AuNPs and the solution was left overnight before being separated on a polyacrylamide gel.

Table 2.3 Restriction Enzymes used to Cut ODNs, their Cut Sites and Buffer Compositions.

Restriction Enzyme	Cut Site	Buffer Composition
HindIII	A ∨ AGCT T T TCGA ∧ A	6 mM Tris-HCl; 6 mM MgCl2; and 100 mM NaCl (pH 7.5)
EcoRI	G ∨ AATT C C TTAA ∧ G	90 mM Tris-HCl; 10 mM MgCl2; and 50 mM NaCl (pH 7.5)
BamHI	G ∨ GATC C C CTAG ∧ G	6 mM Tris-HCl; 6 mM MgCl2; and 100 mM NaCl (pH 7.5)
PstI	C TGCA∨ G G ∧ ACGT C	90 mM Tris-HCl; 10 mM MgCl2; and 50 mM NaCl (pH 7.5)

2.3.3 Restriction Enzyme Digest of ODNs on Nanopatterned Surfaces

A similar protocol to that found in Section 2.3.2 was used to carry out restriction enzyme digest of ODNs bound to nanopatterned surfaces. Following the immobilisation of the ODNs, RE digest was carried out using several restriction enzymes (Table 2.3). RE buffer was mixed gently with 100 units of the RE. This was then added to a total volume of 60 μL and dropped on the surface. The samples were then placed in a humidity chamber and the digest was allowed to proceed overnight at 37 °C. After the incubation, the surfaces were rinsed with DI water, and the surfaces were then imaged using scanning electron microscopy (SEM). To compare the same sample before and after RE digest, dark field and bright field microscopy was used.

Table 2.4. Name, Sequence and 5' Modification of ODNs. The ODNs included in this table refer to those used in Chapter 3.

Name	Sequence (5'-3')	5' Modification
ODN3	ATG GAT CCA TGA AGC TTA TGG AAT TCA TGA TG	Mono-C_8F_{17}
RE_ODN3	ATG GAT CCA TGA AGC TTA TGG AAT TCA TGA TG	None
RE_cODN3	CAT CAT GAA TTC CAT AAG CTT CAT GGA TCC AT	Thiol

2.4 Fabrication of Microarrays and Nanoarrays

2.4.1 Cleaning of Substrates

Substrates were cleaned thoroughly in order to remove any organic contaminants and particles. Firstly, the substrates were sonicated in acetone for 10 minutes, rinsed with isopropanol (IPA) and dried using a nitrogen gun. They were then transferred to a Gala Plasma Prep 5 oxygen plasma asher and ashered for 2 minutes at 100 W.

2.4.2 Silanisation of Substrates

Silane deposition was carried out using a hydrolytic deposition method. This method of silanisation involves four steps that can occur sequentially or simultaneously after the initial hydrolysis step: 1) hydrolysis of the three labile groups; 2) condensation to oligomers; 3) hydrogen bonding between the silane and free hydroxyl groups on the surface; and 4) drying or curing the substrate which drives off the water allowing a covalent Si-O-Si bond to form, Figure 2.2.(59) It is believed in many cases that the self-assembled monolayers resulting from the use of trifunctional silanes form close-packed and well-aligned molecular films where only one bond from each silicon of the organosilane forms between it and the substrate interface. As such, the two remaining silanol groups are present in either a condensed or free form. (60)

To create a sensing area and non-sensing area, two different silanes were used on each surface, Figure 2.3. In order to fabricate the non-sensing regions either n-decyltrichlorosilane (n-DTS, Gelest) or 2- methoxy (polyethyleneoxy) propyl trimethoxysilane (PEG, Gelest) was used due to their propensity to prevent non-specific binding. For the sensing regions, (Heptadecafluoro-1, 1, 2, 2-tetrahydrodecyl) trimethoxysilane) (FDTS, Gelest) or 3-aminopropyl(trimethoxy) silane (APTES, Gelest) was used.

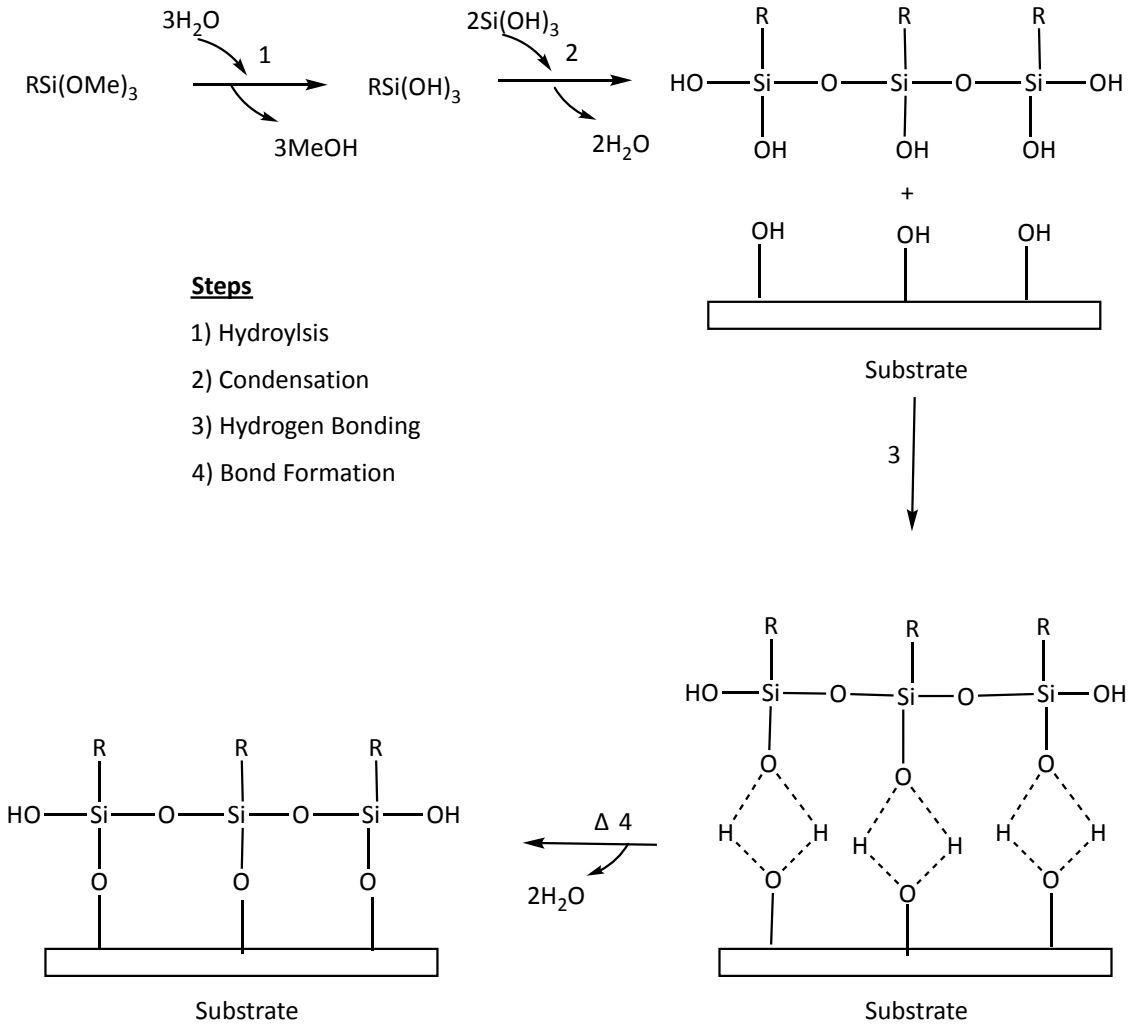

Figure 2-2 Diagram Illustrates the Four Stages of Silane Modification on Substrates via the Hydrolytic Deposition Method. (1) Hydrolysis of the three labile groups; (2) Condensation to oligomers; (3) Hydrogen bonding between the silane and free hydroxyl groups on the surface; and (4) Drying or curing the substrate which drives off the water allowing a covalent Si-O-Si bond to form.

In brief, substrates were placed in a beaker containing a 1 % v/v solution of the silane in toluene whilst being gently agitated. The samples were removed from the beaker, rinsed with fresh toluene and dried under nitrogen. In order to create a denser and higher quality of silane, by promoting lateral polymerisation, the substrates were transferred to a beaker containing deionised water for 10 minutes.(61) This process was repeated twice and finally the substrates were cured in an oven for 30 minutes at 100 °C.

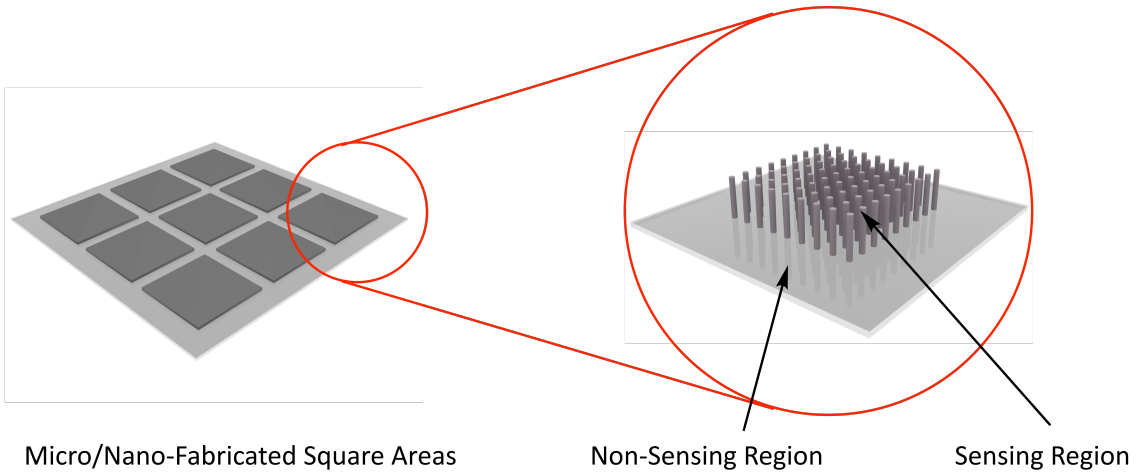

Figure 2-3 Diagram Illustrating the Sensing and Non-sensing Regions on Micro/nano-fabricated Surfaces. Sensing and non-sensing regions were created using either photolithography or electron beam lithography and are defined by the silane that is used.

2.4.3 Photolithography

Lithography allows for a resist image to be created on a surface. Light from an illumination source passes through a predesigned mask, acetate and chrome masks were used in this work, which defines the resist pattern. There are two complementary regions on a mask, one that is opaque and the other transparent, therefore allowing the light to pass through. As the wafer is coated with a photosensitive resist, this process of area specific illumination allows the pattern to be transferred to the wafer. There are two types of photosensitive resist: positive resist and negative resist. Both of these resists undergo a chemical reaction upon exposure to light, however, following illumination from the light source, the positive resist becomes more soluble in the developer, whereas the negative resist becomes cross-linked/polymerised and is not soluble in the developer. (62)

Substrates were spin coated with S1818 (Shiply, USA) at 4000 rpm for 30 seconds to produce a ~1.8 µm thick layer and baked at 95 °C for 3 minutes. Micropatterns were transferred onto the wafer by exposure to UV radiation (SUSS Microtec MA6, Germany) for 4.5 seconds through a chrome or acetate mask. The development of the S1818 resist was performed using a 1:1 ratio of Microposit developer (Shiply,

USA) and reverse osmosis (RO) water for 1 minute. Samples were then dried under nitrogen and patterns checked for over/under exposure using an inverted microscope.

Samples were subsequently ashered for 2 minutes at 100 W to remove the background silane from areas that were going to be re-silanised to create the sensing areas. This was followed by a cleaning step in order to remove the photoresist: substrates were rinsed in acetone and IPA and dried under nitrogen. They were then silanised with FDTS via the protocol outlined in Section 2.4.2.

2.4.4 Electron Beam Lithography

Electron beam lithography (EBL) is a special type of lithography that allows for fabrication of features with size sub 10 nm. In this method, an electron beam, as opposed to a beam of photons, carry energy and transfer said energy into the energy-sensitive polymer material. Following exposure, the resist is developed and the areas exposed to the electron beam are removed. This method surpasses photolithography in the feature sizes that can be achieved: optical microscopy is limited by the optical wavelength. Although electrons have wavelike behaviours, the electron wavelength can be calculated using the following equation:

$$\lambda_e = \frac{1.226}{\sqrt{V}} \text{ nm}$$

Therefore, as the energy of the electrons (V) increases, the wavelength of the electron decreases. This can result in a wavelength that is hundreds of thousands times shorter than the optical wavelength. (63)

2.4.4.1 Design of Patterns

Patterns were designed using L-edit CAD software (Tanner Research Inc.) and exported as a graphical data system file (GDS) containing a multilayer pattern. Layout Beamer (GenlSys Gmbh.) was then used to extract each layer in the GDS file and generate a corresponding file with a defined resolution in VEP format. Each VEP file was then opened in Belle (in-house software) and the substrate size and exposure parameters were defined. Finally the Belle file was transferred to the VB6 machine for writing.

2.4.4.2 Resist Spinning

In order to fabricate the crest designs, electron beam lithography was used. Firstly, the substrates were cleaned and a 2.5 % dilution of 2010 poly-methyl-methacrylate (PMMA) in o-xylene was dropped onto the substrate so that the whole substrate was covered. These were then spun at 5000 rpm for 60 seconds to give a resulting resist layer of 40 nm. This was then baked at 180 °C for 15 seconds to evaporate the solvent. This process was repeated using 2.5 % 2041 PMMA to produce a second layer with a thickness of 50 nm. This process produces a bi-layer of PMMA: with a lower molecular weight resist covered with a higher molecular resist. As such, an undercut profile was obtained allowing for easy lift-off after metallisation.

2.4.4.3 Charge Conduction Layer

A 20 nm layer of aluminium was deposited onto the surfaces of the substrates through electron beam evaporation in a Plassys MEB 4005. This layer acts as a charge conduction layer that prevents the build-up of negative charge in the substrate, which was non-conducting.

2.4.4.4 Patterning using Ebeam Lithography

The samples were then submitted for pattering using the Vistec VB6 UHR EWF electron beam tool. The typical does used for these patterns was 1400 μC/ cm^{-1} and they were written in 1 mm^2 arrays using a 1 nA aperture, 4 nm beam diameter, step size of 1.5 nm and VRU of 3.

2.4.4.5 Development

Following pattern writing, the substrates were placed in Microposit CD- 26 developer (Shiply, USA) to remove the Al layer, rinsed with RO water and dried under nitrogen. The resist was then developed in 2.5:1 ratio of IPA: methyl isobutyl ketone (MIBK) for 45 seconds at 23 °C. PMMA is a positive resist and therefore the areas that were exposed to the electron beam are more soluble than the unexposed regions and can be removed more easily in MIBK, due to polymer chain scission. The substrates were then rinsed with IPA, dried under nitrogen and ashered in an oxygen plasma asher for 30 seconds at 100 W to remove any un-developed resist residue at the bottom of the pattered features.

2.4.4.6 Silanisation of Nanoboxes

Due to the hydrophobic nature of n-DTS (the background silane) PMMA would not stick to the surface following silanisation. Therefore, in order to create sensing and non-sensing regions, an aluminium layer was used as a second resist.

Firstly, the substrates were metallised with aluminium in a Plassys MEB 4005 electron beam evaporator. 20 nm of aluminium was evaporated onto the substrates to produce a metal layer that was thinner than the first layer of PMMA resist. This aids in lift-off.

Lift-off was performed in acetone for 1 hour at 50 °C. This step removes the resist layer and with it, excess metal. Substrates were then rinsed with IPA, dried under nitrogen and transferred to the oxygen plasma asher for 1 minute at 100 W. The substrates were then transferred to a beaker containing n-DTS and silanisation was performed as previously described in Section 2.4.2. The aluminium layer was then removed in Microposit CD-26 developer and the substrate was washed with water and dried under nitrogen. They were then silanised with FDTS by the previously described method, Section 2.4.2.

2.4.5 Immobilisation of ODNs on Micro/Nanopatterned Surfaces

Fluorous-tagged ODNs (Table 2.5) were immobilised onto pattered surfaces functionalised with FDTS silane and n-DTS. An aqueous solution of the fluorous-tagged ODN (1 μM) was spotted onto the surfaces and left for 2 hours (at RT) in a humidity chamber. The surfaces were then rinsed with water (10 mL) and dried under nitrogen. Complementary sequences were then incubated on the surfaces as outline in Section 2.2.3.

2.4.6 Removal of ODNs from the Surfaces & Their Re-immobilisation

The duplexed DNA was removed from the surface by immersing the substrates in a solution containing 50 % MeOH (unless otherwise stated in the text), in hybridisation buffer, overnight. Following this, the substrates were removed, rinsed in hybridisation buffer and imaged. Re-immobilisation of the ODNs, and hybridisation to their complementary sequence was carried out as descried in Section 2.4.5 & 2.2.3.

Table 2.5 Name, Sequence and 5' Modification of ODNs. The ODNs included in this table refer to those used in Chapters 3 &4.

Name	Sequence	5' Modification
ODN1	TGC AGA TAG ATA GCA G	Mono-C_8F_{17}
ODN2	TGC AGA TAG ATA GCA G	-
ODN3	ATG GAT CCA TGA AGC TTA TGG AAT TCA TGA TG	Mono-C_8F_{17}
ODN4	TGC AGA TAG ATA GCA G	Mono-C_8H_{17}
ODN5	TGC AGA TAG ATA GCA G	Mono-C_4F_9
ODN6	TGC AGA TAG ATA GCA G	Mono-C_6F_{13}
ODN7	TGC AGA TAG ATA GCA G	Mono-C_8F_{17}
ODN8	TGC AGA TAG ATA GCA G	Bis-C_8F_{17}
ODN9	TGC AGA TAG ATA GCA G	Tetra-C_8F_{17}
ODN10	ATT TGT GAT GTC CTG C	Bis-C_8F_{17}
cODN1	CTG CTA TCT ATC TGC A	TAMRA
cODN3	CAT CAT GAA TTC CAT AAG CTT CAT GGA TCC AT	Alexa Fluor 488
ncODN1	ATG ATG AAG CTT ATG ATG	TAMRA
cODN10	GCA GGA CAT CAC AAA T	Alexa Fluor 488

2.5 Synthesis, Purification & Immobilisation of DNA Nanostructures

2.5.1 Design of DNA Nanostructures

DNA nanostructures were designed in the Hao Yan Lab (University of Arizona, USA) and tweaked by Dr Henry (University of Glasgow, UK).(64) Chemically modified strands were extended in the 5' direction to allow for all modifications to be on the same plane of the nanostructure.

2.5.2 Synthesis of DNA Nanostructures

The nanostructures were prepared by a standard protocol.(64) Briefly, the scaffold strand and 212 staple strands were mixed together to target concentrations of ~10 nM and ~100 nM, respectfully, in 1 X TAE.Mg buffer. The tubes were then sealed and placed in beaker containing boiling water in a Styrofoam box and left to anneal overnight. Several different structures were synthesised, which differ in the position, chemical modification or both, Table 2.6. The position of the modification is described by a coordinate system as denoted in Figure 2.4.

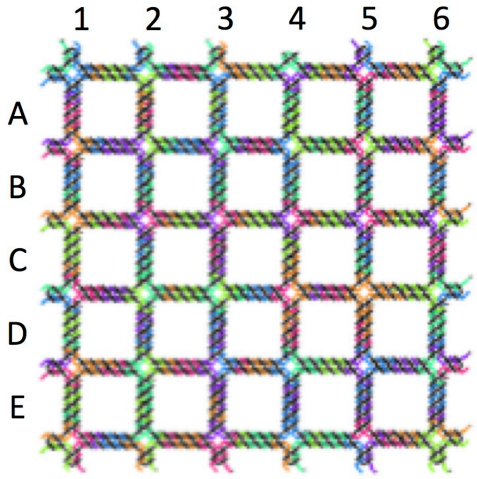

Figure 2-4 Diagram of DNA Nanostructure Template used in Experimental Work. The placement of the modification is described in the text by a coordinate system where the x- position is denoted by a letter and the y-position a number.

Table 2.6 Names used in the Text to Describe the Modified Nanostructures with the Position and the Modification given.

Name of Nanostructure	Biotin Modification	Fluorous Modifications
DNS	**-**	**-**
DNS1	**C3 (Up)**	**-**
DNS2	**C3 (Down)**	**-**
DNS3	**C3 (Up)**	**A1**
DNS4	**C3 (Down)**	**A1**
DNS5	**C3 (Up)**	**A1, E5**
DNS6	**C3 (Up)**	**A1, E1, A5, E5**
DNS7	**C3 (Up)**	**A1, A3, A5, E1, E3, E5**
DNS8	**C3 (Up)**	**A1, A3, A5, B2, B4, D2, D4, E1, E3, E5**
DNS9	**C3 (Down)**	**A1, A3, A5, B2, B4, D2, D4, E1, E3, E5**

2.5.3 Purification of DNA Nanostructures

2.5.3.1 Purification of DNA nanostructures Using a 100 KDa Amicon® Ultra-2 Filter

In order to remove the excess staple strands, the nanostructure solution was added to a 100 KDa Amicon® filter and the buffer was exchanged three times with 1 X TAE.Mg (5000 g, 15 minutes). The sample was then collected (5000 g, 2 minutes) and run on a 1 % agarose gel.

2.5.3.2 Agarose Gel Purification of DNA Origami

The DNA nanostructure solutions were mixed with agarose loading buffer and run on a 1 % agarose gel cast containing Syber Gold (Thermofisher, USA). The gel was run, with 1 XTAE.Mg as the running buffer, for 1.5 hours at 80 V sitting in an ice-water bath. It was then imaged using a Benchtop 3UV™ Transilluminator (Thermofisher, USA) and the band relating to the structure was cut out and chopped up using a razor blade, Figure 2.5. The gel pieces were then transferred to a Freeze n' Squeeze ™ DNA Gel Extraction Spin Column (Bio-Rad, UK), placed in the freezer (- 20 °C) for 5 minutes, and finally spun at RT, 13000 g for 1 minute. The collected liquid was again run through a 100 KDa Amicon® Ultra-2 Filter as previously described and the concentration of the resulting solution was determined using a Nanodrop ND-1000 Spectrophotometer (Thermo, USA).

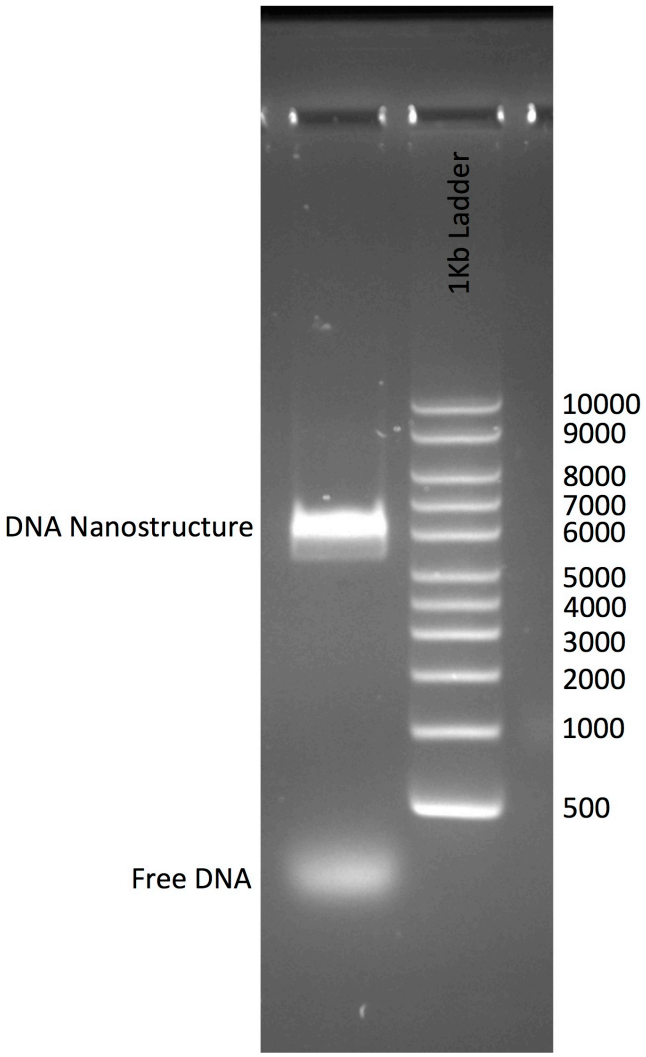

Figure 2-5 1 % Agrose Gel loaded with Unmodified DNA nanostructure. Bands relating to the nanostructure and free DNA are indicated on the gel.

2.5.4 Immobilisation of DNA Nanostructures

2.5.4.1 On Mica

Mica is a negatively charged material and is routinely used to immobilise DNA via a charge bi-layer. As such, mica was freshly cleaved and immediately 4 µL of DNA nanostructure solution (1 nM, 1X TAE.Mg) was spotted onto the surface. The magnesium ions present in the buffer create a positive layer on the mica allowing the origami to be immobilised. (65, 66) The solution was then left to incubate on the surfaces for 10 minutes then dried using a nitrogen gun. The surfaces were then washed with DNAase free water (10 µL) twice with drying in-between and after. In order to prevent damage to the origami, it was necessary to ensure the surfaces were completely dry, Figure 2.6

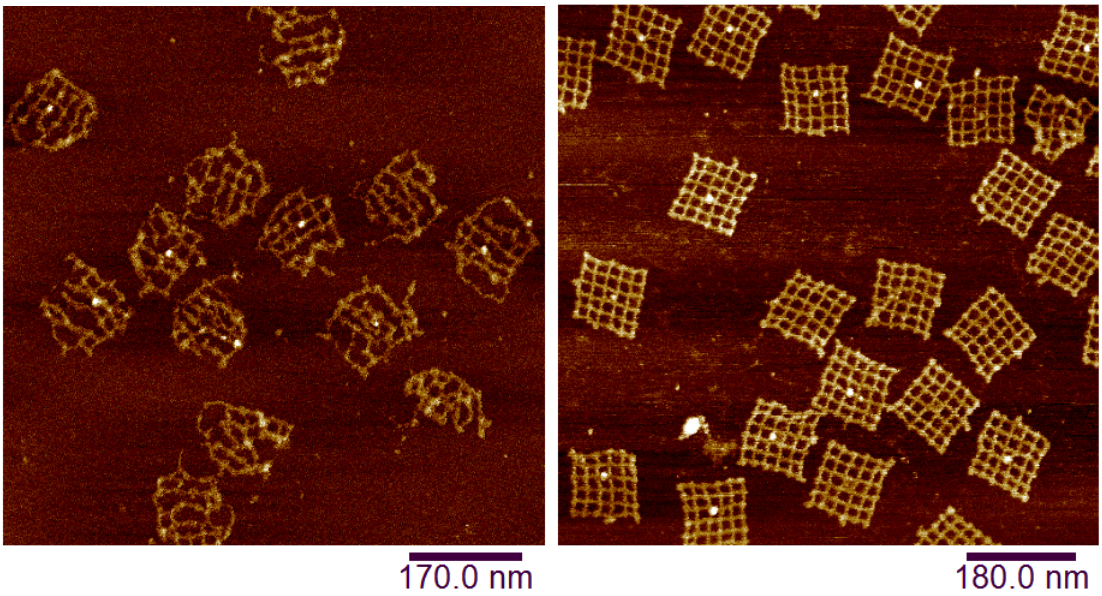

Figure 2-6 Comparison of the Effect that Incomplete Drying has on DNA Nanostructures on Surfaces. Both images are of origami from the same batch. The only difference is that there was incomplete drying on one surface (Left) and complete drying on the second surface (Right).

2.5.4.2 On SiO_2

In order to place DNA nanostructures onto SiO_2, a buffer exchange was required. As such, the DNA origami solution (6 nM, 1 X TAE.Mg) was transferred into a 100 KDa amicon filter and topped up with 10 X TAE.Mg. The sample was spun at 5000 g for 15 minutes and the Amicon filter was again topped up with 10 X TAE.Mg three times in order to ensure buffer exchange from 1 x TAE.Mg to 10 X TAE.Mg. This is

due to the lower negative charge on SiO_2 surfaces compared to mica. Before placement on the SiO_2 surfaces, they were ashered for 30 seconds, 100 W to activate the substrates and ensure the presence of surface silanols as opposed to surface siloxanes.(67) 4 µL of the freshly prepared origami solution (1 nM, 10 X TAE.Mg) was incubated on the surface. This was left for 1 hour at RT in a humidity chamber to prevent evaporation of the droplet, Figure 2.7. Samples were then washed with DNAse free water (20 µL) twice and dried with a nitrogen gun.

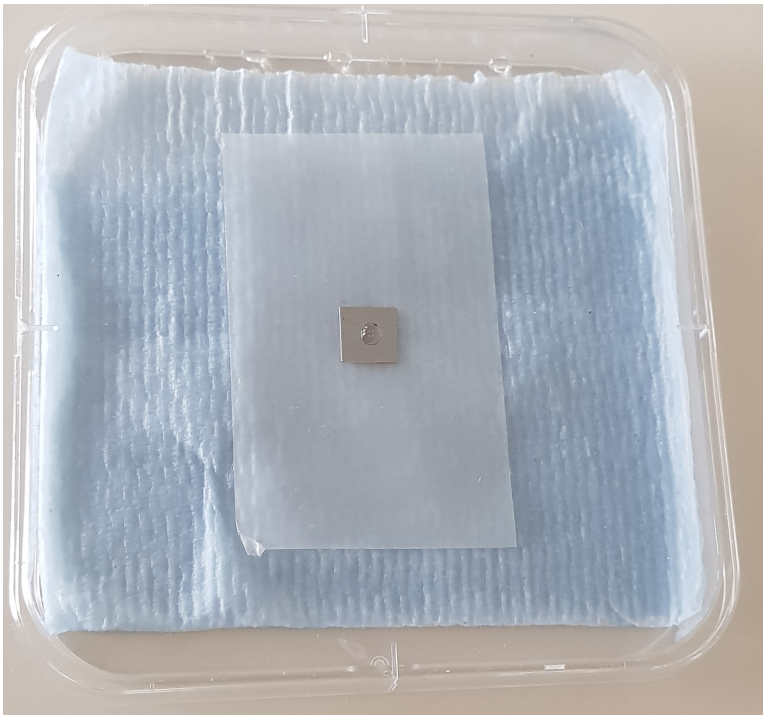

Figure 2-7 Picture of a Humidity Chamber. These chambers were used throughout the experimental section to prevent rapid evaporation of droplets on surfaces.

2.5.4.3 On FDTS/APTES

The same protocol as DNA nanostructure immobilisation on mica was used (Section 2.5.4.1) unless otherwise stated in the text.

2.5.5 Affinity Reaction between Streptavidin and Biotin Modified DNA Nanostructures

2.5.5.1 Incubation and Purification of Streptavidin on Biotin Modified DNA Nanostructures

A solution of DNA origami (1 nM, 1 X TAE.Mg) was incubated with streptavidin (2 uM) for 2 hours at room temperature. The origami were then purified away from the free streptavidin using a 100 KDa Amicon® Ultra-2 Filter using the same protocol as previously described in Section 2.5.3.1. The solution was then deposited onto mica as described in Section 2.5.4.1.

2.5.6 Capture of Fluorous-Tagged molecules onto Fluorous Modified Nanostructures

2.5.6.1 Capture of Fluorous-Tagged Biotinylated ODNs.

Fluorous-tagged, biotinylated ODNs (Table 2.7) were synthesised by Dr Sender & Dr Withers (University of Strathclyde) and diluted to 10 μM in DI water. They were then incubated for 2 hours at RT with streptavidin so that the final concentration of fluorous-tagged biotin was 1 μM and streptavidin was 20 μM. This solution was then incubated overnight with 1 nM of origami solution at 4 °C. Purification of the origami from free streptavidin was carried out as described in Section 2.5.3.1 and the resulting solution was deposited onto mica as outlined in Section 2.5.4.1.

Table 2.7 Name, Sequence and Fluorous Modification of Biotinalayted ODNs used in Section 2.5.6.1.

Name	Sequence	3' Modification	5' Modification
ATS51	TTTT	Biotin	Mono-C_8F_{17}
ATS52	TTTT	Biotin	Bis-C_8F_{17}
ATS53	TTTT	Biotin	Tetra-C_8F_{17}

2.5.6.2 Capture of Fluorous-Decorated Nanoparticles

A fluorous-tagged, thiol bearing ODN (Table 2.8) was obtained from Dr. Sender & Dr Withers (University of Strathclyde) and conjugated to nanoparticles, as outlined

in Section 2.3. Due to aggregation, onto the side of the Eppendorf tube, the samples could not be used.

Table 2.8 Name, Sequence and Fluorous Modified ODNs used in Section 2.5.6.2.

Name	Sequence	3' Modification	5' Modification
NP_ODN	TTTT	Thiol	Mono-C_8F_{17}

2.6 Analytical Techniques

2.6.1 Native Polyacrylamide Gel Electrophoresis (PAGE)

Native gel electrophoresis allows double stranded DNA to retain its double helical structure as it migrates, and separates DNA fragments based on their base pair (bp) number. Due to the uniform negative density of DNA originating from the phosphate backbone, the free solution mobility of DNA is independent of the size of the molecule. However, polyacrylamide (and agrose) gels act as a sieving medium and the relative mobility of any molecule is determined by its ability to navigate a path through the gel pores. In effect, the migration distance of a given DNA strand is proportional to the logarithm of its molecular weight. This is of course a generalisation and the extremes of the size range do not conform to this rule.(68)

Native polyacrylamide gels were prepared and the different compositions for the different percentage gels can be found in Table 2.9. The percentage of acrylamide was determined by the base pair separation required. The components of the gel were added in order shown in table from top to bottom and polymerisation was initiated by the addition of 526 µL tetramethylethylenediamine (TEMED) and 29.4 µL 10 % (w/v) ammonium persulphate (APS). The gel was then left to set for around 1 hour.

Samples were then prepared by adding 20 % v/v of DNA loading dye, and the gel was run for 2-8 hours at 80 V in 1 X TAE.Mg buffer. The gels were then imaged using a Genesyn PXi (Syngene, USA) and the images were analysed using the ImageJ software.

2.6.2 Denaturing Polyacrylamide Gel Electrophoresis (PAGE)

Denaturing gel electrophoresis allows DNA to be separated by its molecular weight only through the inclusion of denaturing agents, such as urea. These agents lower the melting temperature of the DNA, allowing the secondary structure to fall apart at lower temperatures.(69)

In brief, DNA gels were cast depending on the base-pair separation required, Table 2.10. Sample preparation was similar to that described in Section 2.6.1 and the gel was run in TBE buffer at 50 °C for 2-8 hours at 80 V.

Table 2.9 The Composition, and Base Pair Resolution, of the Different Percentage Native PAGE gels used in this work to Analyse DNA Fragments.

	8 %	**12 %**	**15 %**
40 % Acrylamide (19:1)(mL)	14	21	26.2
10 X TAE.Mg (mL)	7	7	7
Water (mL)	49	42	36.8
10 % APS (µL)	526	526	526
TEMED (µL)	29.4	29.4	29.4
Xylene Cyanol Run (bp)	160	70	60
Bromophenol Blue Run (bp)	45	20	15
Resolution (bp)	50-400	35-200	20-150

Table 2.10 The Composition, and Base Pair Resolution, of the Different Percentage Denaturing PAGE gels used in this work to Analyse DNA Fragments. Solutions were made up to 60 mL with DI water.

	8 %	**10 %**	**20 %**
Urea (g)	25.2	25.2	25.2
10 X TBE Buffer (mL)	6	6	6
40 % Acrylamide (19:1)(mL)	12	15	30
10 % APS (µL)	526	526	526
TEMED (µL)	29.4	29.4	29.4
Bromophenol Blue Run (bp)	19	12	8
Xylene Cyanol Run (bp)	75	55	28
Resolution (bp)	35-45	25-35	8-25

2.6.3 Bright Field/Dark Field Microscopy

Microscopy, no matter the technology, follows the laws of physics that define how light interacts with matter. For example, light travelling from one medium to another with a higher refractive index will slow down and change direction dictated by Snell's Law of refractions. Diffraction, on the other hand, describes how light bends around the edges of an object and is defined by Huygens's principle, which states that objects diffract light in a manner directly proportional to its size and spatial distribution. It is the combination of refraction and diffraction that determine what form the image will take and is harnessed in the optical system using lenses to form an image via the controlled convergence and divergence of light.(70)

Bright field microscopy is the fundamental form of microscopy illumination. Its name is derived from the fact that the specimen is dark and the background is light. In contrast, the specimen appears bright and the background dark in dark field microscopy. In this method, the specimen is illuminated at such angles that the direct light is not collected by the microscope objective and thus only diffracted and scattered light are used to form the image. (71)

A Zeiss Axio Imager A1 optical microscope, with a 12 V 100W Tungsten-Halogen bulb as a light source, connected to a Sony NEX-F3, was used to take images of the samples. The exposure time fore each sample was 150 ms, using a 60 X (NA 0.7) objective.

2.6.4 Fluorescence Microscopy

With advances in digital cameras, it is now possible to obtain quantitative data from fluorescence images. When an optical image of the specimen (or surface) is formed by the microscope and recorded by a detector, in this case a charge-coupled device (CCD) camera, a digital image is created. This digital imaged is composed of a two-dimensional grid of equally sized pixels and during the acquisition of the image the photons that are detected at each pixel are converted to intensity values. These values correlate to the number of detected photons or fluorophores present in a sample. (72)

Surfaces were imaged using an Axio Observer Z1 (Zeiss, Germany) (1 second, 20X objective (NA 0.4). In order to obtain quantitative data, the images (8 bit, grey

scale) were imported into ImageJ. The fluorescence intensity was taken from the region of interest (the total analysed area was consistent throughout the analysis) and was normalised by subtracting the fluorescence intensity obtained from an area on the substrate that did not have any sample on it (area of analysis was equal to the area of interest). This was carried out to remove background fluorescence resulting from the detector offset, scattered light from the optics hitting the sensor, difference in the intensity of the illumination source and background light in the room. Therefore the images were normalised to one another allowing quantitative data to be extracted from the images. For each sample, a minimum of 3 repeats was analysed. From this, the average fluorescence intensity and standard deviation was calculated which was plotted for each image.

2.6.5 Quartz Crystal Microbalance

A quartz crystal microbalance (QCM) monitors changes of mass and viscosity on a surface in real-time.(73) QCM, with dissipation, measurements were performed on silicon dioxide coated QCM-D crystals (25 mm, 5 MHz) using an OWLS QCM-I (MicroVacuum, Hungary) attached to a mechanical pump to introduce the samples. The QCM crystals were silanised according to Section 2.4.2. Prior to being mounted into the QCM-D unit, the crystals were soaked in buffer overnight. A crystal was then mounted into the unit where water was flushed through at 20 °C until a stable baseline was established. The flow rate and temperature (40 µL/minute; 20 °C) remained constant throughout the experiment unless otherwise stated. Solutions were introduced slowly through an injection loop (total volume was 500 µL).

Following the stabilisation of the QCM, the change in the frequency and dissipation was measured. The frequency data was then normalised to the fundamental frequency by dividing it by its overtone number. The data obtained from the 3rd, 5th and 7th overtone was then plotted on the same graph to give qualitative data at different depths from the surface.

2.6.6 Atomic Force Microscopy

Atomic force microscopy (AFM) uses a cantilever with a sharp tip to scan over a sample surface and reads out a three-dimensional topographical image with nano-scale precision.(74)

AFM images were taken in tapping mode (air) on a Dimension Icon ScanAsyst (Bruker, USA). ScanAsyst-Air nitride cantilevers with a 2 nm radius silicon tip were used for imaging. Images were then analysed using Nanoscope Analysis 1.5 software.

2.6.7 Fourier Transform Infrared Attenuated Total Reflection Spectroscopy

Fourier transform infrared spectroscopy (FT-IR) in an invaluable tool for the rapid analysis of microsamples.(75) Attenuated total reflection (ATR), in conjunction with infrared spectroscopy (IR), allows samples to be examined directly in the solid or liquid state without further preparation. FT-IR spectra were obtained on a Vertex 70 (Bruker, USA) using a Platinum ATR attachment with a resolution of 2 cm^{-1} and 128 scans. Samples were prepared by grinding the substrates, pre-silanisation, to a fine powder using a mortar and pestle.

2.6.8 Water Contact Angle Measurements

Contact angle measurements were made using 5 µL of DI water on a DSA25 (Kruss, Germany). The contact angle is geometrically defined as the angle formed at the interface between a droplet of liquid, and the surface under examination. This relatively simple technique was used to characterise the surfaces, as the hydrophobicity/hydrophilicity could be rapidly determined. Furthermore, due to the non-destructive nature, as well as rapid throughput, this technique was used as a quality control measure for all silanised surfaces.(76)

2.6.9 Scanning Electron Microscopy

Scanning electron microscopy (SEM) images are generated by probing the specimen with a focused high-energy beam of electrons. The electrons interact with the sample surface, specifically the atoms, which generate a signal that contains information about the specimen surface topography and characteristic features.(77)

SEM images were obtained using a Hitachi S-4700 SEM operating at 10 kV. Before loading the samples in the SEM, they were coated with Au using an in-house sputter coater operating at 15 mA for 2 minutes.

3 Reversible DNA Micro-Patterning using the Fluorous Effect

3.1 Introduction

Microarrays allow for biomolecular interactions to be probed using minimum sample volumes. The typical set up of a microarray involves the probe molecule covalently bonded to a substrate.(54) For this to succeed, the probe molecule must be chemically modified.(78) However, the processes required to chemically modify biomolecules are often tricky and can hamper the overall synthesis. Therefore, new methods to attach biomolecules to solid supports are extremely valuable. This led to the seminal work by Pohl et al., whom suggested a simpler concept for microarray formation relying on the non-covalent fluorous effect. This method of attachment, through a mono-C_8F_{17} tail, was demonstrated to be sufficient to bind carbohydrates to a fluorinated solid support and allowed for the screening of small molecules.(36)

3.1.1 Fluorous-based Microarrays

The term 'fluorous' refers to a class of perfluorinated organic compounds, similar to hydrocarbon chains, with the general formula C_nF_{2n+1}. Tagging molecules with a fluorous chain results in the compound having three distinct regions: (1) a perfluorocarbon group (R_f) to allow for separation; (2) a hydrocarbon spacer (2-3

carbons) to shield the high electronegativity of the R_f group; and (3) an organic compound that dominates its reactivity. In these cases, the fluorous region can be viewed as a phase tag, often referred to as a fluorous "ponytail".(40)

The chemical and physical properties of fluorous "ponytails" differ significantly from their hydrocarbon counterparts. Notably among these differences is their tendency to exclude themselves from both aqueous and organic phases in order to reduce the unfavourable interactions of fluorine atoms with other elements. However, they are known to have strong non-covalent interactions with other fluorous compounds or solvents.(79) This observation is known as the 'fluorous effect' and in 2005 it was exploited by Nichola Pohl to both purify synthetic carbohydrate intermediates and to direct their immobilisation for the production of carbohydrate microarrays. In this work, fluorous-tagged monosaccharides were anchored onto a fluorinated-solid support and then screened with fluorescently labelled carbohydrate-binding proteins. This method bested other non-covalent immobilisation strategies for carbohydrates, such as on nitrocellulose-coated glass slides, in the fact that there was control over the orientation of the sugar on the surface. (80, 81) Further to this, it was demonstrated that only a small fluorous tag (mono-C_8F_{17}) was required to pattern the carbohydrates, and they could withstand multiple washing steps and routine screening against carbohydrate-binding proteins.(36) This work was then built upon by expanding the scope of these arrays for the immobilisation of many molecules including disaccharides, histone deacetylase inhibitors, peptides, and proteins.(82-85) Further to this, unlike traditional microarrays, it was shown that fluorinated-substrates could be rinsed and re-used multiple times with little background fluorescence.(37)

3.1.2 Context & Aim of Result Chapter

The tagging of biomolecules with fluorous "ponytails" has emerged as an attractive method for the immobilisation of biomolecules onto fluorinated-solid supports. This is due to the associated advantages: (i) strong and specific affinity for molecules containing fluorous "ponytails", (ii) high signal-to-noise ratios, (iii) high resistance to non-specific binding, (iv) low and uniform background fluorescence, and (v) simple fabrication workflows.(85) Furthermore, fluorous "ponytails" are often chemically inert, compatible with a wide range of functional groups, and the

tag itself can aid in product purification following solution phase parallel synthesis by means of fluorous-solid phase extraction, reverse fluorous-solid phase extraction and liquid-liquid extraction. (86)

Nevertheless, to our best knowledge, this method of attachment has not yet been applied to the immobilisation of ODNs for the fabrication of microarrays. The work carried out in this section hopes to address this issue with the following aims:

1. Determine if the fluorous effect can be used to immobilise ssODNs onto fluorinated-solid supports without inhibiting the self-recognition properties of the ODN for its complementary sequence.
2. Determine if the fluorous effect can be used to fabricate re-usable surfaces for ODN immobilisation.
3. Determine if the incorporation of a mono-C_8F_{17} tag on the 5' end of an ODN impacted the ability of restriction enzymes to recognise the strand as a substrate.

3.2 Results & Discussion

3.2.1 Characterisation of FDTS Surfaces

Silanisation of borofloat wafers, using FDTS, was investigated by comparing the hydrophobicity of the modified surfaces to unmodified surfaces and by ATR-FT-IR spectroscopy (Figure 3.1). Hydrophobicity was determined using static contact angle measurements for unmodified and FDTS-modified surfaces. It was found that following the silanisation procedure the contact angle measurement increased from ~10˚ ± 7.8 for the unmodified, cleaned glass to ~114.2˚ ± 8.7. This was found to be consistent with other reported values for FDTS modified surfaces, which demonstrated typical contact angle measurements of 110-116˚. (86) (87)

In interpreting the spectra of FDTS silanised borofloat wafers, focus was placed on the region above 700 cm^{-1}. This region is less congested and the band assignments can be found in Table 3.1.(88) Presence of peaks in the region 1200-1400 cm^{-1} are consistent with the deposition of FDTS onto wafers and the enhancement of the methylenic signals at 2850 cm^{-1} and 2935 cm^{-1} reveals a great amount of grafted organic matter.(89) Furthermore, the characteristic asymmetric stretching mode of Si-O-Si shifts from ~1080 to ~1100 cm^{-1}. This has been associated with the successful silanisation of glass substrates and is attributed to the abstraction of –OH to form a monolayer on Si-O-Si.(90) As such, it was concluded that the silane was deposited onto the surface.

Table 3.1 Band Assignment for the Infrared Spectra of FDTS silanised borofloat wafer. Assignments are based on Ref (88, 91-93)

Frequency (cm^{-1})	Intensity	Description
1375	Medium	Antisymmetric CF_2 stretch, CF_2 rock
1260-1200	Strong	Antisymmetric CF_2 stretch, CF_2 rock, CC stretch, CCC bend
2935	Very Strong	Anitsymmetric CH_2 stretch
2850	Very Strong	Symmetric CH_2 stretch

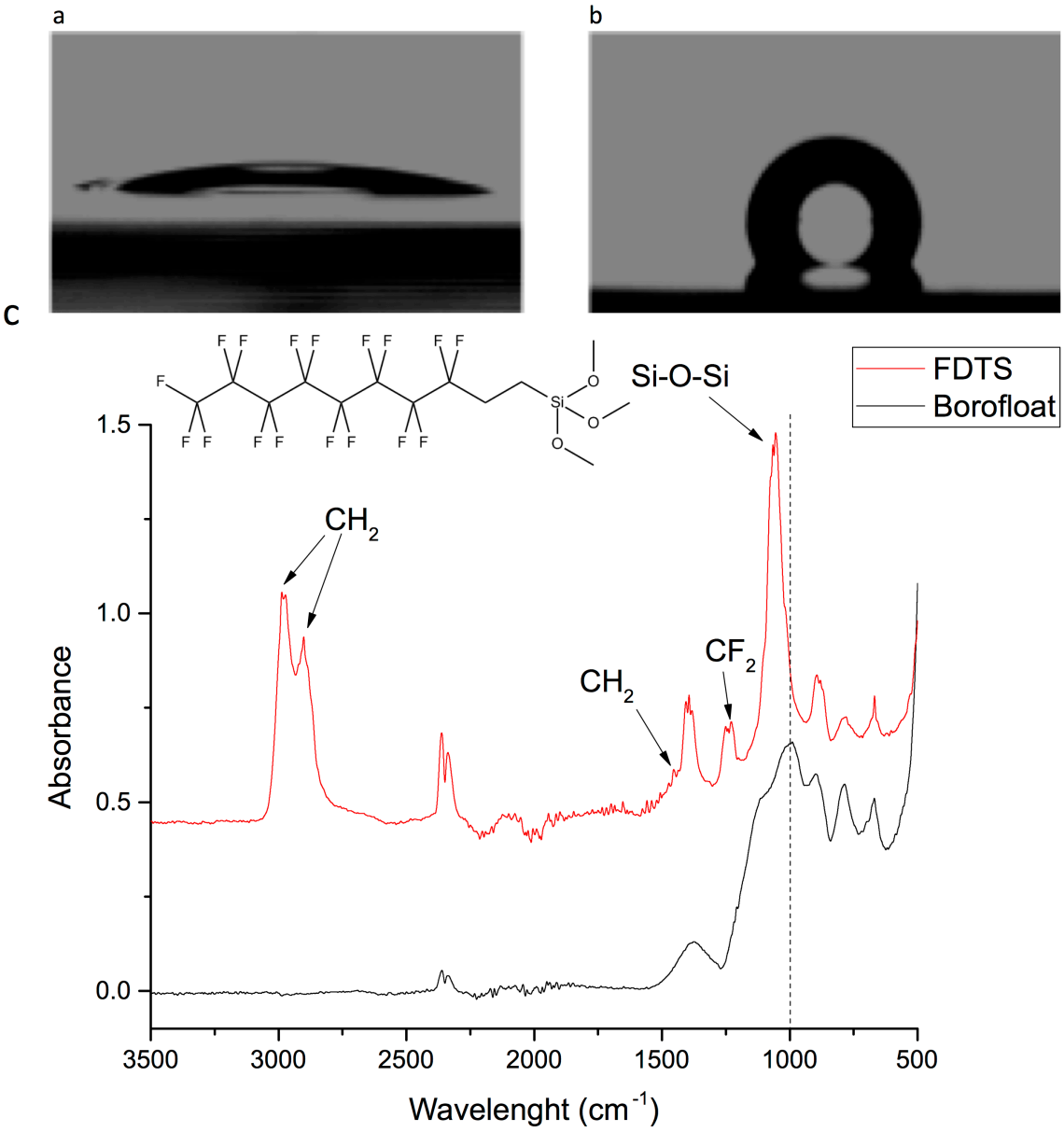

Figure 3-1 Characterisation of FDTS Silanised Borofloat Wafers using FT-IR-ATR Spectroscopy & Contact Angle Measurements. (a) Contact angle measurements were taken before and (b) after silanisation of borofloat wafers. (c) FT-IR-ATR spectra were obtained for the substrates before (in black) and after silanisation (in red) and bands relating to FDTS (structure can be seen above spectra) are indicated on the spectra.

3.2.2 Immobilisation of Fluorous-Tagged DNA

Crucial to the fabrication of DNA microarrays is the retention of the self-recognition properties of the immobilised probe strand, low non-specific binding and high reproducibility of the immobilisation technique. (78) As such, the fluorous effect, as a means to immobilise ODNs for microarray development, was tested against these criteria.

The steps involved in the immobilisation procedure can be seen in Figure 3.2 (a). Briefly, surfaces were fabricated using standard photolithography in order to create chemically distinct regions (Section 2.3.3). This included fluorous modified square arrays surrounded by a non-fluorous background (nDTS). Following this, the mono-C_8F_{17} fluorous-tagged 16-mer ODN (ODN1) was incubated onto the surfaces. This was followed by a washing step to remove non-specifically bound ODN1 and the complementary sequence (cODN1) was introduced to the substrate. In order to detect the presence of cODN1 on the surfaces using fluorescence microscopy, the stand was fluorescently labelled (TAMRA). Incubation of a non-complementary sequence (ncODN1, TAMRA label) was also carried out on surfaces with anchored ODN1. The surfaces were then imaged using fluorescence microscopy (Figure 3.2 (c (i) & (ii))). The corresponding fluorescence intensity values were determined using ImageJ and plotted against one another (Figure 3.2 (b)). These measurements allowed a comparison of the relative concentrations of fluorescently labelled strands, which can be inferred from the fluorescence intensity values, to be made.(72) Hence, it was observed that the described method of attachment for DNA microarray production was suitable in the fact that little fluorescence was detected for the ncODN1. This suggested that there was little of the non-complementary sequence on the surface and thus the surfaces showed low non-specific binding properties. Further to this, as the fluorescence intensity value for the cODN1 was comparably high to the ncODN1, it was inferred that OND1 was in an orientation that permitted hybridisation to its complementary sequence and therefore neither the fluorous-tail nor the fluorinated-substrate inhibited the self recognition properties of ODN1.

In order to determine if the ODN was immobilised through the fluorous effect, a 16-mer ODN was synthesised without a fluorous-tag (ODN2) for comparison of the binding/hybridisation efficiency. This was deposited onto a fluorous array and

incubated with cODN1 (Figure 3.2 (c (iii))). Again, the fluorescence intensity values were low for these samples indicating low non-specific binding of ODN2 onto fluorinated-substrates. As such, from this data it was deduced that the ODN1 was immobilised through the fluorous effect (Figure 3.2 (b)).

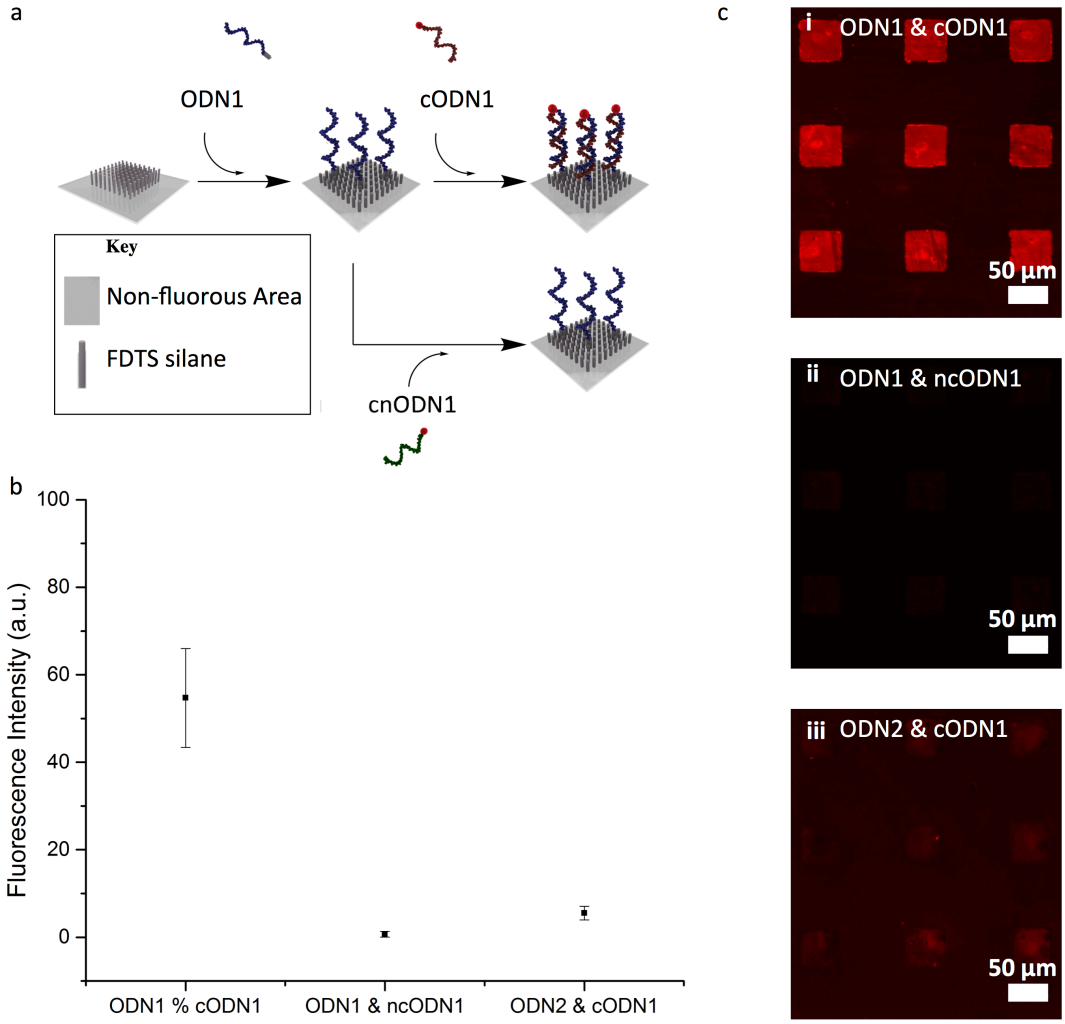

Figure 3-2 Immobilisation & Hybridisation of Fluorous-Tagged ssDNA (ODN1) onto Fluorous Microarrays. (a) Schematic shows the immobilisation of ODN1 onto photo-lithographically defined fluorous-arrays and subsequent hybridisation to its complementary sequence (cODN1) or incubation with a non-complementary sequence (ncODN1). (b) Graph and (c) the corresponding fluorescence images show the fluorescence intensity measurements for the immobilisation and incubation of (i) ODN1 with cODN1, (ii) ODN1 and ncODN1, and (iii) ODN2 and cODN1.

3.2.3 Immobilisation of Fluorous-Tagged DNA – QCM Investigation

The immobilisation, of ODN1, and hybridisation, of cODN1, were also investigated using a quartz crystal microbalance with dissipation monitoring (QCM-D) on both FDTS-modified QCM chips (Figure 3.3 - 3.5) and unmodified QCM chips (Figure 3.6 – 3.8). QCM has been extensively used to investigate the immobilisation and hybridisation of DNA on surfaces.(94-97) A change in the mass of material deposited on the sensor surface generates a shift in the frequency of oscillation, ƒ, relative to the original baseline frequency. This change in frequency (Δƒ) is detected by the sensor and relates to the mass change of the molecular film according to the Sauerbrey equation ($\Delta m = -C \Delta f / n$; where Δm is the change in the density of the immobilised mass (ng cm^{-2}), n is the overtone number and C is a constant value of 17.7 ng cm^{-2} s^{-1}).(73)

The special variation of this technique, QCM-D, allows for the label-free simultaneous measurement of the changes in the induced energy dissipation (ΔD) and the frequency (Δƒ) in real-time. This change in dissipation can be related to the energy loss of the system, or the viscoelastic properties of the adlayer and thus QCM-D measures two distinct properties of the immobilised layer.(98) This technique has been used to probe the conformational changes or secondary structures of DNA molecules.(99-101)

In this work, QCM-D measurements were carried out to determine if the ODN1 was immobilised non-specifically onto an unmodified, SiO_2 coated QCM chip. The purpose of this experiment was to monitor the immobilisation of this strand onto the surface as it was not fluorescently labelled and could therefore not be monitored using fluorescence microscopy.

As shown in Figure 3.3, after a short wash with buffer (flow rate 40 μL/min) , the ODN1 (1 μM) was loaded into the chamber containing a fluorous modified QCM chip. Immediately a dramatic decrease in the frequency (-Δƒ) was detected. The Δƒ then plateaued around 8 Hz indicating surface “saturation”. Following this, buffer was flowed into the chip to remove any non-specifically bound ODN1 and the frequency change again plateaued at around 6 Hz. As stated, dissipation data was also recorded during these measurements. Initially, after the loading step, a large increase in the dissipation was observed. This is consistent with non-specific adsorption, the formation of a non-rigid film, or a change in density of the buffer.

(98, 102)As the Sauerbrey equation is only valid for acoustically rigid films with low dissipation, the increase in mass could not be plotted for these measurements using this model as ΔD and Δ*f* have become coupled. However, it can be taken as an approximation that Δ*f* mainly reflects changes in surface mass and ΔD is predominantly influenced by the viscoelastic properties of the surface-immobilised layer.(73) Therefore, a decrease in the frequency was attributed to the immobilisation of ODN1 onto the surface (Figure 3.3 (b)).

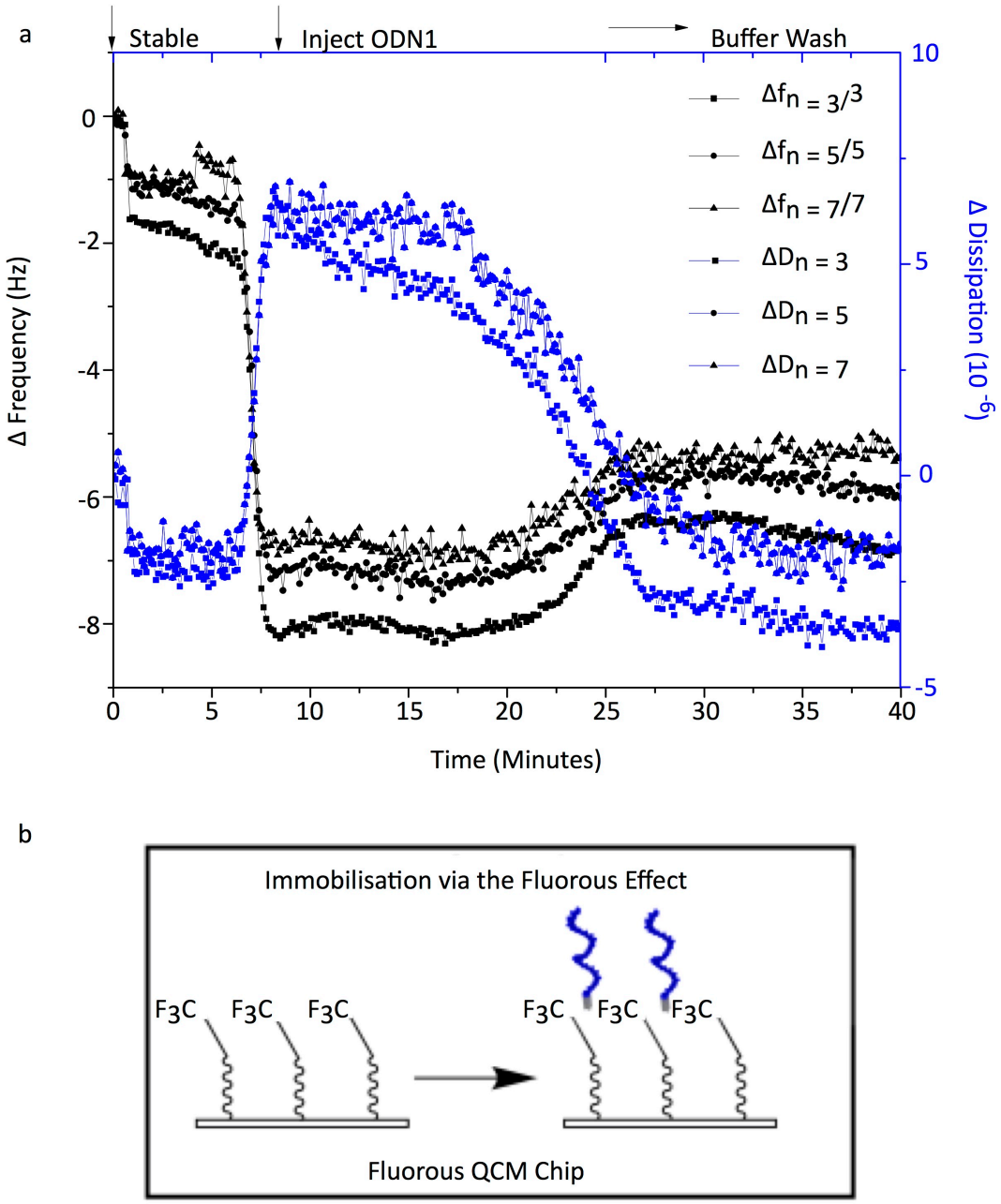

Figure 3-3 QCM Measurements taken during the Immobilisation of ODN1 onto Fluorous Silanised QCM Chips. (a) Frequency and dissipation data

obtained during the immobilisation of ODN1 onto a FDTS modified QCM chip. (b) Schematic of immobilisation of ODN1 onto a fluorous QCM chip. Key: $\Delta f_n = {}^{3}/_{3}$ is the change in the frequency arising from the 3rd overtone normalised to the fundamental by dividing it by its overtone number; $\Delta f_n = {}^{5}/_{5}$ is the change in the frequency arising from the 5th overtone normalised to the fundamental by dividing it by its overtone number; $\Delta f_n = {}^{7}/_{7}$ is the change in the frequency arising from the 7th overtone normalised to the fundamental by dividing it by its overtone number; $\Delta D_n = 3$ is the change in the dissipation data arising from the 3rd overtone; $\Delta D_n = 5$ is the change in the dissipation data arising from the 5th overtone; and $\Delta D_n = 7$ is the change in the dissipation data arising from the 7th overtone.

Following the injection of cODN1 (1 μM) into the chamber, a smaller and slower decrease in the frequency was observed (Figure 3.4 (a)). This was attributed to hybridisation events occurring on the surface (Figure 3.4 (b)). Nevertheless, there was little change in the dissipation. This could suggest the formation of a rigid layer due to the hybridisation of the cODN1 to the ODN1 on the surface, which reduces the persistence length associated with single-stranded DNA.(101, 103)

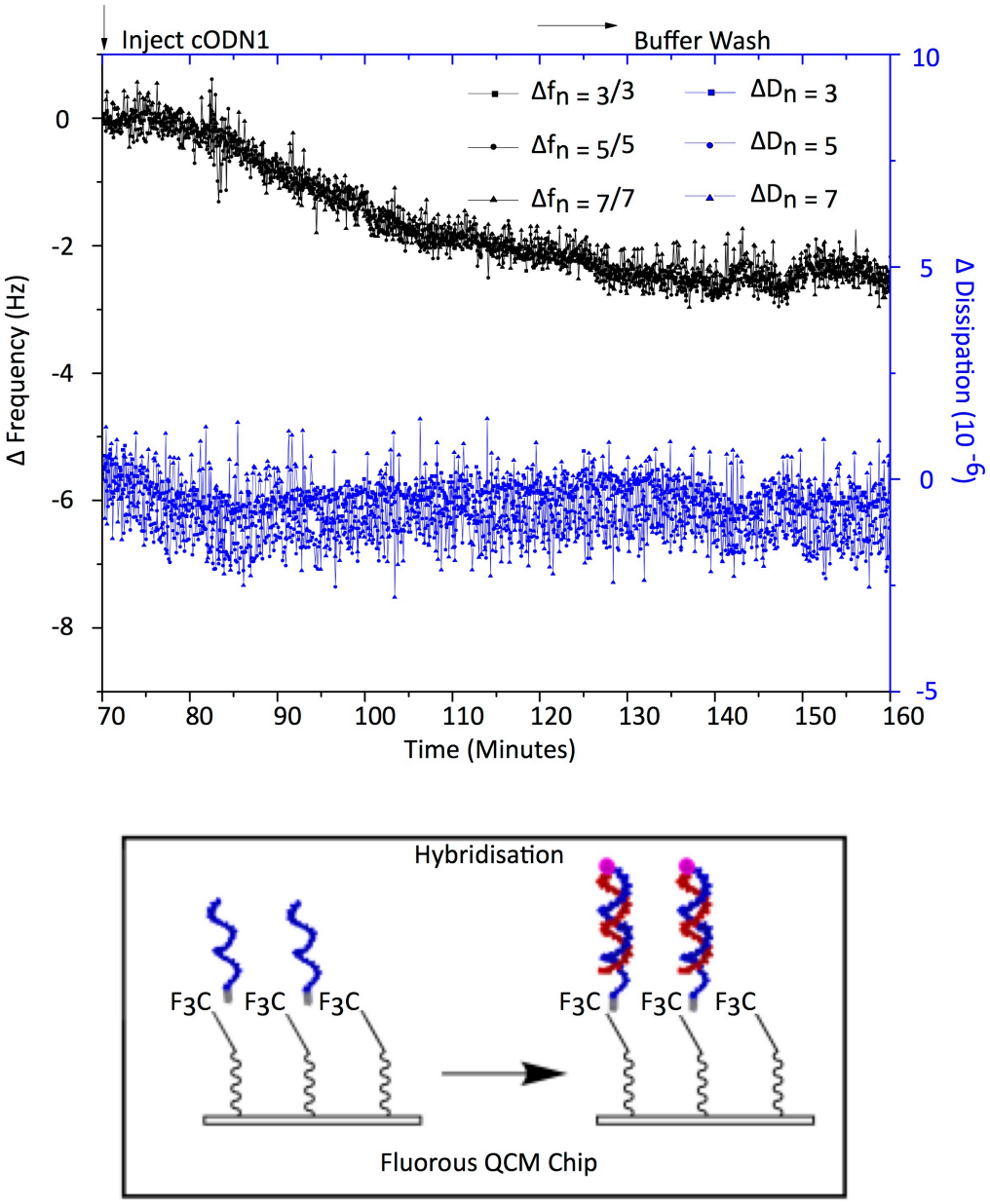

Figure 3-4 QCM Measurements taken during Hybridisation of cODN1 to ODN1 on Fluorous Silanised QCM Chips. (a) Frequency and dissipation data for the hybridisation of cODN1 with ODN1. (b) Schematic of hybridisation of cODN1 with ODN1 immobilised onto fluorous modified QCM chip. Key: $\Delta f_n = {}^{3}/_{3}$ is the change in the frequency arising from the 3rd overtone normalised to the fundamental by dividing it by its overtone number; $\Delta f_n = {}^{5}/_{5}$ is the change in the frequency arising from the 5th overtone normalised to the fundamental by dividing it by its overtone number; $\Delta f_n = {}^{7}/_{7}$ is the change in the frequency arising from the 7th overtone normalised to the fundamental by dividing it by

its overtone number; ΔD_n= 3 is the change in the dissipation data arising from the 3rd overtone; ΔD_n= 5 is the change in the dissipation data arising from the 5th overtone; and ΔD_n= 7 is the change in the dissipation data arising from the 7th overtone.

To characterise the immobilisation of ODN1 onto the FDTS-modified surface and to gain more qualitative information about the interactions occurring at the solid-liquid interface, the ΔD was plotted against the Δƒ (Figure 3.5 (a)).(104) It was found that with an increase in the mass on the surface, which was attributed to the immobilisation of ODN1 onto the FDTS-modified QCM chip, the dissipation energy also increased until a critical mass on the surface was obtained and the dissipation suddenly dropped to the starting value (Figure 3.5 (a)). This profile of events has been observed for supported lipid bilayer (SLB) formation from vesicle rupture. This process is described as a three-step model: (1) vesicle adsorption; (ii) vesicle stress in the form of bending and intervesicular crowding; and finally (iii) vesicle rupture into a confluent SLB. (105) As such, the QCM data was analysed in this context as the formation of spherical micelles with a perfluorocarbon core and a DNA corona has been reported elsewhere (Figure 3.5 (c)). (106) It was thus postulated that the fluorous-DNA micelles approached the surface and were non-specifically bound. This could explain the large change in the dissipation during the injection stage (Figure 3.3 (a)). Finally, once a critical mass of the fluorous-DNA micelles was reached on the surface, they ruptured causing a reduction in the dissipation data consistent with the formation of a more rigid layer.

The same analysis for the cODN1 hybridisation events was carried out (Figure 3.5 (b)). This plot showed that a linear relationship existed between the Δƒ and ΔD indicating that no conformational changes occurred during the hybridisation process. Further to this, the gradient was very small indicating slow adsorption/hybridisation kinetics for the cODN1. (107)

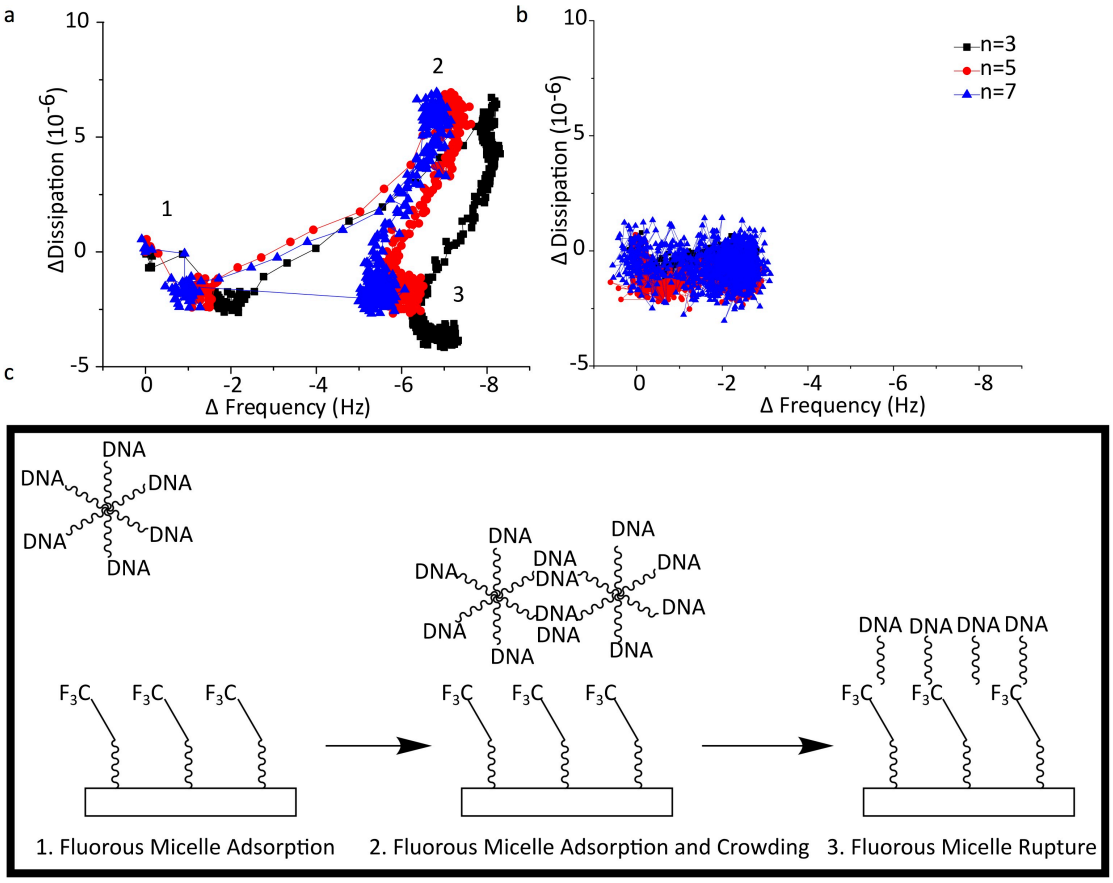

Figure 3-5 Plots of the Change in Dissipation as a function of the change in Frequency for Immobilisation & Hybridisation of Fluorous Tagged ssDNA on Fluorous Silanised QCM Chips. (a) Graph illustrates the change in dissipation with the change in frequency measured during the immobilisation of ODN1 onto fluorous surfaces. Upturned "v" is consisted with lipid vesicle adsorption and rupture on a surface and could be correlated to fluorous micelle adsorption onto surfaces as outlined in schematic (c). (b) Change in dissipation with the change in frequency measured during hybridisation of cODN1 to immobile ODN. Key: n= 3 is the frequency and dissipation data obtained from the 3rd overtone; n= 5 is the frequency and dissipation data obtained from the 5th overtone; n= 7 is the frequency and dissipation data obtained from the 7th overtone.

As stated, the immobilisation events of ODN1 onto unmodified QCM chips (with deposited SiO_2 layers) were probed using QCM using the same conditions as previously explained (Figure 3.6 - 3.7). In relation to the FDTS-modified QCM chips, a comparable decrease in frequency (6 Hz) was found for these surfaces following the introduction to the fluorous-tagged DNA (Figure 3.6). This suggested

that the DNA was immobilised onto the surface. However, the energy dissipation for these surfaces was comparably higher than that of ODN1 immobilisation onto FDTS-modified QCM chips. It is difficult to pinpoint the exact reason for this, however it could suggest more water adsorption in the adlayer due to the fact that the surface is hydrophilic as opposed to hydrophobic like the FDTS-modified layer.(104) However, as the penetration depth of an acoustic wave is proportional to the $\sqrt{f}$, collecting data at multiple frequencies (overtones) can give further information as to the structure of the immobilised layer. Therefore, the overtone dependence displayed during the immobilisation of ODN1 onto the unmodified surface could hint at different viscoelastic properties at different penetration depths. This could therefore indicate the formation of a non-homogenous layer. (101, 108)

Examination of the QCM frequency and dissipation data following the injection of the cODN1 showed no change (Figure 3.7 (a)). Therefore, it was concluded that the immobilised ODN1 was not in the correct orientation to permit hybridisation and no cODN1 was immobilised onto the surface.

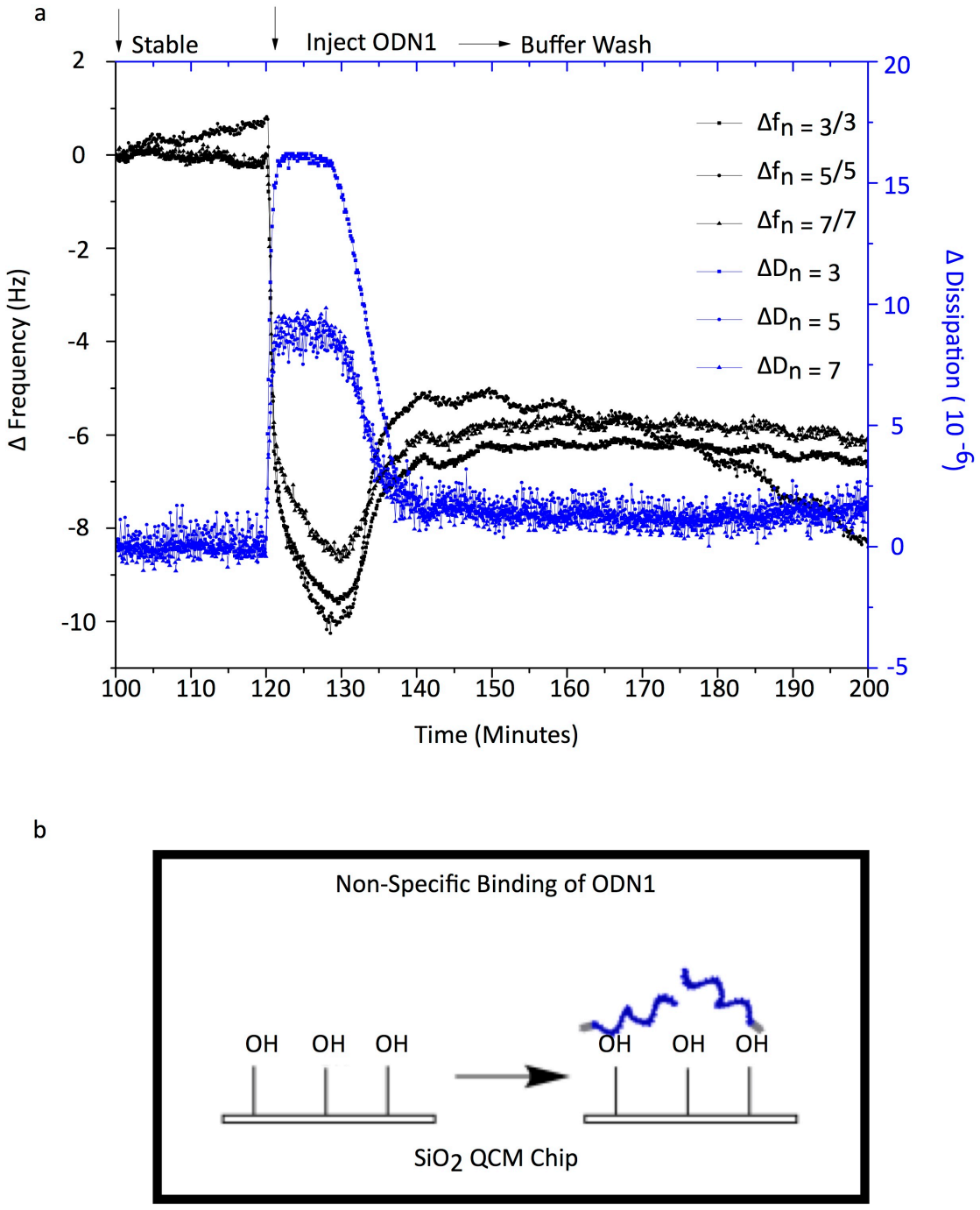

Figure 3-6 QCM Measurements of Immobilisation of ODN1 onto SiO_2 coated QCM Chips. (a) Frequency and dissipation data obtained during the non-specific immobilisation of ODN1 onto SiO_2 coated QCM chip. (b) Schematic of non-specific immobilisation of ODN1 onto SiO_2 coated QCM chip related to theorised events occurring in (a). Key: $\Delta f_n = {}^{3}/_{3}$ is the change in the frequency arising from the 3rd overtone normalised to the fundamental by dividing it by its overtone number; $\Delta f_n = {}^{5}/_{5}$ is the change in the frequency arising from the

5th overtone normalised to the fundamental by dividing it by its overtone number; $\Delta f_n = {}^{7}/_{7}$ is the change in the frequency arising from the 7th overtone normalised to the fundamental by dividing it by its overtone number; $\Delta D_n = 3$ is the change in the dissipation data arising from the 3rd overtone; $\Delta D_n = 5$ is the change in the dissipation data arising from the 5th overtone; and $\Delta D_n = 7$ is the change in the dissipation data arising from the 7th overtone.

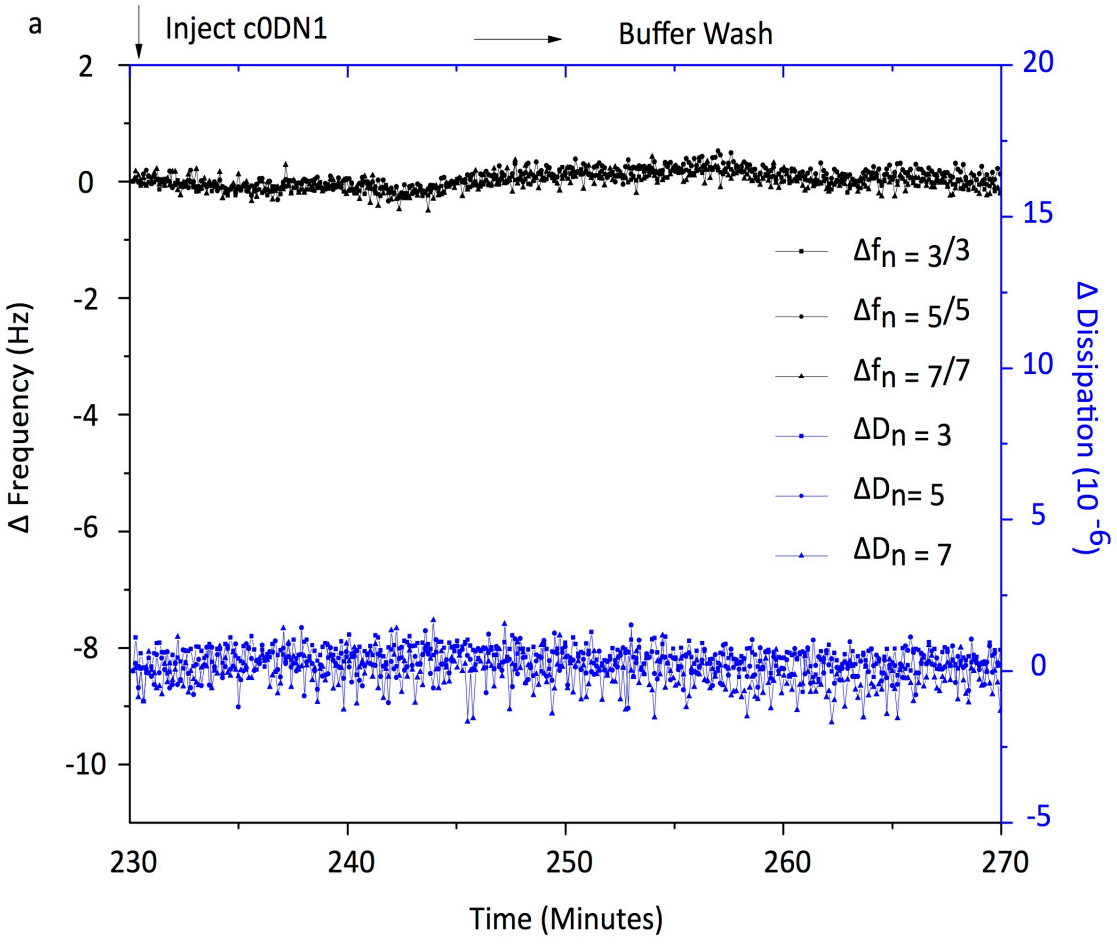

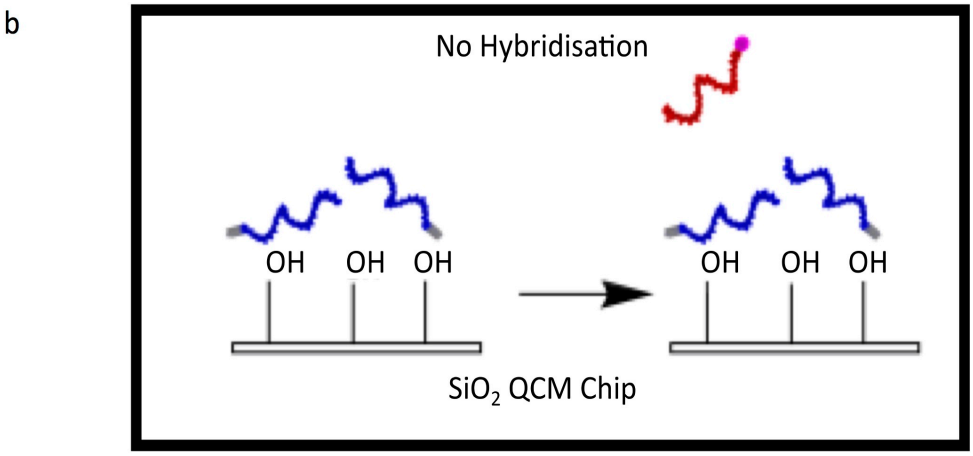

Figure 3-7 QCM Measurements Following the Injection of cODN1 into chamber containing SiO_2 coated QCM Chips with previously immobilised ODN1. (a) Frequency and dissipation data obtained after cODN1 was injected into the QCM chamber. (b) Schematic showing that the ODN1 is not in the correct orientation to permit hybridisation and is related to theorised events occurring in (a). Key: $\Delta f_n = {}^{3}/_{3}$ is the change in the frequency arising from the 3rd overtone normalised to the fundamental by dividing it by its overtone number; $\Delta f_n = {}^{5}/_{5}$ is the change in the frequency arising from the 5th overtone normalised to the fundamental by dividing it by its overtone number; $\Delta f_n = {}^{7}/_{7}$ is the change in the frequency arising from the 7th overtone normalised to the fundamental by dividing it by its overtone number; $\Delta D_n = 3$ is the change in the dissipation data arising from the 3rd overtone; $\Delta D_n = 5$ is the change in the dissipation data arising from the 5th overtone; and $\Delta D_n = 7$ is the change in the dissipation data arising from the 7th overtone.

Again, qualitative data was obtained by plotting the Δf vs. ΔD (Figure 3.8). This hinted at the same set of events described for the immobilisation of ODN1 onto FDTS-modified QCM chips (Figure 3.5). However, due to lack of frequency data following the injection of cODN1 into the QCM chamber (suggesting that no hybridisation events occurred) it was postulated that the ODN1 was immobilised in an orthogonal arrangement, following micelle rupture, but with the fluorous "ponytails" pointing away from the surface.

A comparison between the Δf vs. ΔD for ODN1 on FDTS-modified and unmodified QCM chips showed that the initial adsorption kinetics were a lot faster for the immobilisation of ODN1 onto FDTS-modified surfaces (due to the steeper gradient).(101) Further to this, slight curvature during the initial immobilisation step of the ODN1 onto the unmodified QCM chip could hint at conformational changes on the surface. (107)

In summary, this body of work was used to gain qualitative data about the immobilisation of fluorous-tagged DNA onto both fluorous modified and unmodified SiO_2 surfaces. It was shown in both of these cases that the fluorous-DNA was immobilised onto the surface. Analysis of the dissipation data pointed at possible fluorous-micelle rupture on the surfaces causing the formation of a layer

of fluorous DNA on the surface. However, following the incubation of the complementary DNA onto the surfaces, only the fluorous modified chips showed frequency response consistent with the hybridisation of the probe DNA to the target DNA. Therefore it was postulated that the fluorous DNA specifically orientated itself, following micelle rupture on the surface, whereby the fluorous tail either interacted with the surface enabling hybridisation (as seen on the FDTS modified surfaces) or pointed towards the bulk solution preventing hybridisation (as seen on the unmodified SiO_2 surfaces). This was attributed to the fluorous tail trying to orientate itself in such a manner to reduce unfavourable interactions with other elements. Unfortunately, QCM-D can give more qualitative data than presented here including the layer thickness and dissociation kinetics. However, it was not possible to carry out this analysis due to software limitations. Therefore, further investigation should be carried out on this work to gain more quantitative data. Furthermore, it could be interesting to probe the surface further and determine if, following rupture of the fluorous micelle on the surface, a fluorous bilayer could be formed.

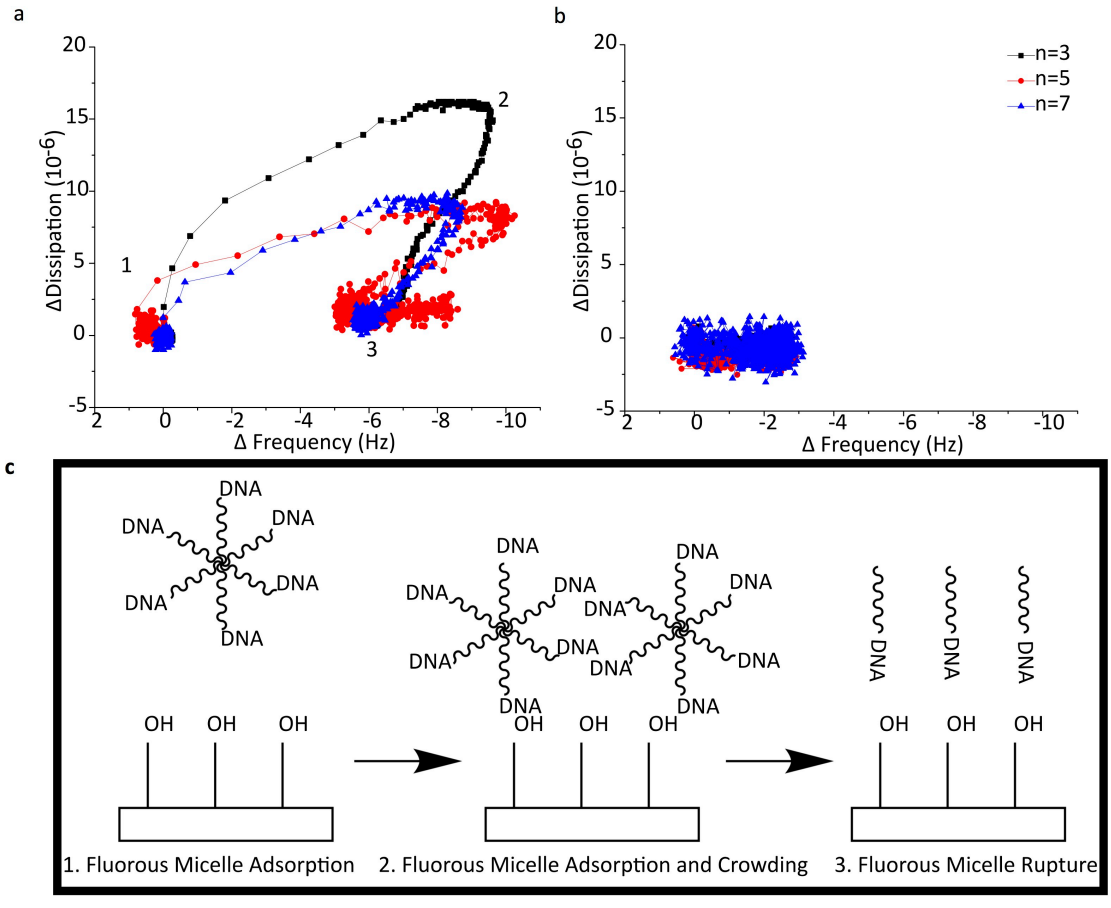

Figure 3-8 Plots of the Change in Dissipation as a function of the change in Frequency for Immobilisation of ODN1 onto SiO_2 coated QCM Chips and Following Injection of cODN1. (a) Graph illustrates the change in dissipation with the change in frequency measured during the immobilisation of ODN1 onto SiO_2 surfaces. Upturned "v" is consisted with lipid vesicle adsorption and rupture on surface and could be correlated to fluorous micelle adsorption onto surfaces as outlined in schematic (c). Due to the lack of binding of the cODN1 to the surface it is postulated that ODN1 is immobilised on the surface with the fluorous tails pointing away from the surface preventing both hybridisation of cODN1 with ODN1 or non-specific binding of the cODN1 onto the surface. (b) Change in dissipation as a function of the change in frequency measured during injection of cODN1 into QCM chamber. Key: n= 3 is the frequency and dissipation data obtained from the 3rd overtone; n= 5 is the frequency and dissipation data obtained from the 5th overtone; n= 7 is the frequency and dissipation data obtained from the 7th overtone.

3.2.4 Immobilisation and Removal of Fluorous-Tagged DNA onto Fluorous Surfaces

Many DNA immobilisation techniques used in the fabrication of microarrays are often static in nature and therefore do not provide any opportunity to modify the composition of the substrate after the initial immobilisation step. (109, 110) This limits the potential use of the surfaces, particularly in biosensing and diagnostics, as they are restricted to single use applications.(16) Therefore, the development of new chemistries that allow for the reuse of the sensing platforms would provide a route towards more versatile systems and devices.

The current method employed to reuse microarray slides relies on a stripping mechanism that refreshes the substrates between each reuse.(13) However, this method does not permit the probing of different genetic information. Fluorous-fluorous interactions on the other hand have demonstrated potential as a method for removing anchored small molecules from surfaces. (37) This work demonstrated the ability to probe small molecule-protein interactions with the added benefit of being able to reuse the same substrate up to five times with low background fluorescence following a simple methanol/dichloromethane wash.(37)

It was therefore hypothesised that applying this technique to the fabrication of DNA microarrays could permit reusable ODN screening applications.

In order to investigate this, fluorous arrays were fabricated using standard photolithography and the ssDNA with a fluorous tag, ODN1, was incubated on the substrates. This was then hybridised to its complementary sequence, cODN1, allowing for its detection using standard fluorescence microscopy. Due to the non-covalent nature of the fluorous interaction, by employing a simple methanol/PBS wash, the duplex was removed from the surface thus regenerating it and allowing for new DNA to be immobilised onto the surface (Figure 3.9).

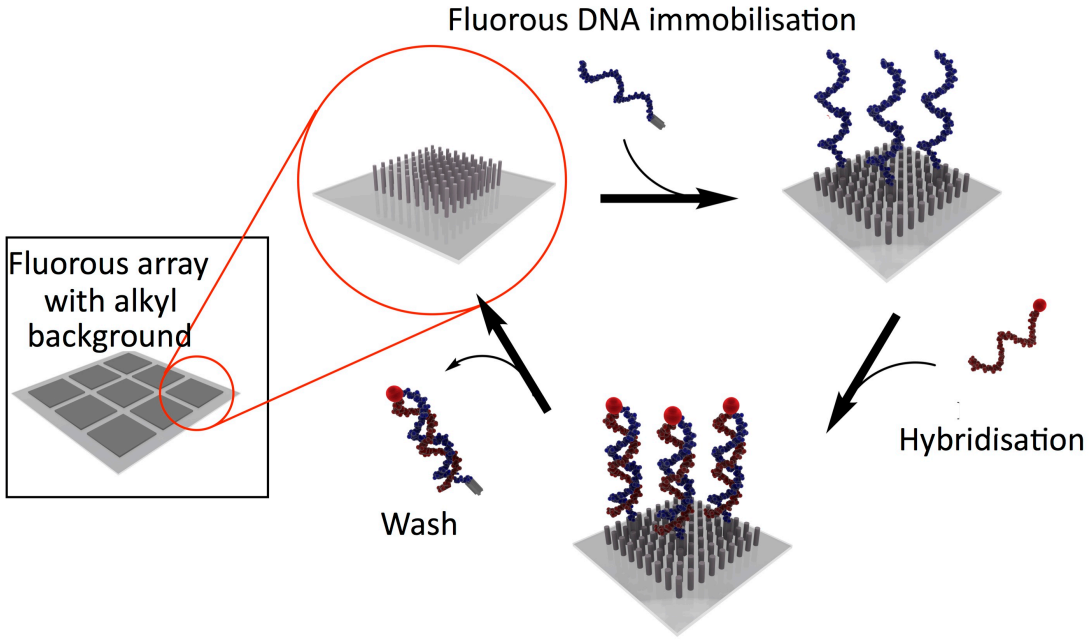

Figure 3-9 Schematic of Fluorous Tagged ssDNA Immobilisation & Hybridisation to Fluorescently tagged complementary sequence.

In order to assess the removal of ODN1 from the surface, label free QCM measurements were necessary (Figure 3.10). As such, FDTS-modified QCM chips were incubated overnight with ODN1. These were then inserted into the QCM chamber and washed with PBS buffer to remove any non-specifically bound ODN1. Once equilibrium was reached the buffer was changed to 50 % MeOH in PBS. This resulted in a large and sudden decrease in the frequency, which was attributed to a change in the density of the buffer.(111) Finally, the buffer was switched back to PBS to allow for a comparison between the starting and final frequency values which was found to increase to ~100 Hz. This increase in the frequency was

attributed to a reduction in the mass on the surface. In comparison, modified QCM chips with no immobilised ODN1 were subjected to the same cycle of events and showed a decrease in the frequency, which was attributed to ion adsorption onto the surface (Figure 3.10 (b)). The Δf vs. ΔD was plotted for the removal events of ODN1 from the FDTS-modified QCM chip (Figure 3.11). This showed a linear decrease in the dissipation with an increase in the frequency. This was attributed to fast dissociation kinetics with no change in the conformation on the surface. The two-phase response from the control was attributed to a change in the density of the buffer and then a steady linear increase in mass with no change in the dissipation due to the adsorption of ions from the buffer (Figure 3.11 (b)).

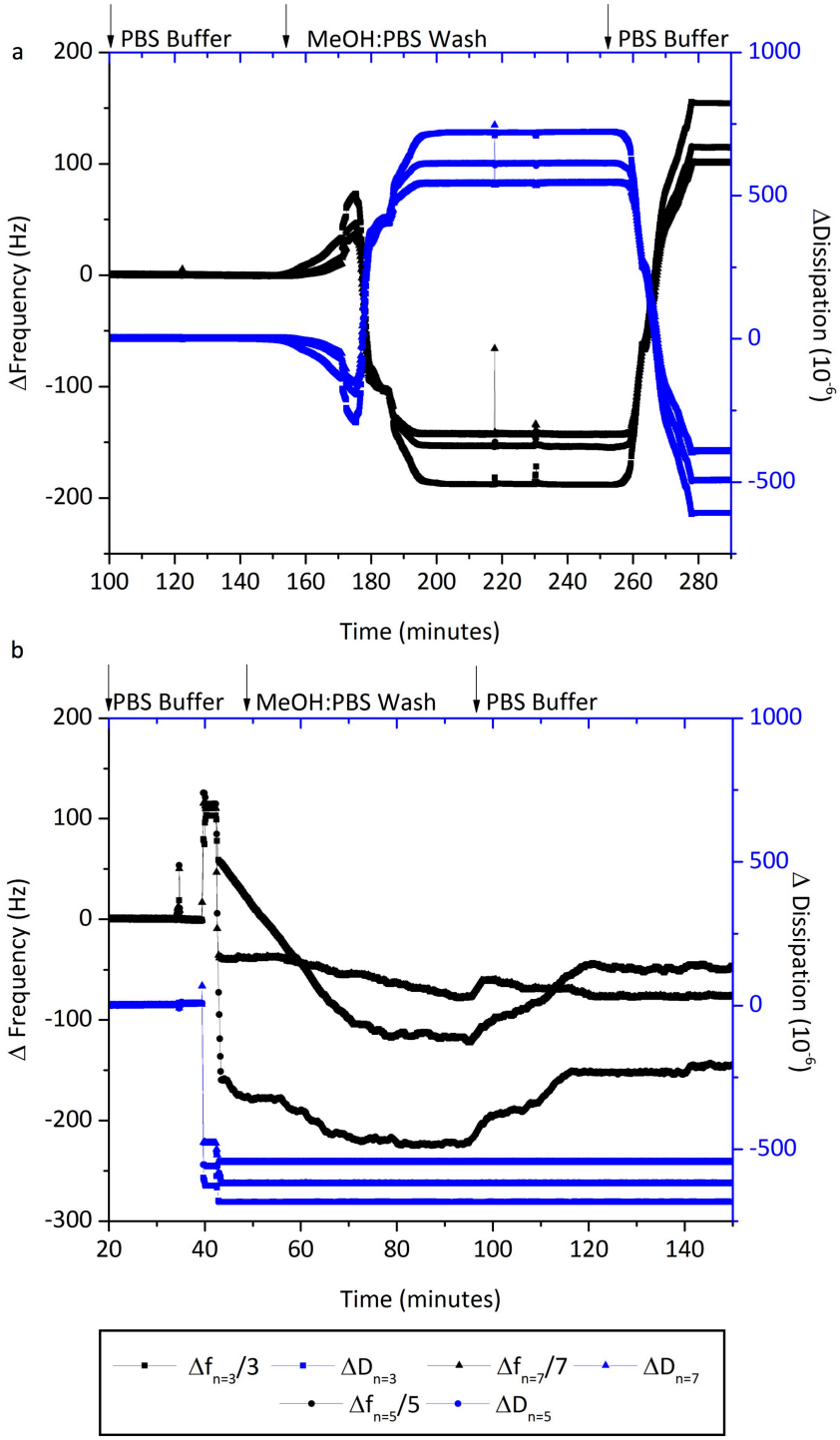

Figure 3-10 QCM Measurements Obtained During the Removal of ODN1 from Fluorous QCM chips using a 50 % MeOH (PBS) wash. (a) Frequency and dissipation data obtained during the stabilisation of the QCM, washing with solvent buffer and then final stabilisation in PBS buffer showing the removal of ODN1 indicated by an increase in the frequency. (b) Frequency and dissipation data for negative control whereby fluorous chips, with no anchored ODN1, were put into the QCM chamber. Key: $\Delta f_n = {}^{3}/_{3}$ is the change

in the frequency arising from the 3rd overtone normalised to the fundamental by dividing it by its overtone number; $\Delta f_n = {}^{5}/_{5}$ is the change in the frequency arising from the 5th overtone normalised to the fundamental by dividing it by its overtone number; $\Delta f_n = {}^{7}/_{7}$ is the change in the frequency arising from the 7th overtone normalised to the fundamental by dividing it by its overtone number; $\Delta D_n = 3$ is the change in the dissipation data arising from the 3rd overtone; $\Delta D_n = 5$ is the change in the dissipation data arising from the 5th overtone; and $\Delta D_n = 7$ is the change in the dissipation data arising from the 7th overtone.

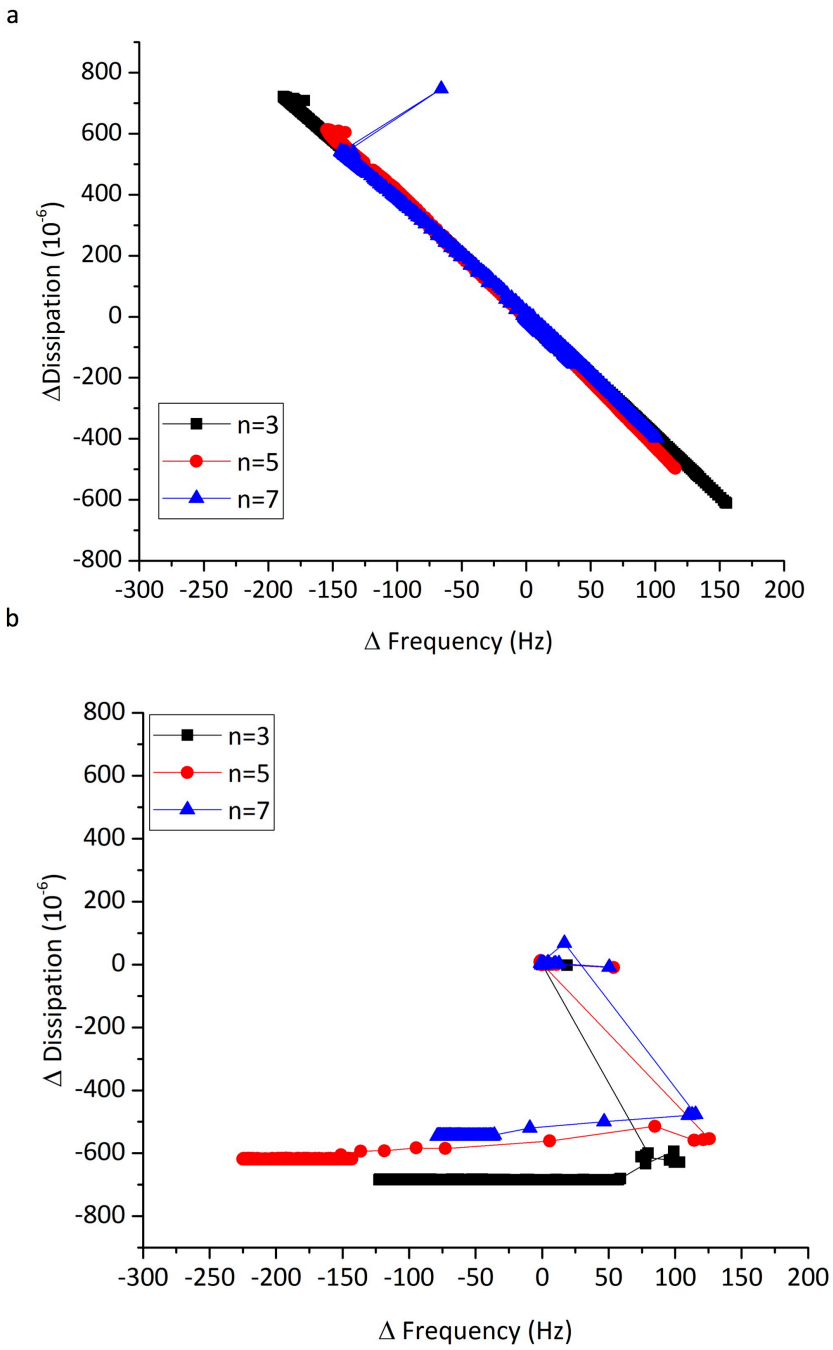

Figure 3-11 Plots of the Change in Dissipation as a function of the change in Frequency for Removal of ODN1 from Fluorous QCM chips using a 50 % MeOH (PBS) wash. (a) Change in Dissipation with the change in frequency measured during the removal of ODN1 from fluorous surfaces. As the frequency increased, corresponding to a mass decrease, the dissipation decreased indicating that the surface was becoming more rigid. (b) Change in Dissipation with the change in frequency measured for negative control. Key: n= 3 is the frequency and dissipation data obtained from the 3rd overtone; n=

5 is the frequency and dissipation data obtained from the 5th overtone; n= 7 is the frequency and dissipation data obtained from the 7th overtone.

To further investigate the re-usability potential of these surfaces, fluorescence microscopy was carried out as a complementary technique to QCM (Figure 3.12).

Immobilisation techniques for DNA microarray development must adhere to several stringent requirements, including reproducibility.(78) As such, after each washing and immobilisation step, fluorescence images were obtained and the fluorescence intensity values were compared (Figure 3.12 (a) and (b)). This showed low background fluorescence after each washing step with an average remaining fluorescence intensity of 1.3 % (± 0.8 %) of the initial fluorescence intensity before the washing step. This suggested that the majority of the cODN1 was removed. Furthermore, comparable fluorescence intensities were recorded after five subsequent hybridisation events with a coefficient of variation of 4.5 % over all the washing steps. This indicated similar immobilisation/hybridisation densities on the surfaces. As such, it was proposed that the surface was completely regenerated allowing for similar anchoring densities on the surfaces. Controls were performed to rule out photobleaching as a major contributing factor for the detected decrease in fluorescence intensity (Figure 3.13 (a)) and it was found that 22.2 % of the reduction in fluorescence intensity was attributed to this. Furthermore, in order to determine if the reduction in intensity was due to the denaturation of the strand, as opposed to removal of the duplex, the complementary sequence was incubated onto a freshly washed substrate (Figure 3.13 (b)). This again showed that the decrease in fluorescence intensity was due to the removal of the ODN1/cODN1 duplex from the surface as no binding events were observed. Therefore, it was concluded that the duplex was being removed via the fluorous-phase tail from the surface.

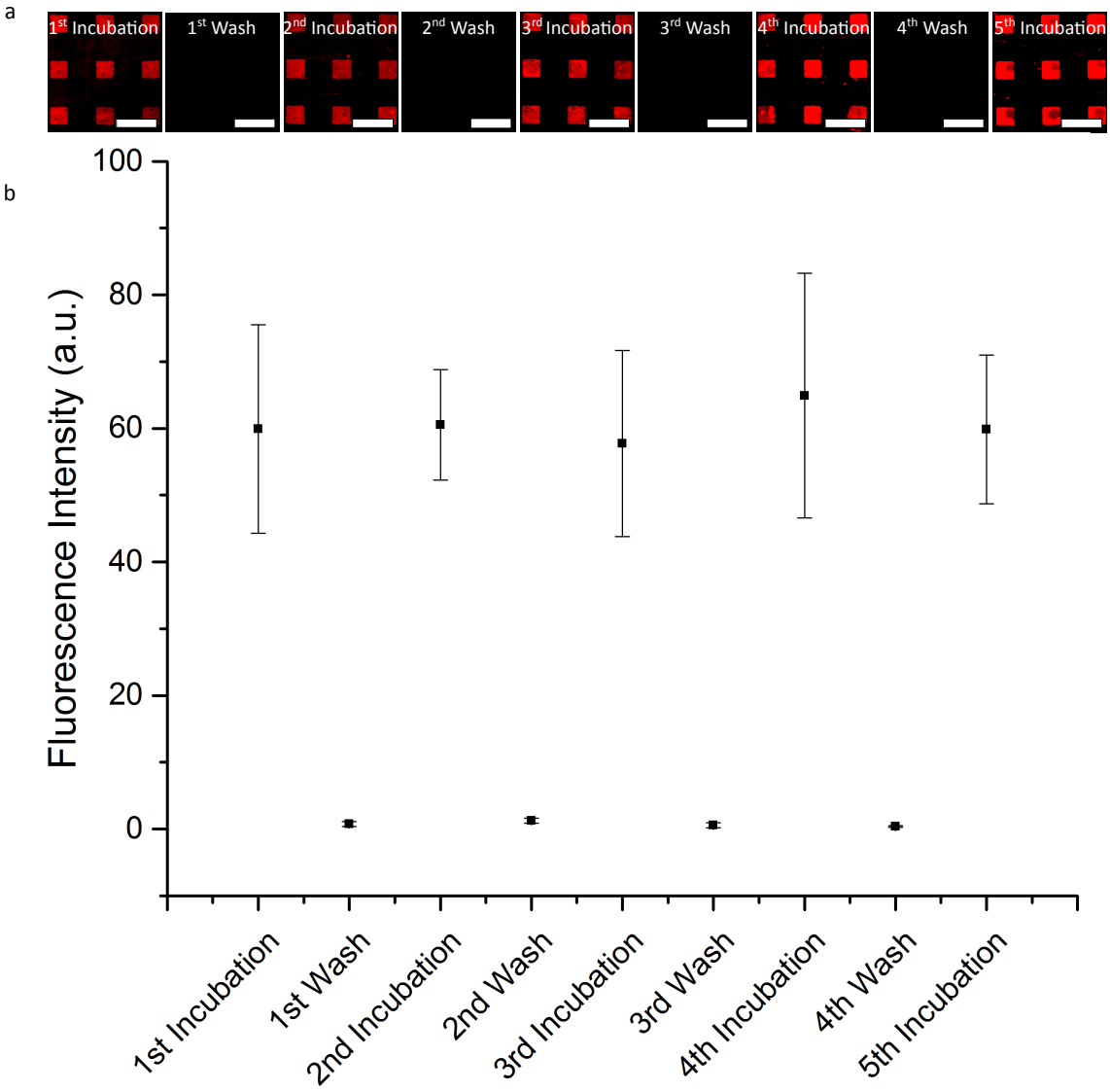

Figure 3-12 Reversible DNA Attachment using the Fluorous Effect. (a) Fluorescence images obtained during the immobilisation/removal cycles. (b) Graph shows the corresponding fluorescence intensity measurements taken after each immobilisation /removal cycle. Scale bar = 100 µm.

a

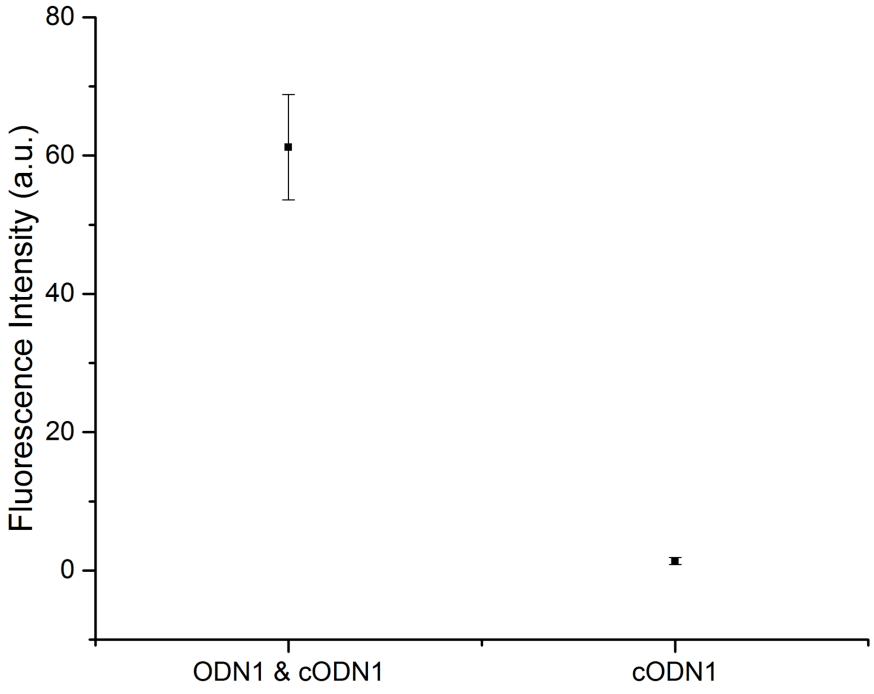

b

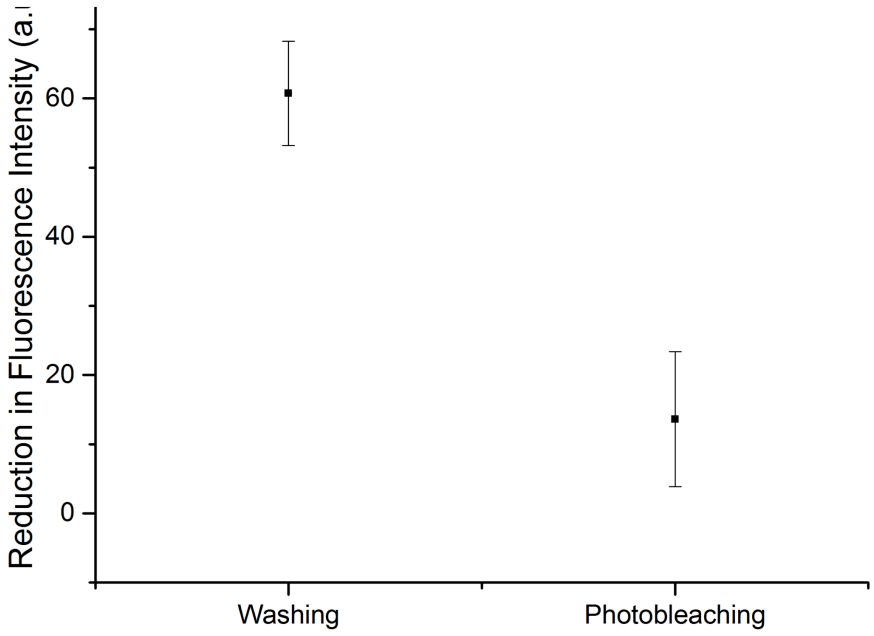

Figure 3-13 Control Experiments for Reversible DNA Attachment using the Fluorous Effect. (a) Graph shows the increase in fluorescence intensity following the immobilisation of ODN1 (and hybridisation to cODN1) compared to the incubation of cODN1 on a freshly washed fluorous surface (after BSA block). This was carried out to determine if the duplex was

completely removed after each washing step as opposed to denaturation of the strand on the surface. (b) Graph shows the reduction in fluorescence intensity due to photobleaching compared to solvent wash.

3.2.5 Fabrication of Re-writable Surface

As stated, in order to reuse microarray platforms, a denaturing protocol is used allowing the substrate to be salvaged multiple times.(13) However, it only allows for the same set of genetic information to be detected. Therefore, to better this method would be to use the same sensing platform for sequential detection of different sets of genetic information. These surfaces would be both reusable and rewritable.

Therefore, in order to test if the fluorous effect could be used to fabricate said platforms, a 32-mer fluorous-tagged DNA (ODN3) was synthesised along with more intricate patterns, using electron-beam lithography, with feature sizes as small as 500 nm (Figure 3.14 (a)).

The same protocol was used for these substrates as described before. Briefly, ODN1 was immobilised onto the patterns, hybridised to its complementary sequence and imaged using fluorescence microscopy (Figure 3.14 (b)). The surface was then washed, imaged, and ODN3 was immobilised and hybridised to its complementary sequence (cODN3, Alexa-Fluor 488) (Figure 3.14 (c-d)). This was followed by a final washing step (Figure 3.14 (e)). Here we see the potential of these surfaces for the fabrication of re-writable DNA surfaces, different to re-usable surface, in which the same surface can be used to detect different targets. Furthermore, in the case of ODN3, the fluorous tag comprised less than 2 % of the total mass but was sufficient to immobilise the water-soluble strand and remain bound to the surface during aqueous washing steps.

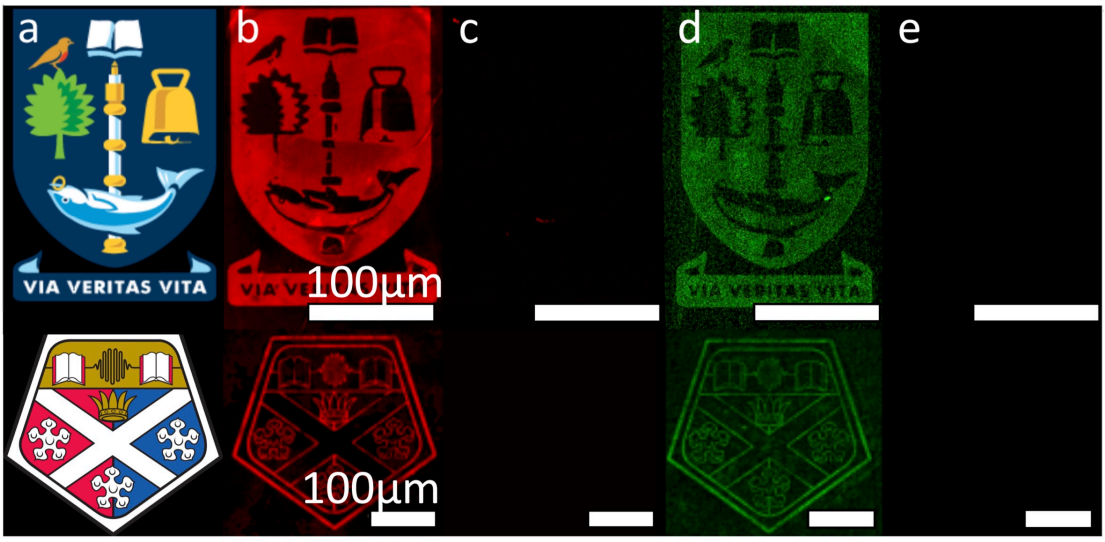

Figure 3-14 Re-writable DNA Attachment using the Fluorous Effect. (a) Ebeam template used to fabricate the University of Glasgow & University of Strathclyde crests. (b) Fluorescence image obtained following the immobilisation and hybridisation of ODN1 to cODN1. (c) Fluorescence image obtained following solvent wash. (d) Fluorescence image obtained following immobilisation and hybridisation of ODN3 to cODN3. (e) Fluorescence image obtained following final solvent wash.

Atomic force microscopy (AFM) was also used, in conjunction with fluorescence microscopy, to obtain height profiles before and after the washing step (Figure 3.15 (a & b)). This showed a reduction in the height following the removal of ODN3/cODN3. This further supports the conclusion that the duplex was removed via the fluorous-tag from the surface.

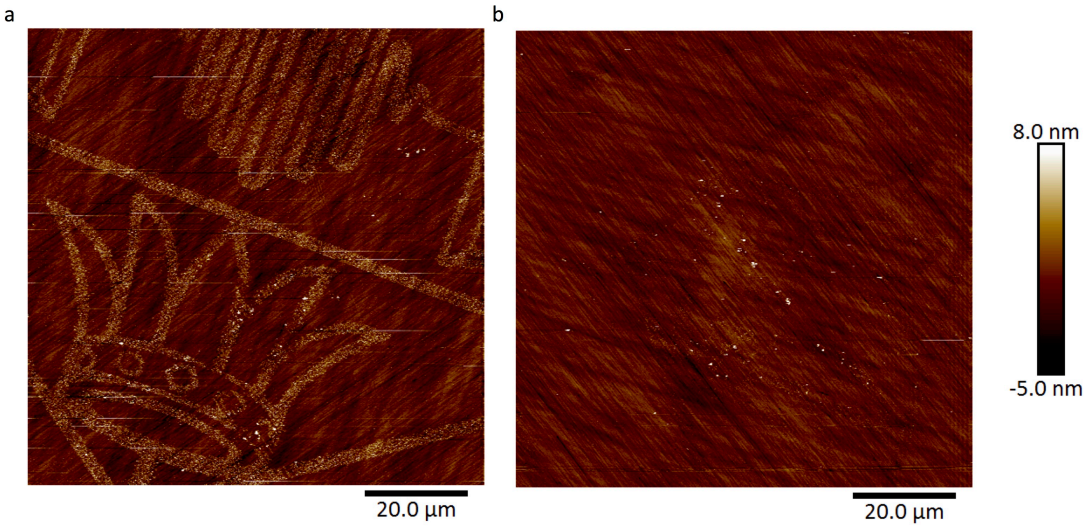

Figure 3-15 AFM images of Re-writable DNA Attachment using the Fluorous Effect. (a) AMF image of crown present in University of Strathclyde crest after immobilisation and hybridisation of ODN3 to cODN3. (b) AMF image of crown present in University of Strathclyde crest after solvent wash showing a reduction in the height profile consistent with that of the duplex being removed from the surface.

3.2.6 Restriction Enzyme Digest of Fluorous Tagged ODNs

A growing avenue of research is in the fabrication of surfaces that can be modified *in situ* through biological means. For example, restriction enzymes (RE) have been shown to cleave DNA attached to a surface.(112) This work was built upon by adsorbing a restriction enzyme onto an AFM tip allowing for area specific cleavage of the DNA attached to the surface.(113) Furthermore, the combination of a restriction enzyme and a DNA polymerase allowed for the fabrication of multi-layered surfaces.(114) Therefore, incorporating restriction enzyme sites within the fluorous-tagged ODNs, and immobilising said strands onto surfaces, could lead to the fabrication of surfaces that can be continually re-designed or updated in response to specific ques.

In order to test this hypothesis, ODN3 was incubated with several restriction enzymes. Briefly, the fluorous stand (ODN3) and an exact copy of the strand without a fluorous tag (RE_ODN3) were annealed to their complementary sequence (RE_cODN3), which was modified with a thiol group. These dsODNs were

then incubated overnight with BamHI, HindIII, EcoRI and PstI and the products were run on a 12 % polyacrylamide gel, Figure 3.16.

Both the dsODNs had recognition sites for BamHI, HindIII and EcoRI. Incubation with PstI was carried out as a control. Following the incubation of the fluorous and non-fluorous dsODNs with EcoRI and HINDIII, RE digestion was observed. Therefore, it was postulated that the fluorous-tag did not inhibit the ODNs digestion by REs. However, no cut was obserevd following the incubation with BamHI for either the fluorous or non-fluorous tagged dsODN. This was attributed to the recognition site for BAMHI being too close to the thiol group.

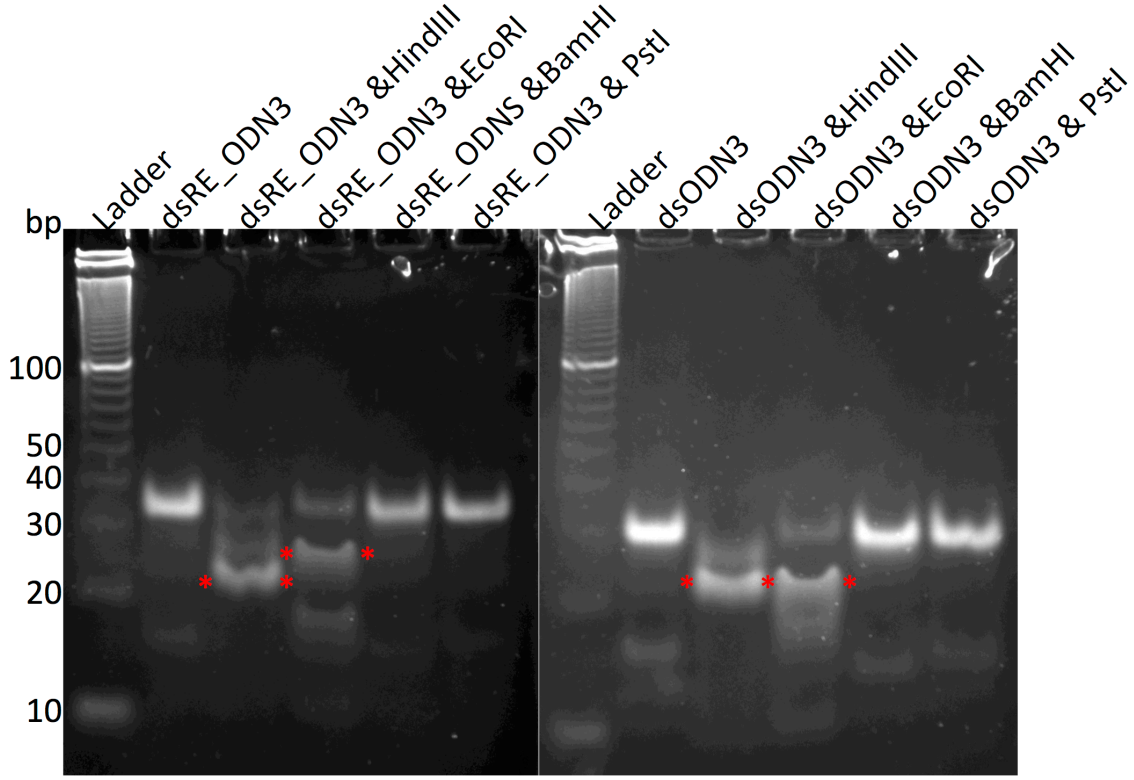

Figure 3-16 Polyacrylamide Gel Showing the Results from the Restriction Enzyme Digest of dsODN3 and dsRE_ODN3 (non-fluorous strand). ODNs were incubated with EcoRI, HindIII, BamHI. The red stars indicate the position of the RE digest products.

The dsODN3 was then conjugated to a 20 nm Au Nanoparticle, and restriction enzyme digest was then carried out using EcoRI and HindIII. Once again, PstI was used as the control, Figure 5.17. Again restriction enzyme digest was observed for the the conjugated and unconjugated dsODN3.

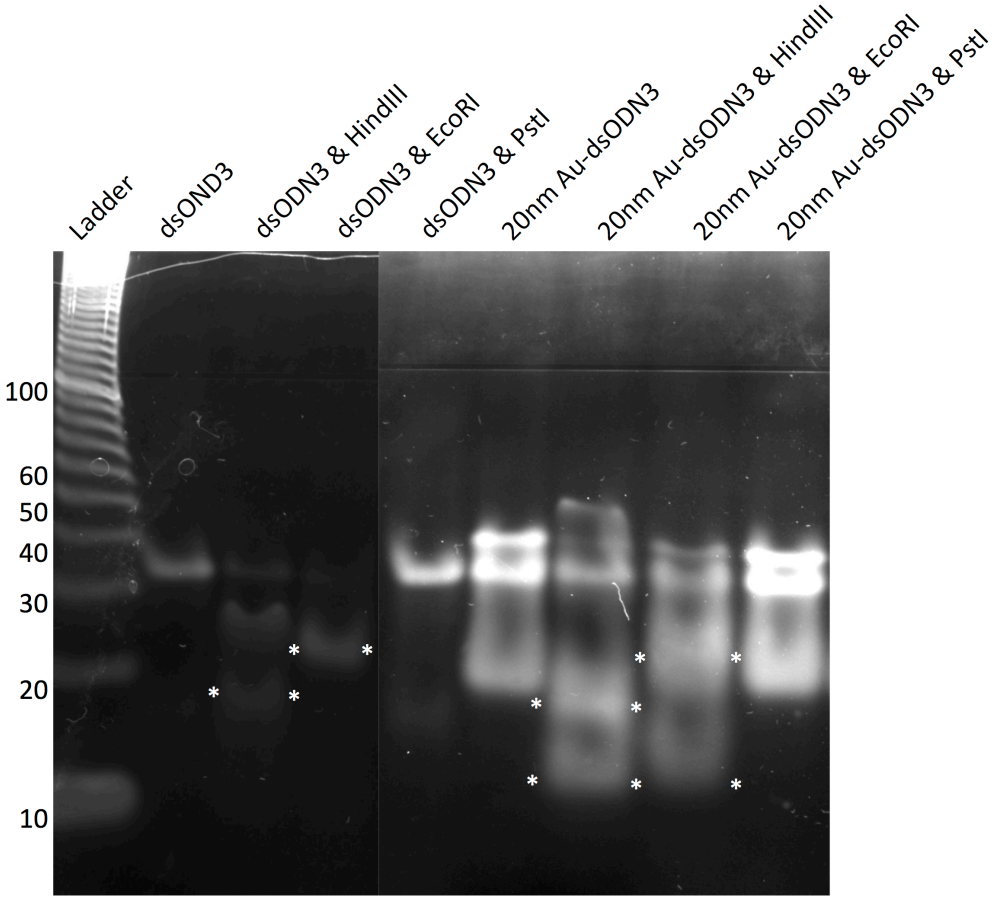

HindIIISite EcoRI Site

Uncut (32bp)
5'-C_8F_{17}-ATG GAT CCA TGA AGC TTA TGG AAT TCA TGA TG-3'
3'-TAC GTA GGT ACT TCG AAT ACC TTA AGT ACT AC-thiol-5'

After EcoRI Cut (25 bp)
5'-C_8F_{17}-ATG GAT CCA TGA AGC TTA TGG -3'
3'-TAC GTA GGT ACT TCG AAT ACC TTA A-5'

After EcoRI Cut (11 bp)
5'-AAT TCA TGA TG-3'
3'-GT ACT AC-thiol-5'

After HindIII Cut (16 bp)
5'-C_8F_{17}-ATG GAT CCA TGA -3'
3'-TAC GTA GGT ACT TCG A-5'

After HindIII Cut (20 bp)
5'-AGC TTA TGG AAT TCA TGA TG-3'
3'-AT ACC TTA AGT ACT AC-thiol-5'

Figure 3-17 12 % Polyacrylamide Gel Showing the Results from the Restriction Enzyme Digest of dsODN3 attached to a 20 nm Au nanoparticle. ODNs were incubated with EcorRI, HindIII & PstI. The restiction enzyme products can be seen below the gel and are indicated on the gel by white stars.

As it was determined that the dsODN3 conjugated to a nanoparticle could undergo RE digest, the strands were immobilised onto nanopatterned arrays, Figure 3.18. Initially, the dsRE_ODN3 was incubated onto a fluorous nanoarray, Figure 3.18 (a) as a binding control. No immobilisation was observed in any of the 3 repeats. Therefore, the dsODN3 was incubated onto the nanoarrays, and binding was observed, Figure 3.18 (b-d). It was therefore concluded the dsODN3 conjugated to a 20 nm Au Nanoparticle was immobilised via the fluorous effect.

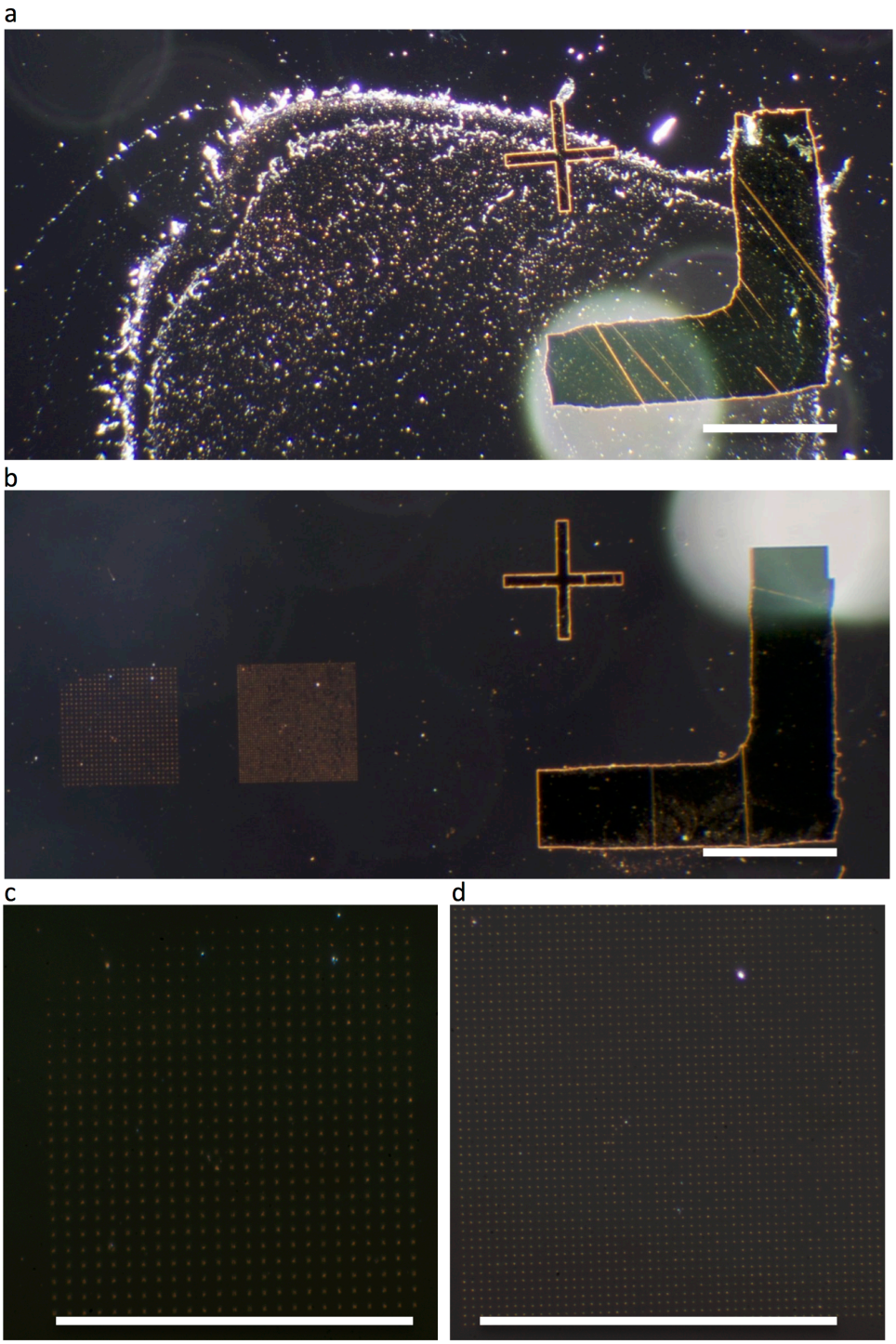

Figure 3-18 Immobilisation of ODN3, Conjugated to a 20 nm Au Nanoparticle, via the Fluorous Effect. Dark field microscopy was used to image (a) nanopattered fluorous surface following the incubation of dsRE_ODN3 conjugated to a 20 nm AuNP (10 X objective); (b) nanopattered fluorous surface following the incubation of dsODN3 conjugated to a 20 nm AuNP (10 X objective) (c) Close up of left hand side array of fluorous nanopattered squares seen in "b" following the incubation of dsODN3 conjugated to a 20

nm AuNP (60 X objective); and (d) Close up of right hand side array of fluorous nanopattered squares seen in "b" following the incubation of dsODN3 conjugated to a 20 nm AuNP (60 X objective). Scale bars = 100 µm.

Finally, the surfaces were incubated with the RE, Figure 3.19. Unfortunately, no RE digestion was observed on the surfaces following the incubation with either EcoRI, or HindIII. This was attributed to the hydrophobic nature of the fluorinated surface. (115)

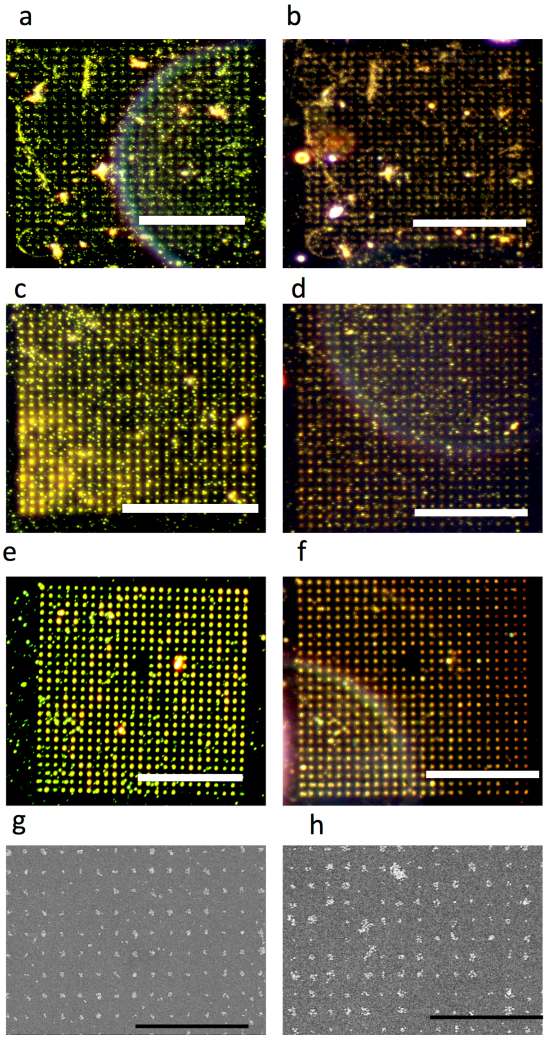

Figure 3-19 Incubation of Restriction Enzymes on Surface Bound dsODN3 Conjugated to a 20 nm Au Nanoparticle. (a) DF image of surface before incubation with PstI; (b) DF image of surface after incubation with PstI; (c) DF image of surface before incubation with HindIII; (d) DF image of surface after incubation with HindIII; (e) DF image of surface before incubation with EcoRI; (f) DF image of surface after incubation with EcoRI; (g) SEM image of surface before incubation with EcoRI; and (h) SEM image of surface after

incubation with EcoRI. Scale bars for the DF images are 50 µm and 3 µm for the SEM images.

3.3 Conclusions & Future Work

Presented in this chapter is the demonstration that the fluorous effect can be used for the immobilisation of fluorous-tagged DNA onto fluorinated-solid supports. This method of attachment fulfils several important criteria for DNA microarray immobilisation strategies. These criteria include low non-specific binding and the retention of the self-recognition properties of the bound DNA strand.(78) Further to this, it was shown that the substrate could be re-used up to five times with comparable immobilisation/hybridisation densities and could be used to sequentially detect different sets of genetic information. Therefore, this immobilisation chemistry could, in the future, be exploited across many research fields. This is of particular importance in DNA microarray development, where progress is already being made in fabricating re-useable sensing platforms.(116)

However, our understanding of the strength and utility of the fluorous effect is still in its infancy.(117) Future work in this line of research should include determining the detection limits of this immobilisation technique and determination of the strength of the fluorous interaction by means of AFM. (118) Additionally, probing the limitations of the fluorous content for tag-mediated DNA microarray formation should be carried out in order to reduce the build up of perfluorinated compounds in the environment. (119) Extending this idea would be to use branched fluorous tags and to determine if, and at what fluorous content, the fluorous-fluorous interaction could have dissociation constants comparable to that of covalent bonds. This data would enhance our understanding of the fluorous effect, which is pivotal for the development of this technique as an immobilisation strategy.

It was also shown in this chapter that tagging ODNs with a fluorous ponytail did not affect the activity of restriction enzymes. However, following the immobilisation of the ODNs onto fluorinated solid supports, no RE digest was observed. This was attributed to the hydrophobic nature of the fluorous solid support. In order to further develop this, longer ODN strands could be investigated which would increase the distance between the fluorinated solid support and the restriction enzyme recognition point.

Another avenue of research would be the use of the fluorous-effect as a means to direct the immobilisation of DNA origami onto surfaces. As hypothesised in this section, fluorous-tagged DNA was immobilised on SiO_2 with the fluorous-tag orientated away from the surface. Therefore, the incorporation of these tags into DNA nanostructures could aid in the development of this research field in regard to building up from surfaces by directing the face on which the DNA nanostructures are deposited onto mica/SiO_2. In conjunction with this would be to use the fluorous effect as a means to reversibly attach DNA origami onto fluorous surfaces.

4 CHANGING THE FLUORINE CONTENT OF FLUOROUS-PHASE TAGS

4.1 Introduction

The environmental persistence of perfluorinated compounds (PFCs), and their potential adverse physiological effects, is becoming a major concern.(120, 121) Consequently, there is intense interest in the development of fluorous "ponytails" that are functionalised and/or based upon smaller perfluorinated units to order to promote biodegradability. This is because six carbon, and shorter, perfluoroalkyls are known to be less persistent and bioaccumulative than longer perfluoroalkyl chains.(40, 122) This concern has now reached those involved in using the fluorous effect as a means to immobilise biomolecules onto fluorinated-solid supports.(119)

4.1.1 Fluorous-Phase Tails

Typically the mono-C_8F_{17} fluorous-phase tag has been employed in the immobilisation of biomolecules onto fluorinated-solid supports for microarray development.(36, 82, 84, 117) However, growing concerns as to their safety has seen other tags being investigated. For example, comparison has been made

between the use of mono-C_8F_{17}- and mono-C_6F_{13}-fluorous-phase tags for the immobilisation of biotin onto fluorinated-solid supports. In this study, it was found that the mono-C_8F_{17}-fluorous-phase tagged biotin showed better results in terms of spot intensity, size and morphology for use in biotin-avidin microarrays.(37) As mono-C_6F_{13}-fluorous-phase tags, and most likely shorter fluorous-phase tags, were not viable for the production of microarrays, Pohl et al. set out to discover a tag that could form strong non-covalent fluorous-fluorous interactions for microarray development without reliance on the C_8F_{17}-motif.(119) In this work, branched fluorous-tags, based on the C_6F_{13} motif, were investigated for use in microarray development as opposed to the traditional single, mono-tagged carbohydrates. Direct comparison was made between bis-C_6F_{13}- and mono-C_6F_{13}- fluorous-phase tagged sugars. This showed that the mono-C_6F_{13}-tagged sugars could not withstand the necessary washing procedures for microarray development. Conversely, the bis-C_6F_{13}-tagged sugars could withstand multiple washing steps with little change in the fluorescence intensity. Comparison between the bis-C_6F_{13}- and mono-C_8F_{17}-fluorous-phase tag was also made. This indicated that the fluorous-fluorous interactions between the bis-C_6F_{13}-tag and the fluorinated-solid support were stronger than those between the surface and the mono-C_8F_{17}-tag. Consequently, it was shown that the bis-C_6F_{13}-tag had superior binding ability compared to both the mono-C_8F_{17}- and mono-C_6F_{13}-tags. Although not mentioned in the work, this could be due to the bis-C_6F_{13}-tag having a higher fluorous partioning coefficient: meaning that it is better retained on a fluorous-solid phase compared to the mono-C_8F_{17}-tag. Furthermore, different linkers were used between the bis-C_6F_{13}-tag and the carbohydrate and the mono-C_6F_{13}-/mono-C_8F_{17}-tag and the carbohydrate. As such, the effect of the different linkers used was not explored and could therefore account for the observed differences in binding capability and strength.

4.1.2 Fluorous Solid Phase Extraction

Partion coefficients quantify the equilibrium distribution of a solute between two immiscible phases. In terms of fluorous partion coefficients, they constitute a direct measure of the fluorophilicity: this term is used interchangeably with fluorous phase affinity.(40)

Standard fluorous solid phase extraction (FSPE) is based on the partioning between a fluorous solid phase and a fluorophobic liquid phase. Following the addition of the reaction mixture, usually a combination of fluorous and non-fluorous components, the fluorous column is washed with a fluorophobic solvent (40-80 % MeOH-H_2O, 40-60 % MeCH-H_2O, 80-90 % DMF-H_2O, or 100 % DMSO). This elutes the non-fluorous fractions. To elute the fluorous fraction, a fluorophilic solvent (such as water free MeOH, MeCN, THF) is required. (79, 123)

Like FPSE, fluorous high performance liquid chromatography (F-HPLC) utilises a fluorous-solid phase. However, this method can be used to separate fluorous molecules based on their fluorous content: with molecules containing a higher fluorine content exhibiting longer retention times on F-HPLC columns.(49, 124, 125)

4.1.3 Context & Aim of Result Chapter

As such, our understanding of the strength and utility of the fluorous effect is still in its infancy.(117) An area of research that has not yet been fully explored is determining how the fluorous content of a fluorous-phase tail effects the immobilisation and removal of bound biomolecules. Therefore, the work carried out in this section hopes to address this issue with the following aims:

1. Determine the effect of increasing the fluorine content of mono-fluorous-phase tails on the immobilisation and hybridisation densities of ODNs on fluorinated-solid supports.
2. Determine the effect of using branched fluorous-phase tails on the immobilisation and hybridisation densities of ODNs on fluorinated-solid supports.
3. Determine the effect of increasing the fluorine content on the washing conditions required to remove the ODN duplex from the surface.
4. Determine the effect of the linker, present between the fluorous-phase tail and the ODN, on the binding capabilities.

4.2 Results & Discussion

4.2.1 Characterisation of Fluorous-Phase Tags Attached to ODNs

Dr Andrea T. Sender and Dr Jamie M. Withers, University of Strathclyde, carried out the synthesis and purification of the fluorous-tagged ODNs, Table 4.1.

Table 4.1 Name, Linker and Fluorous Tag used in work.

Name	Fluorous Tag	Linker
ODN1	Mono-C_8F_{17}	HEG
ODN2	No Tag	None
ODN4	Mono-C_8H_{17}	HEG
ODN5	Mono-C_4F_9	HEG
ODN6	Mono-C_6F_{13}	HEG
ODN7	Mono-C_8F_{17}	None
ODN8	Bis-C_8F_{17}	None
ODN9	Tetra-C_8F_{17}	None

As can be seen in Figure 4.1, three mono-fluorous-phase tags were synthesised and attached to the 5'-end of a 16-mer ODN via a hexaethyleneglycol (HEG) hydrophilic block. This was carried out using standard solid-phase methods where the ODN was synthesised from the 3'- to the 5'- end.(126) Additionally, the same 16-mer ODN was tagged with a C_8H_{17}-alkyl-tag as a control for the C_8F_{17} tag. It is noteworthy that the incorporation of highly hydrophobic motifs into ODNs is often tricky.(127) However, to date there have been several studies related to the tagging of ODNs with mono-perfluorinated phase tags using solid phase synthesis.(128-130)

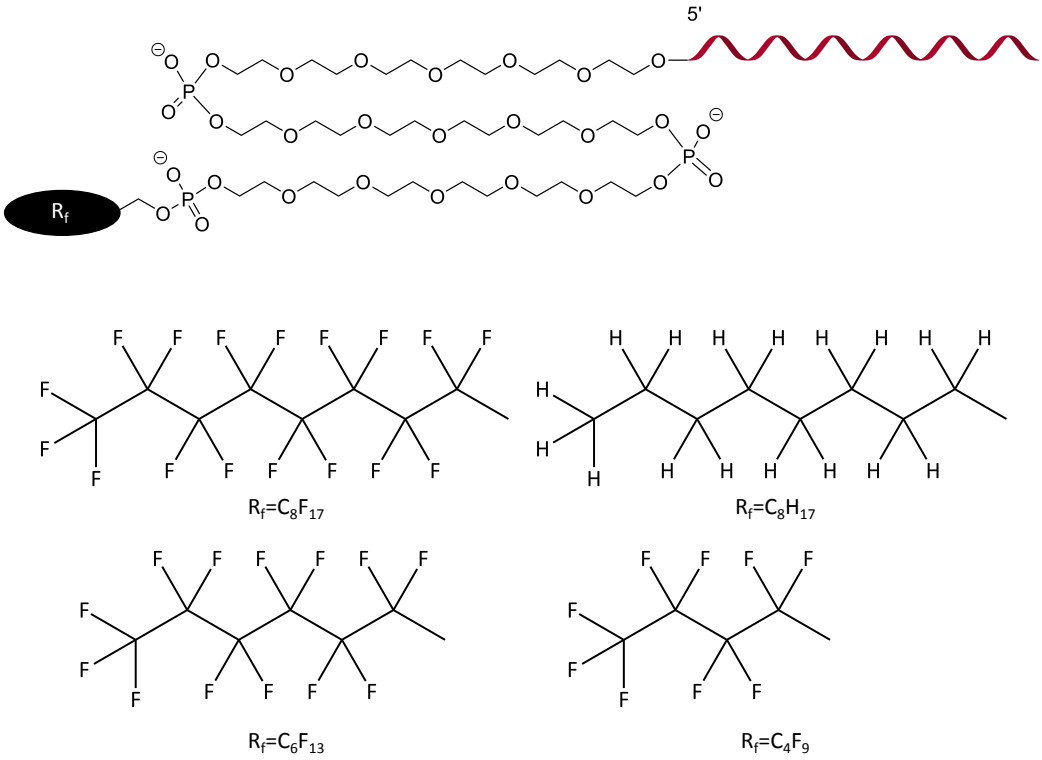

Figure 4-1 Schematic of the Four Different Tags Attached to the 5'-end of a 16-mer ODN.

The tagging of ODNs with branched fluorous tags is less prevalent in the literature. (106) Again, automated phosphoramidite chemistry was used to synthesise the ODNs from the 3'- to the 5'- end. However, the ODNs differentiate from the mono-tagged ODNs in the absence of a HEG spacer group between the fluorous tag and the ODN, Figure 4.2. This was carried out to reduce the cost of the synthesis procedure.

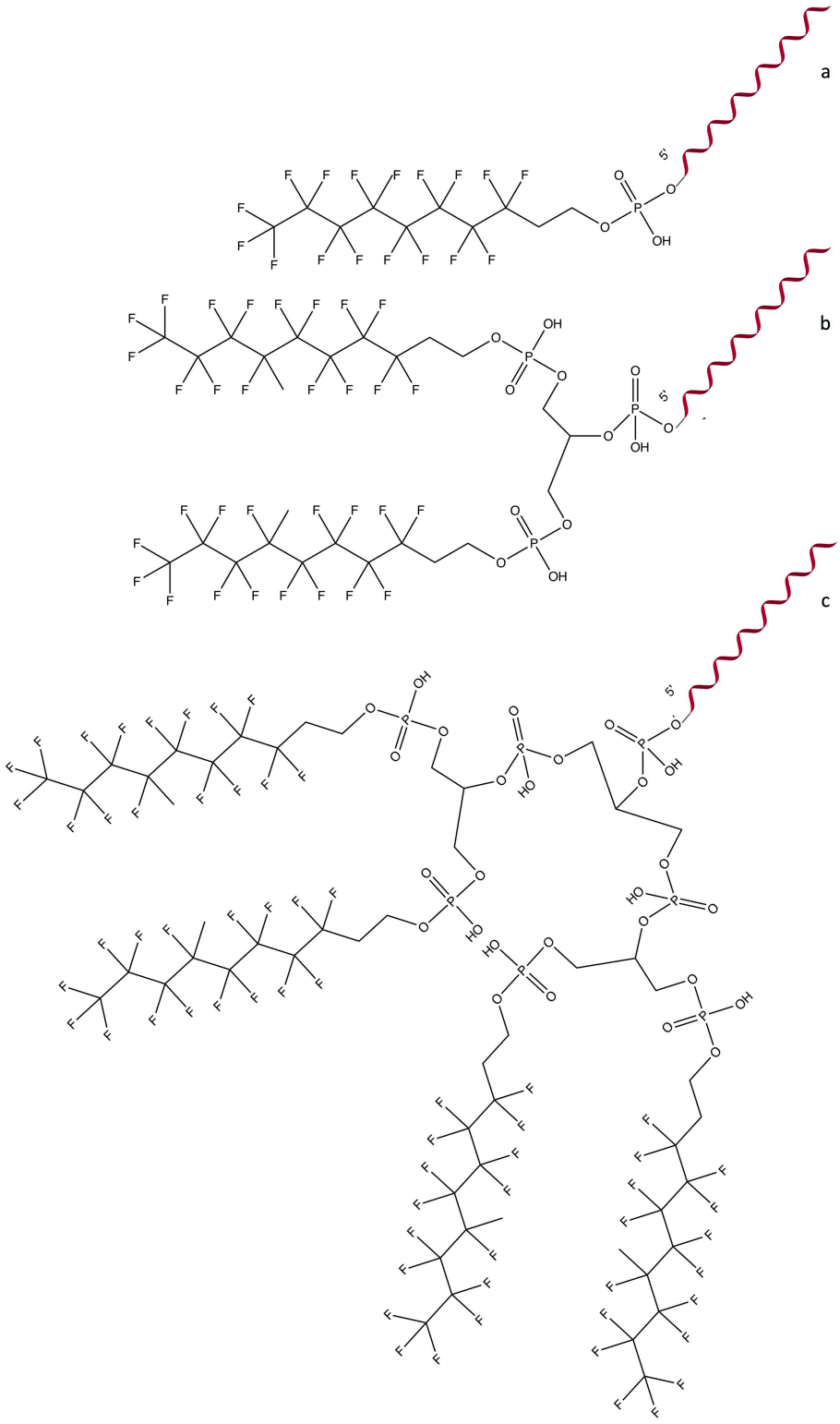

Figure 4-2 Schematic of the Different Branch Fluorous-Phase Tags Attached to the 5'-end of a 16-mer ODN. (a) ODN7; (b) ODN8; and (c) ODN9.

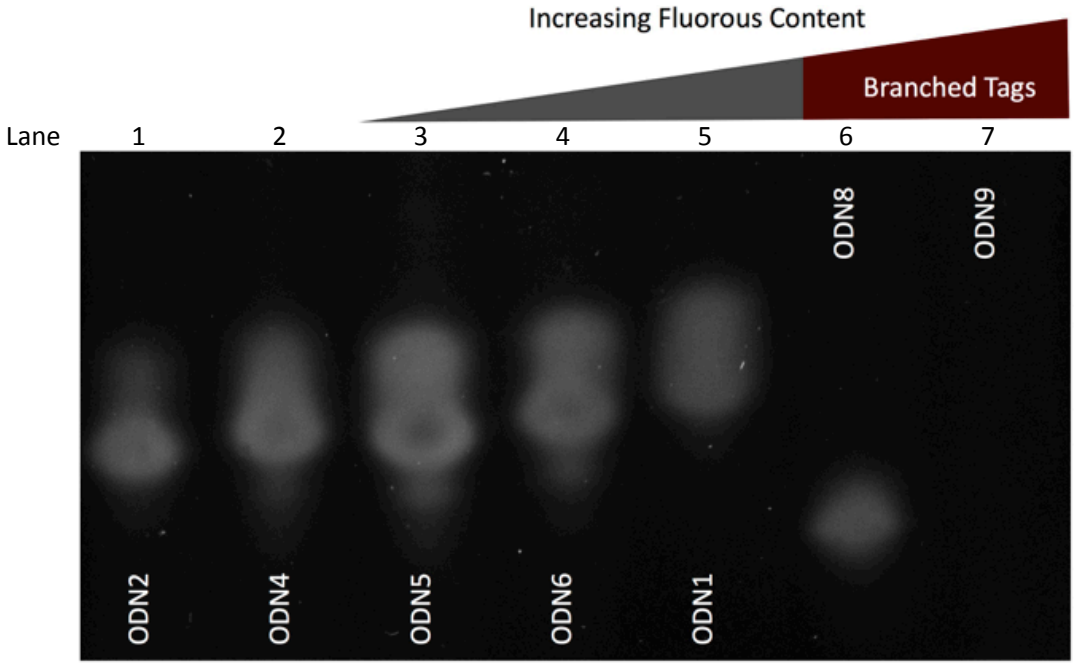

Figure 4-3 15 % Denaturing PAGE Analysis of Fluorous-Tagged ODNs. Lane 1: 16-mer ODN with no tag (ODN2); Lane 2: 16-mer ODN with a mono-C_8H_{17} tag (ODN4); Lane 3: 16-mer ODN with a mono-C_4F_9-tag (ODN5); Lane 4: 16-mer ODN with a mono-C_6F_{13}-tag (ODN6); Lane 5: 16-mer ODN with a mono-C_8F_{17}-tag (ODN1); Lane 6: 16-mer ODN with a bis-C_8F_{17}-tags (ODN8); and Lane 7: 16-mer ODN containing a tetra-C_8F_{17}-tags (ODN9).

Denaturing gel electrophoresis was performed in order to determine the electrophoretic mobility of the ODNs with respect to their tag, Figure 4.3. In general it was found that increasing the fluorous content of the mono-fluorous-phase tail decreased the mobility of the ODN through the gel (Lanes 3-5). Denaturing gel electrophoresis allows separation based solely on the molecular weight: higher molecular weight ODNs present themselves at higher positions in the gel compared to lower molecular weight ODNs. As such, the retardation of the ODNs with higher fluorine content was expected due to the associated increase in molecular weight. Again, the effect of the molecular weight is evident from the decreased mobility of ODN1 (mono-C_8F_{17}-tag) compared to ODN 4 (mono-C_8H_{17}-tag) whereby the hydrogen atoms were replaced by fluorine atoms leading to a higher molecular weight. (131, 132) However, ODN8 was present much further down the gel compared to the single fluorous tagged ODNs. This was attributed to the mass difference between ODN8 and the mono-tagged ODNs (ODN5 and ODN6) due to the lack of a HEG linker group used in the synthesis of ODN8. Furthermore,

ODN9 did not pass into the gel. This was attributed to the formation of fluorous micelles, reported elsewhere, and as such they were too large to pass into the gel.(106)

4.2.2 Effect of Increasing the Fluorous Content on the Hybridisation Density using Mono-Tagged Probe Strands

Key to the success of microarray-based technologies is the hybridisation of the target strand to the probe strand. In theory, this recognition and binding event is dependent on the thermodynamic equilibrium between bound ODNs and the free ODNs.(133) However, this is not always the case for surface bound ODNs, as the thermodynamic equilibrium conditions may not be reached without excessive incubation times. Furthermore, hybridisation may be kinetically or sterically inaccessible for some probe sequences or for some probe densities.(134-136) For this reason, in order to determine the effect of increasing the fluorine content on the immobilisation and hybridisation densities of the ODNs, fluorous microarrays were fabricated and the immobilisation and hybridisation steps were carried out overnight to ensure the highest probe and hybridisation densities. Furthermore, it must be noted that the immobilisation densities could not be determined using fluorescence microscopy: the fluorous-tagged ODNs were not fluorescently labelled. Therefore, the fluorescence intensity refers to the cOND1 density on the surfaces as it was fluorescently tagged (TAMRA). However, as the utility of a DNA microarray is based on the hybridisation events, this method was sufficient to determine the effectiveness of the different mono-fluorous-tags to immobilise the probe strands and permit hybridisation events for the fabrication of fluorous DNA microarrays.

As previously described, a 16-mer ODN was tagged using 3 different fluorous "ponytails": ODN5 was tagged using a mono-C_4F_9 motif; ODN6 was tagged with a mono-C_6F_{13} motif; and ODN1 was tagged with a mono-C_8F_{17} motif. In order to determine the effect of the fluorine content on the hybridisation densities, the ODNs were immobilised onto separate fluorous arrays and incubated with the complementary sequence (cODN1). As the sequences were the same for all of the ODNs, the complementary ODN was also the same. This allowed for direct comparison to be made between the fluorous tags used; as changing the sequence of the ODN would have an effect on the thermodynamic conditions required for

hybridisation reactions. Two control ODNs (same 16-mer ODN used previously) were also immobilised onto fluorous microarrays. These included ODN2, which was not tagged, and ODN4, which was tagged with a mono-C_8H_{17} motif. This was carried out to determine the background fluorescence due to non-specific binding of the cODN1 onto the surface. As such, low levels of fluorescence were detected. This was used to determine the difference between specifically bound ODNs and non-specifically bound ODNs. Therefore, it was found that all of the fluorous-tagged ODNs (ODN1, ODN5 and ODN6) were specifically bound to the surface and permitted hybridisation reactions with the cODN1. Furthermore, once the duplex had formed, and was bound to the surface, the fluorous-fluorous interactions were strong enough to withstand the washing steps used. This is contrary to other reported work that suggest that perfluoroalkyl chains with 6 or fewer carbons are not sufficient to bind biomolecules to surfaces for microarray development.(37, 119) However, the success of these tags to capture ODNs from solution, and immobilise them onto fluorinated-solid supports, could be due to the conditions used. In this work, the ODNs were suspended in DI water; in other work the biomolecules have been suspended in methanol/DMSO/water.(119) As such, it is postulated that the fluorous-fluorous interactions could be more favourable between the ODNs and the surface in water due to the differences in the fluorophilicity of the solvents used.(40) Furthermore, it was found that increasing the fluorine content of the tag led to an increase in the hybridisation efficiency, with the strongest signal being obtained for the mono-C_8F_{17} tagged ODN. Owing to the same immobilisation and hybridisation conditions being used for the different tags, it was postulated that the difference in the average fluorescence intensity between the different tagged ODNs was due to the removal of bound ODNs during the washing steps. This was found for the immobilisation of fluorous-tagged carbohydrates on fluorinated solid supports and was attributed to the weaker fluorous-fluorous interactions of perfluoroalkyl chains with six or less carbons.(119) However, it could also be due to an increase in the fluorine content of the tag. This could result in the immobilisation of more probes thus permitting higher hybridisation densities. Furthermore, the sensitivity of a microarray is affected by the signal-to-noise ratio. Therefore, for ODN5 and ODN6, the calculated lower hybridisation density could be a result of higher non-specific binding onto the alkylated background.(137) Nevertheless, the highest average fluorescence

intensity was found for the mono-C_8F_{17}-tagged ODN. As such, this tag was determined to be the most effective tag for the immobilisation of ODNs. It was postulated that this was due to the ODN and the surface having identical perfluoroalkyl chains, as enhanced fluorous-fluorous interactions for molecules containing identical chains has been reported elsewhere.(138)

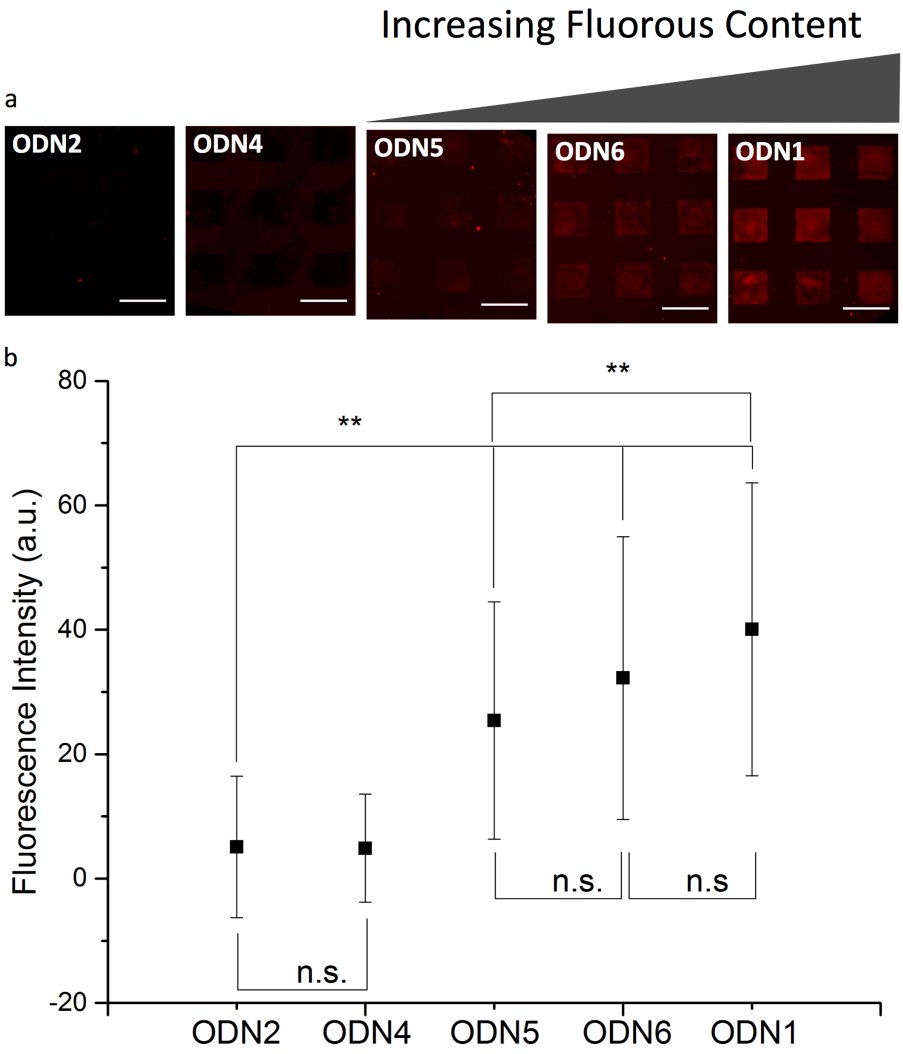

Figure 4-4 Effect of the Fluorous content on the Hybridisation Densities obtained using mono-tagged probe strands. (a) Fluorescence images obtained following the immobilisations/hybridisation of ODNs on fluorous microarrays, (b) Graph shows the corresponding fluorescence intensity measurements taken after each immobilisation/hybridisation event. n.s. p>0.1 * p< 0.05 **p<0.01. Scale bar = 50 µm.

4.2.3 Optimising the Washing Conditions to specifically remove the Mono-Tagged Duplex ODNs based on their Fluorous Tag.

As stated previously, F-HPLC can be used to separate fluorous molecules from other fluorous molecules based on their fluorine content.(138) This has resulted in extensive systematic investigations being conducted on the effect of the fluorine content of the fluorous tags on their retention times in F-HPLC columns.(124, 139) Consequently it was found that increasing the fluorine content of the tag resulted in longer retention times on fluorous columns.(140) Therefore, an investigation was carried out to determine if the same process could be mimicked on fluorous microarrays by tuning the methanol content of the washes. In theory, increasing the methanol content of the washes should increase their fluorophilic properties. This would allow for the sequential removal of ODNs from a microarray based on the wash and the fluorous-phase tag used.(141) Therefore, this work could be used to purify immobilised ODNs from other ODNs on fluorous-microarrays for further analysis or could be used for the fabrication of dynamic surfaces where the removal of specific ODNs can be pre-programmed.

Again, fluorous square arrays were fabricated using standard photolithography and the ODNs were immobilised overnight, rinsed with DI water and then the cODN1 was incubated on the substrates. The substrates were then washed overnight in hybridisation buffer and the fluorescence intensity was determined. This was carried out to determine the collective starting fluorescence intensity and allowed for the change in the fluorescence intensity to be detected upon placement in washing buffer. Following this, the substrates were split up and put into beakers containing different washing buffers (MeOH content ranged from 10-50 %) overnight. The results from these experiments can be seen in Figures 4.5 – 4.7. As stated previously, the background fluorescence intensity was determined from that of non-specifically bound cODN1 (Figure 4.4). This data was used to determine the methanol content of the wash required to remove the ODN duplex from the surface as the fluorescence intensity value that was not significantly different ($p>0.1$) to that of non-specifically bound cODN1.

The effect of the methanol content of the washing buffer on the removal of the ODN5/cODN1 duplex can be seen in Figure 4.5. It was found that complete removal was observed following a 10 % MeOH wash.

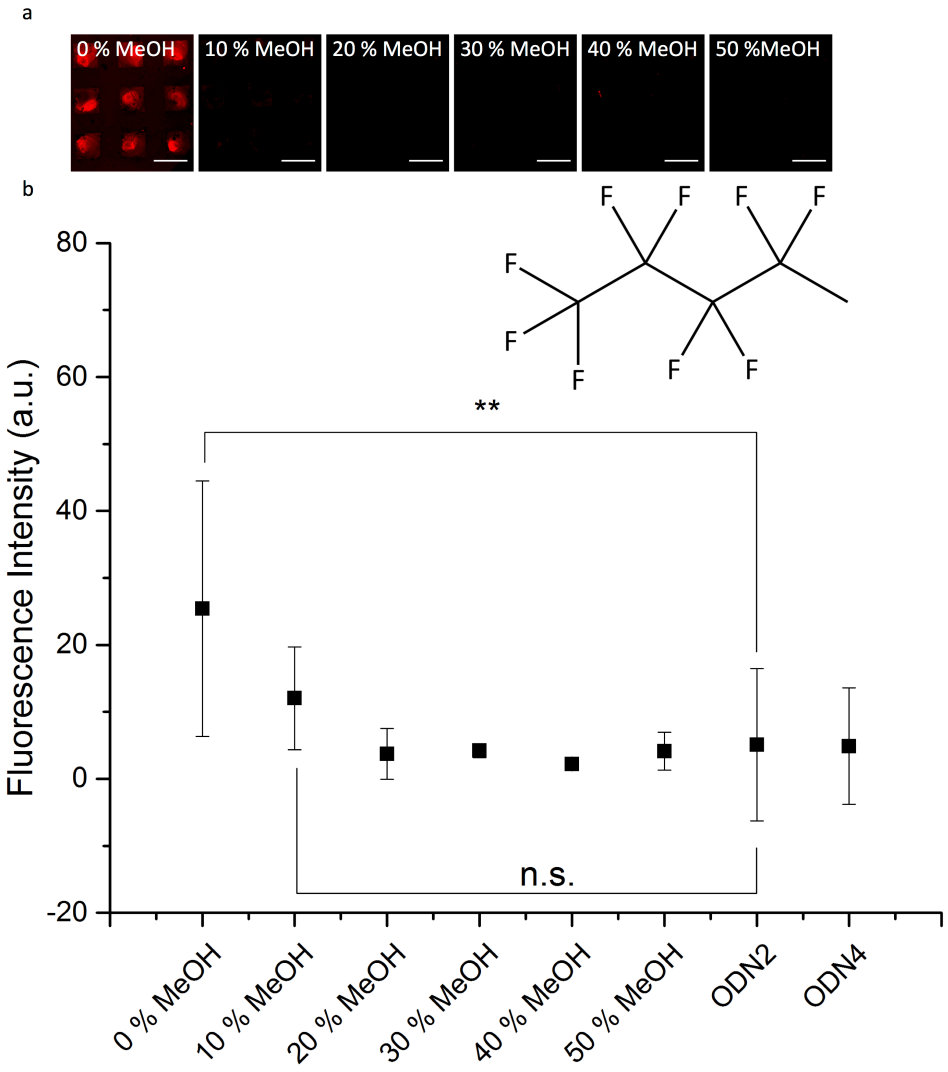

Figure 4-5 Effect of MeOH content of washing buffer on removal of ODN5/cODN1 duplex from Fluorous Microarrays. (a) Fluorescence images obtained of the fluorous microarrays following washes: the MeOH content of the washes increases going left to right. b) Graph shows the corresponding fluorescence intensity measurements taken after each washing step. n.s. p>0.1 * p< 0.05 **p<0.01. Scale bar = 50 µm.

The effect of the methanol content of the washing buffer on the removal of the ODN6/cODN1 duplex can be seen in Figure 4.6. It was observed that increasing the methanol content of the wash led to a gradual decrease in the density of the duplex on the surface and complete removal was achieved following a 30 % MeOH wash. This trend was also observed for the ODN1/cODN1 duplex and complete removal was achieved following a 40 % MeOH wash, Figure 4.7.

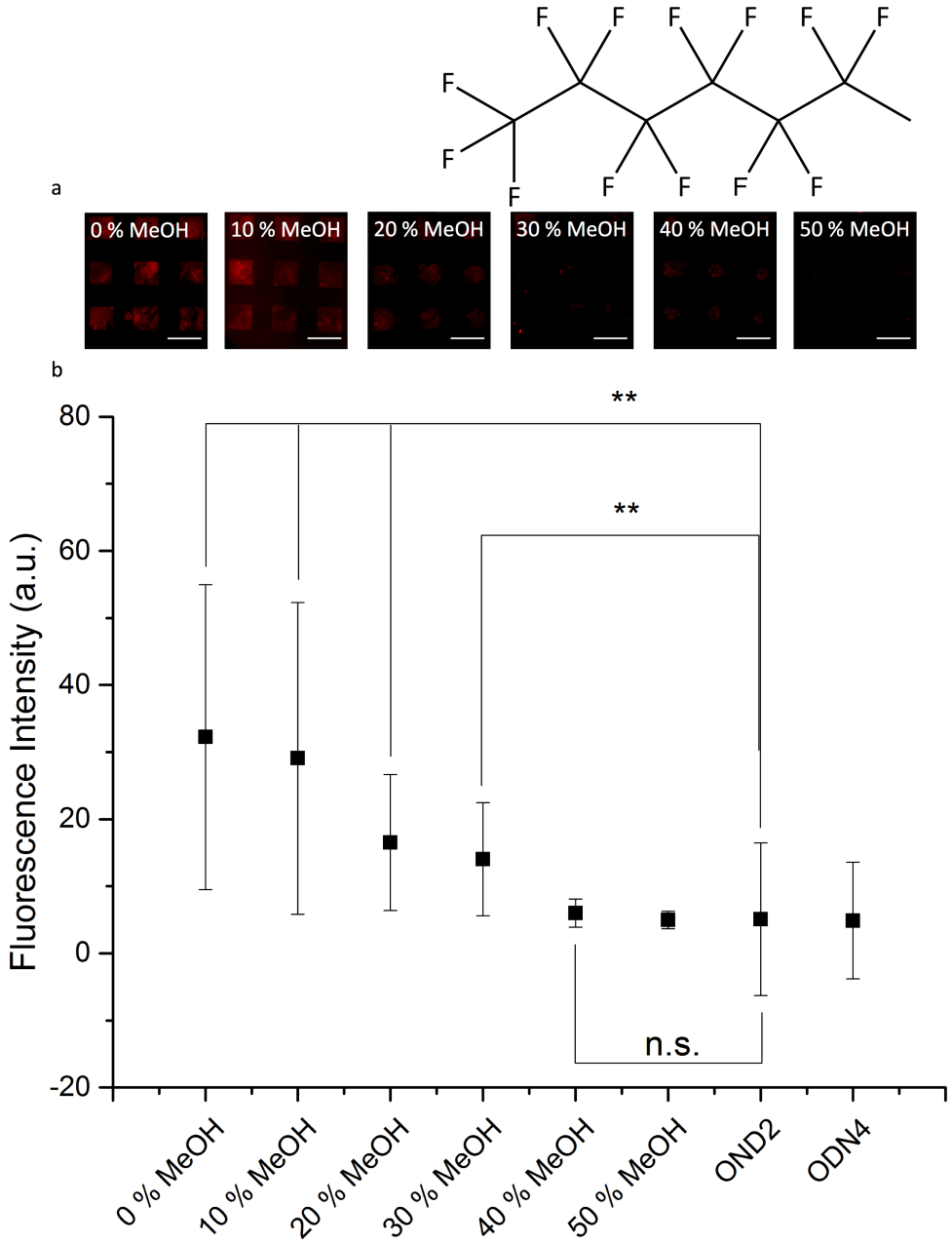

Figure 4-6 Effect of MeOH content of washing buffer on removal of ODN6/cODN1 duplex from Fluorous Microarrays. (a) Fluorescence images obtained of the fluorous microarrays following washes: the MeOH content of the washes increases going left to right. b) Graph shows the corresponding fluorescence intensity measurements taken after each washing. n.s. p>0.1 * p< 0.05 **p<0.01. Scale bar = 50 µm.

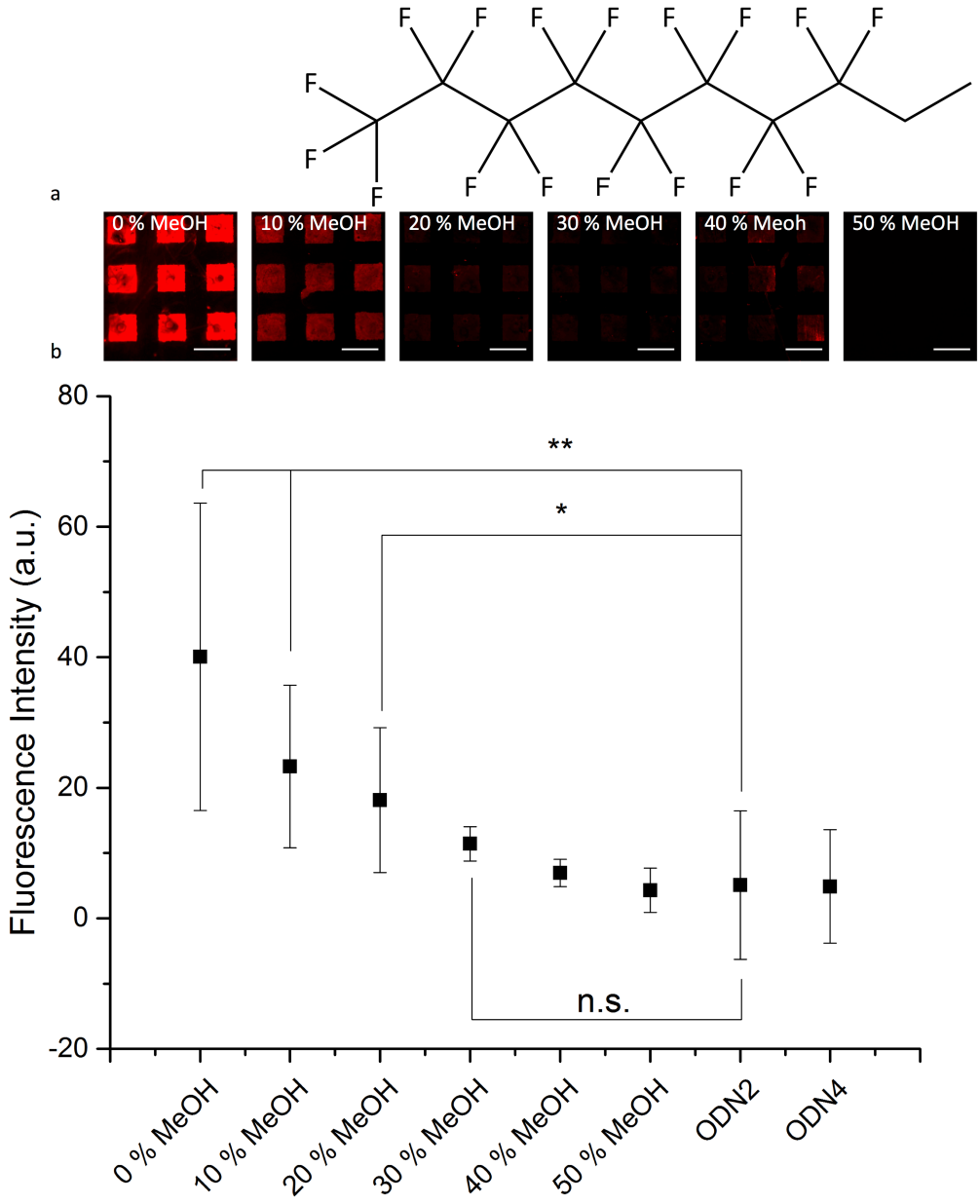

Figure 4-7 Effect of MeOH content of washing buffer on removal of ODN1/cODN1 duplex from Fluorous Microarrays. (a) Fluorescence images obtained of the fluorous microarrays following washes: the MeOH content of the washes increases going left to right. b) Graph shows the corresponding fluorescence intensity measurements taken after each washing step. n.s. p>0.1 * p< 0.05 **p<0.01. Scale bar = 50 µm.

The results of these experiments are in good agreement with the literature: as the fluorine content of the tag increased so did the methanol content of the wash required to completely remove the duplex from the fluorinated solid support. For this reason, it was postulated that increasing the fluorine content of the tag

increased the strength of the fluorous-fluorous interaction, which is the reason behind the observed longer retention times of mono-C_8F_{17}-tagged molecules compared to C_6F_{13}-tagged molecules in F-HPLC columns.(138)

4.2.4 Effect of Linker Molecule on Hybridisation Densities

Due to the different linkers used between the mono-fluorous-tagged ODNs and the bis-C_8F_{17}- and tetra-C_8F_{17}- fluorous-tagged ODNs, an investigation into the effect of the linker molecule had to be carried out. The effect of linker molecules on the retention of the recognition properties of fluorous-tagged biomolecules has been reported elsewhere. In fact, it was found that a polyethylene glycol spacer unit was required between a biotin moiety and a fluorous tag in order to permit protein interactions following its immobilisation onto a fluorinated-solid support.(37)

Therefore, comparison between ODN1 and ODN7 was carried out, Figure 4.8. Both of these ODNs were tagged with a mono-C_8F_{17}-fluorous ponytail. However, the ODNs differed in the linker molecule used: a HEG linker was present between the mono-C_8F_{17}-fluorous ponytail for ODN1 whereas there was no linker for ODN7. This had a drastic effect on the hybridisation densities observed, Figure 4.8. As such, the fluorescence intensity value for ODN1 (containing a HEG linker) was significantly higher.

The observed difference in the fluorescence intensity values was attributed to the highly hydrophobic nature of ODN7 and lack of a linker molecule. As such, the presence of the HEG group modifies the properties of the tagged-molecule by increasing its flexibility. Therefore, its presence is vital in the synthesis of ODNs tagged with fluorous motifs, as it greatly enhances the hybridisation densities observed.(142) Consequentially, without the HEG group, it is possible that the ODN was too close to the hydrophobic fluorinated solid support. Therefore, the ODN was potentially sterically hindered preventing it from taking part in hybridisation reactions. However, the reduction in the fluorescence intensity observed for the ODN7 compared to the ODN1 could be due to a reduced immobilisation density of the ODN7 on the fluorinated support. Unfortunately, this hypothesis could not be tested, as the fluorous-tagged ODNs were not fluorescently labelled.

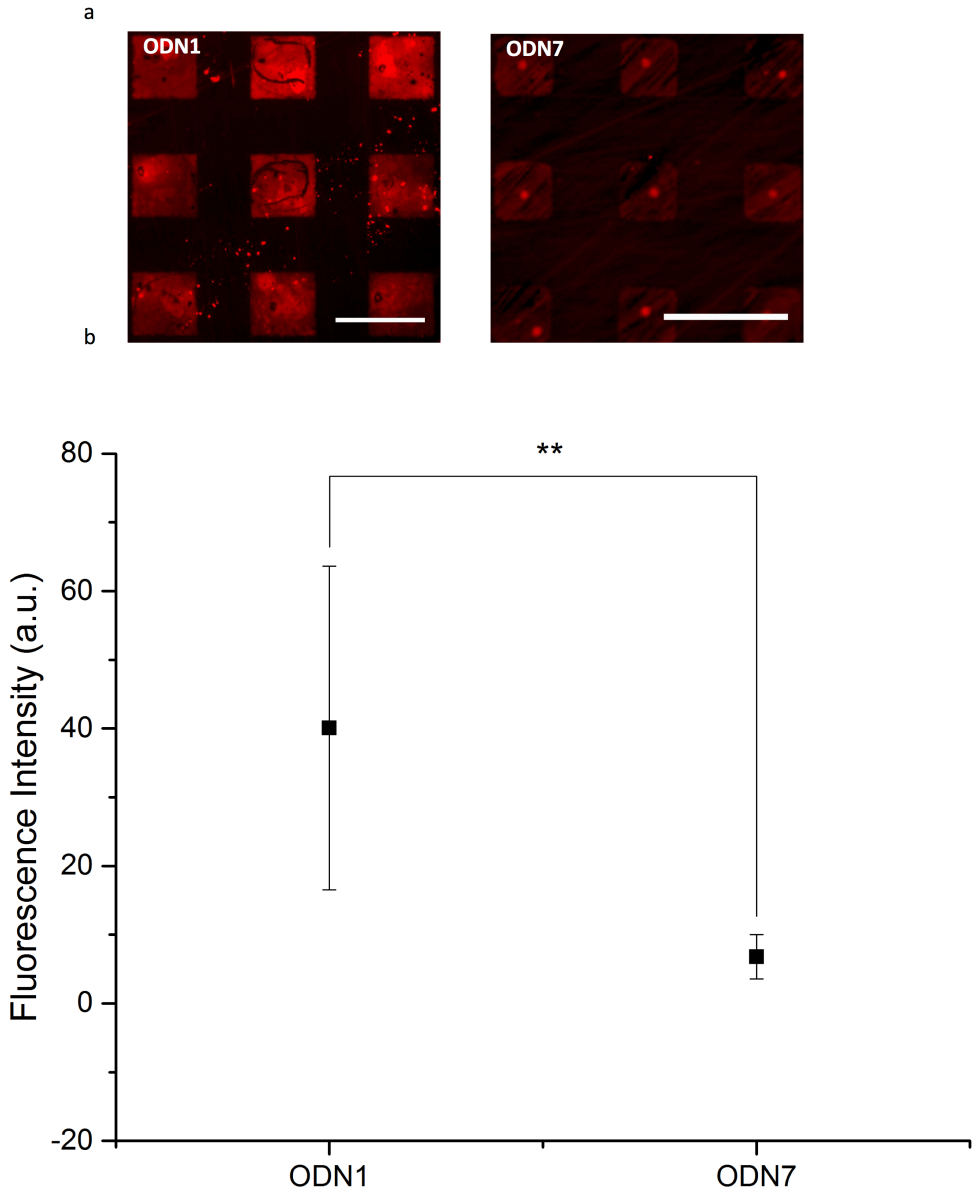

Figure 4-8 Effect of the Linker Molecule on the Hybridisation Density of mono-C_8F_{17}-tagged ODNs on Fluorinated Solid Supports. (a) Fluorescence images obtained following the immobilisation of ODN1 (HEG linker group) and ODN7 (no HEG linker group) and hybridisation to the complementary sequence (cODN1). b) Graph shows the corresponding fluorescence intensity measurements taken after the immobilisation/hybridisation of the ODNs/cODN1. n.s. p>0.1 * p< 0.05 **p<0.01. Scale bar = 50 µm.

4.2.5 Effect of Branched Fluorous Tags on Hybridisation Densities

Branched fluorous-tags (bis-C_6F_{13}) have shown superior binding capabilities for biomolecules onto fluorinated-solid supports compared to mono-C_8F_{17} and mono-C_6F_{13} tagged biomolecules.(119) Therefore, an analysis into the effects of using branched fluorous tags based on the C_8F_{17}-motif was carried out to determine if these ODNs showed enhanced binding capabilities compared to the mono-C_8F_{17} tagged ODN, Figure 4.9. Specifically we used a bis-C_8F_{17} fluorous tag (ODN8) and a tetra-C_8F_{17} tag (ODN9). However, it must be noted that these compounds did not contain a HEG linker and therefore the hybridisation capabilities of these compounds could not be compared to the mono-C_4F_9-, mono-C_6F_{13}- and mono-C_8F_{17}-tagged ODNs used in Section 4.2.2.

Upon examination of the fluorescence intensity values obtained following hybridisation on surfaces with immobilised ODN7, ODN8 and ODN9, it was found that by moving from the mono-C_8F_{17} tag to the bis-C_8F_{17} tag the hybridisation density increased four fold on the surface, Figure 4.9. However, moving from the bis-C_8F_{17} tag to the tetra-C_8F_{17} tag did not have a significant effect on the detected fluorescence intensity/hybridisation density. The jump in the hybridisation density moving from the mono-C_8F_{17} tag to the bis-C_8F_{17} tag is consistent with other reports. This observation is thought to due to the enhanced stability of the fluorous effect, resulting in better retention on surfaces following the required washing procedures.(119) Furthermore, it is proposed that the increase in hybridisation densities observed for the branched-fluorous tagged ODNs compared to the mono- C_8F_{17} tagged ODNs could be due to an increase in the distance of the ODNs from the surface: ODN7 was only one CH_2-O-PO_4H unit away from the surface whereas ODN 8 was 2 units away and ODN9 was 3 units away. The increase in distance from the surface could both shield the ODN from the hydrophobic surface and impart greater flexibility to the ODN. This could explain the observed increase in the hybridisation efficiency on the surfaces due to the ODN being less sterically hindered. Therefore, the effect of the linker molecule was determined to be more important on the immobilisation and retention of the self-recognition properties than the fluorous-tag used. Furthermore, the plateau in the fluorescence intensity moving from the bis-C_8F_{17} tag to the tetra-C_8F_{17} tag could be due to surface saturation. This assumption was based on the hybridisation

densities observed for ODN1, Figure 4.4. As is, the fluorescence intensity value for the mono-C_8F_{17} fluorous-tagged ODN (containing a HEG group) is comparable to the values obtained for the branched structures. Therefore, it is thought that the surface is saturated with probes and the maximum hybridisation density has been reached on all of these surfaces.

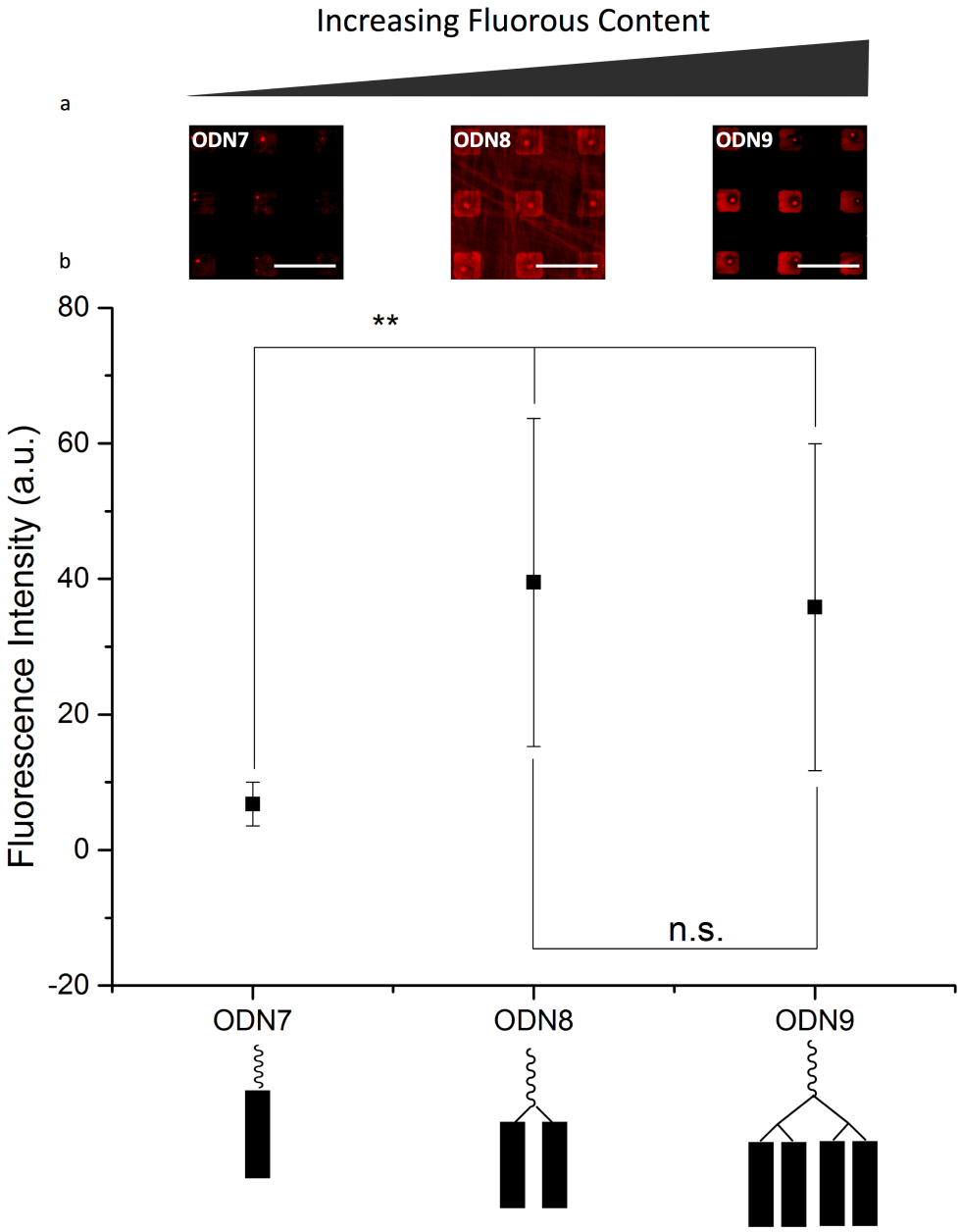

Figure 4-9 Effect of the Branched-Fluorous-Tags on the Hybridisation Densities. (a) Fluorescence images obtained following the immobilisations/hybridisation of ODNs on fluorous microarrays, (b) Graph shows the corresponding fluorescence intensity measurements taken after

each immobilisation/hybridisation event. n.s. p>0.1 * p< 0.05 **p<0.01. Scale bar = 50 µm.

4.2.6 Optimising the Washing Conditions to specifically remove the Branched-Tagged Duplex ODNs.

It has been observed that branched fluorous motifs have greater retention times on F-HPLC columns compared to their mono-fluorous tagged counterparts. This has been attributed to cooperative effects between the branched tags leading to stronger fluorous-fluorous interactions. Therefore, it was hypothesised that by increasing the number of C_8F_{17}-motifs on an ODN, we could increase the fluorous-fluorous interaction. In effect, this should result in a higher methanol content wash required to remove the duplex from the surface.

Again, fluorous square arrays were fabricated using standard photolithography and the ODNs were immobilised overnight, rinsed with DI water and then the cODN1 was incubated on the substrates. The substrates were then washed overnight in hybridisation buffer and the fluorescence intensity was determined. Following this, the substrates were split up and put into a beaker containing different washing buffers (MeOH content ranged from 10-80 %) overnight.

The change in the fluorescence intensity value following different percentage MeOH washes for the mono-C_8F_{17}-tagged ODN (ODN7) tag can be seen in Figure 4.10. As can be seen, the starting fluorescence value was not significantly different from the non-specific binding control. Therefore, from this analysis, the ODN cannot be established as being bound to the surface through fluorous-fluorous interactions.

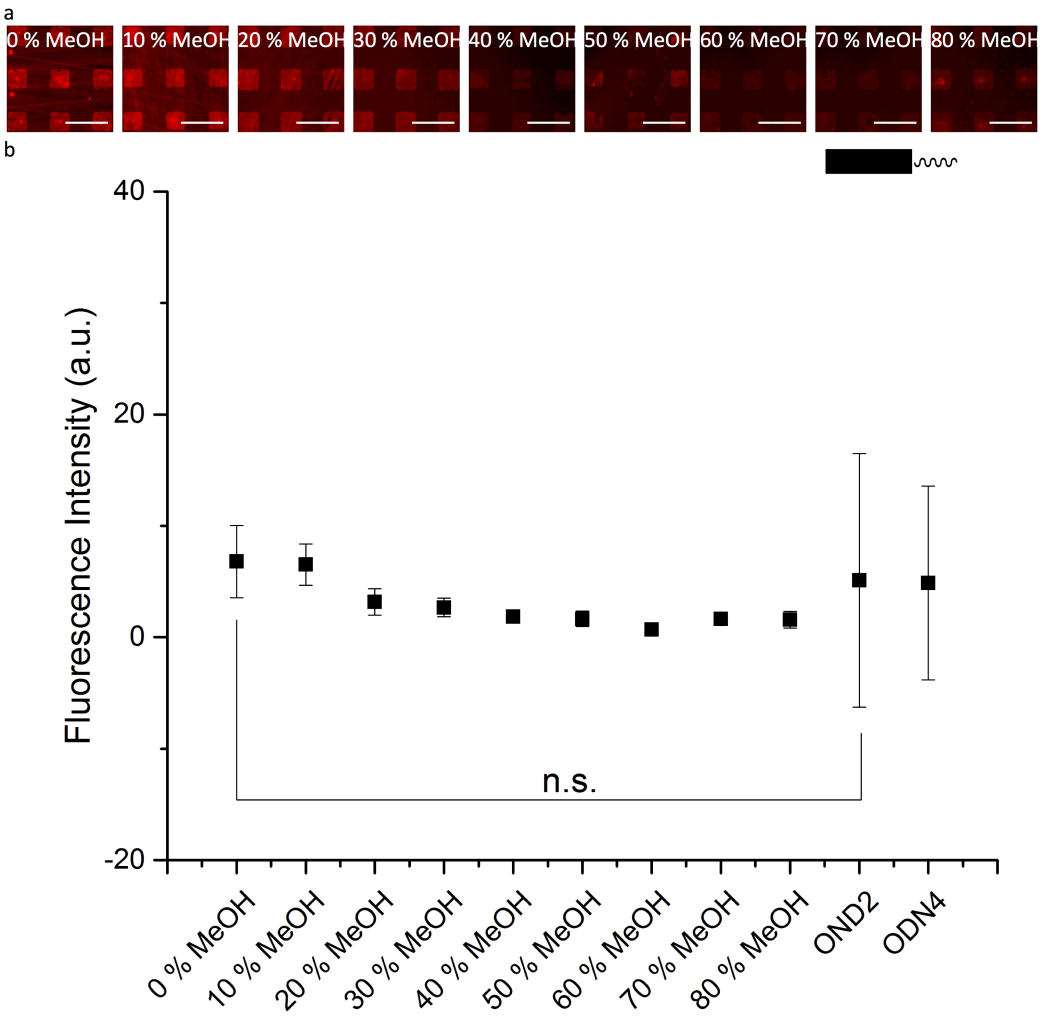

Figure 4-10 Effect of MeOH content of washing buffer on removal of ODN7/cODN1 duplex from Fluorous Microarrays. (a) Fluorescence images obtained of the fluorous microarrays following washes: the MeOH content of the washes increases going left to right. b) Graph shows the corresponding fluorescence intensity measurements taken after each washing step. n.s. p>0.1 * p< 0.05 **p<0.01. Scale bar = 50 µm.

The change in the fluorescence intensity value following different percentage MeOH washes for the bis-C_8F_{17}-tagged ODN (ODN8) and tetra-C_8F_{17}-tagged ODN (ODN9) can be found in Figure 4.11 and 4.12 respectfully.

Following a 10 % MeOH wash, the fluorescence intensity value for the bis-C_8F_{17}-tagged ODN (ODN8) did not change significantly from the starting fluorescence intensity. In fact, the average fluorescence intensity increased. This could be due to an increase in the signal-to-noise ratio due to a reduction in non-specific binding of the cODN1 on the background. Following this, a gradual decrease in the

fluorescence intensity was observed leading to complete removal of the duplex after a 50 % MeOH wash, Figure 4.11. This is a higher MeOH percentage wash than was required to remove the mono-tagged ODNs containing a HEG group. Again, the enhanced stability of the fluorous-fluorous interaction was attributed to cooperative effects between the C_8F_{17} branches.

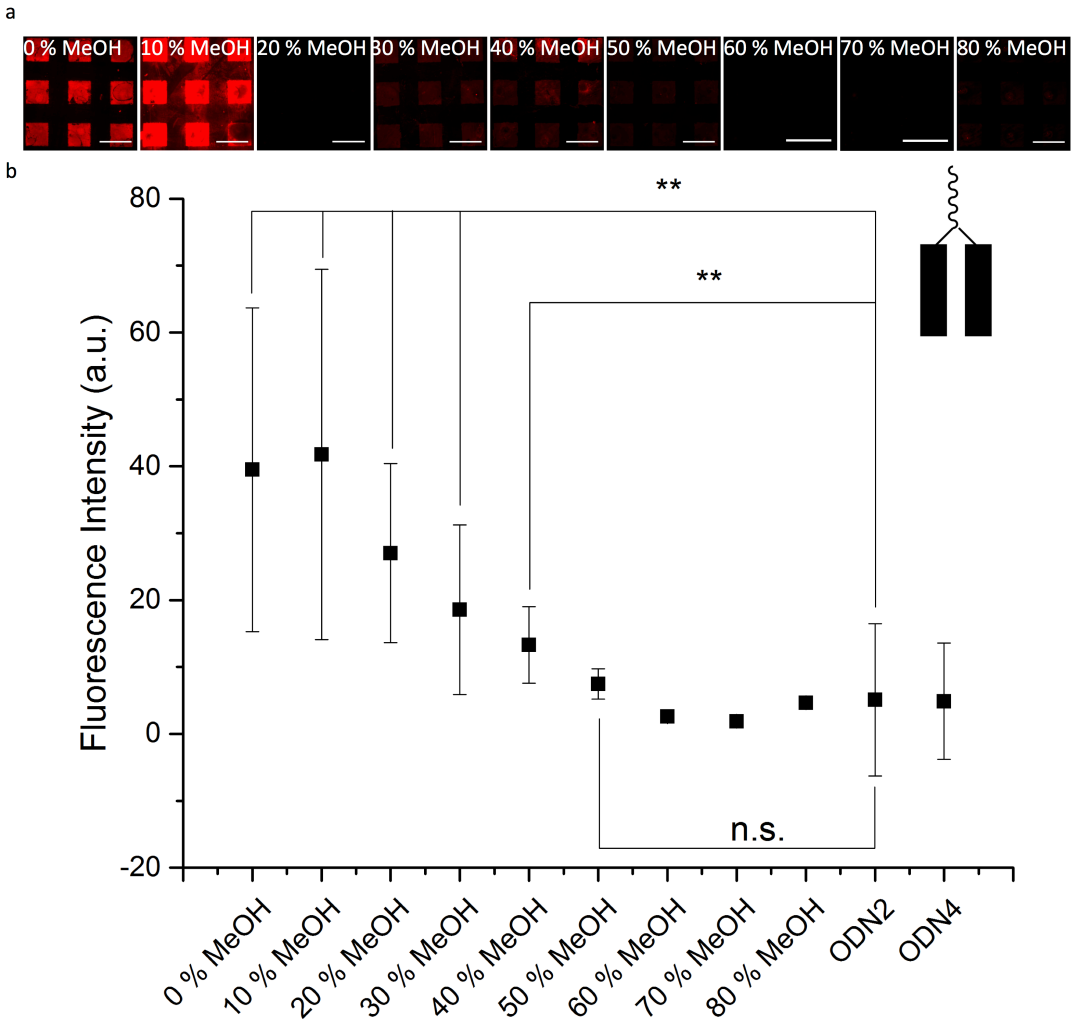

Figure 4-11 Effect of MeOH content of washing buffer on removal of ODN8/cODN1 duplex from Fluorous Microarrays. (a) Fluorescence images obtained of the fluorous microarrays following washes: the MeOH content of the washes increases going left to right. b) Graph shows the corresponding fluorescence intensity measurements taken after each washing step. n.s. p>0.1 * p< 0.05 **p<0.01. Scale bar = 50 µm.

Moving from the bis-C_8F_{17}-tagged ODN to the tetra- C_8F_{17}-tagged ODN showed a further enhanced stability of the fluorous-fluorous interaction, Figure 4.12. Again, little change in the fluorescence intensity was observed following washes up to 50

% MeOH, bar the results from the 20 % MeOH wash. Again, the signal-to-noise ratio was enhanced following a 10 % MeOH wash, suggesting the removal of non-specifically bound cODN1 from the background. Furthermore, the percentage of MeOH required to remove the ODN from the surface increased compared to the bis-C_8F_{17}-tagged ODN: following a 60 % MeOH wash, the fluorescence intensity decreased to below the threshold assigned to non-specific binding. This again was attributed to the enhanced fluorous-fluorous interactions resulting from a higher fluorous content in the tetra-C_8F_{17}-tag.

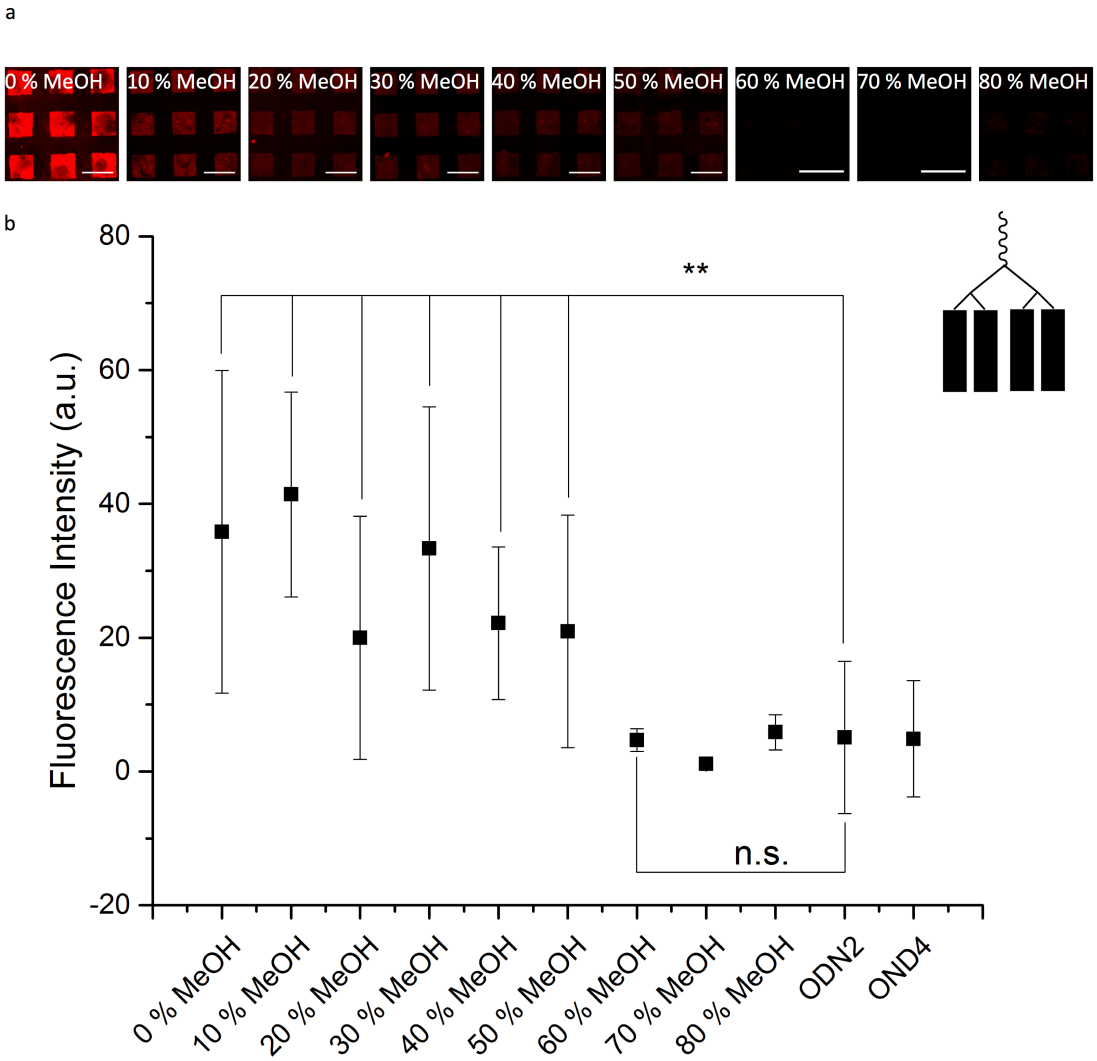

Figure 4-12 Effect of MeOH content of washing buffer on removal of ODN9/cODN1 duplex from Fluorous Microarrays. (a) Fluorescence images obtained of the fluorous microarrays following washes: the MeOH content of the washes increases going left to right. b) Graph shows the corresponding fluorescence intensity measurements taken after each washing step. n.s. p>0.1 * p< 0.05 **p<0.01. Scale bar = 50 µm.

Through this work, it was found that increasing the fluorine content, by increasing the number of fluorous branches, increased the fluorous-fluorous interaction, leading to a direct effect on the percentage of MeOH required in the washing buffer to remove the duplex from the surface. However, comparison of the methanol content required to remove the mono-C_8F_{17}-tagged ODN with a HEG linker (ODN1) and the mono-C_8F_{17}-tagged ODN without a HEG linker (ODN7), indicated that the linker molecule may also have an effect on the retention capabilities of the fluorous-tag on a fluorinated solid support. However, as the initial fluorescence intensity values for these two compounds was significantly different, it is difficult to determine if this is in fact the case and more work needs to be conducted.

4.2.7 Selective Removal of ODNs based on the Fluorine Content of the Tag

As a preliminary study, an investigation was carried out to determine if the washing conditions could be tuned to selectively remove one ODN over another ODN on the surface, depending on the fluorine content of the ODN. As such, ODN9/cODN1 (tetra-C_8F_{17}) and ODN10/cODN10 (bis-C_8F_{17}) duplex were immobilised onto the same surface, Figure 4.13. Neither of these ODNs contained a HEG linker and therefore a direct comparison can be made between them.

Following the immobilisation of both ODN9/cODN1 and ODN10/cODN10 onto the same surface, the fluorescence intensity value for ODN9/cODN1 dropped compared to it being immobilised on its own. However, the fluorescence intensity for the ODN10/cODN10 increased. This was attributed to the spectral overlap of the adsorption spectra of the dye attached to cODN1 (TAMRA) with the emission spectra of the dye attached to cODN10 (Alexa Fluor 488).

Washing the substrate with 50 % MeOH/PBS buffer was found to specifically remove the ODN10/cODN10 duplex and leave ODN9/cODN1 duplex' intact on the surface. Again, the increase in the fluorescence intensity, from the ODN9/cODN1 duplex, following the washing step was again attributed to the spectral overlap between the dyes used and not an increase in ODN9/cODN1 on the surface.

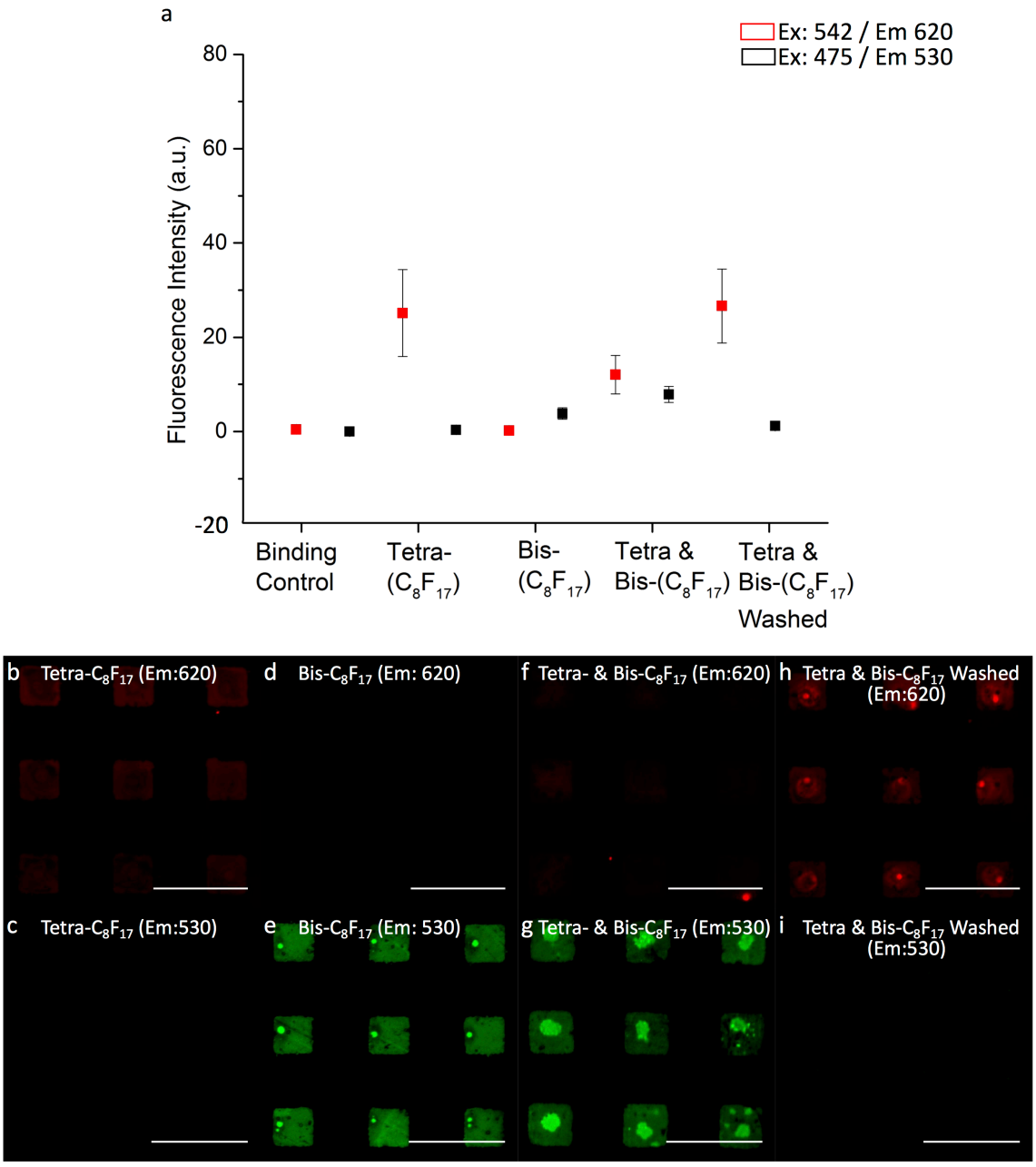

Figure 4-13 Selective removal of an ODN based on the wash used and the fluorine content of the tag. (b) Fluorescence image of surface following the immobilisation of ODN9/cODN1 (Ex: 542/ Em: 620 nm); (c) Fluorescence image of surface following the immobilisation of ODN9/cODN1 (Ex: 475/ Em: 530 nm); (d) Fluorescence image of surface following the immobilisation of ODN10/cODN10 (Ex: 542/ Em: 620 nm); (e) Fluorescence image of surface following the immobilisation of ODN10/cODN10 (Ex: 475/ Em: 530 nm); (f) Fluorescence image of surface following the immobilisation of ODN9/cODN1 and ODN10/cODN10 (Ex: 542/ Em: 620 nm); (g) Fluorescence image of surface following the immobilisation of ODN9/cODN1 and ODN10/cODN10

(Ex: 475/ Em: 530 nm); (h) Fluorescence image of surface with ODN9/cODN1 and ODN10/cODN10 after wash in 50 % MeOH/PBS (Ex: 542/ Em: 620 nm); and (g) Fluorescence image of surface with ODN9/cODN1 and ODN10/cODN10 after wash in 50 % MeOH/PBS (Ex: 475/ Em: 530 nm). (a) Graph showing the fluorescence intensity values for the sample.

4.3 Conclusions & Future Work

In this results chapter we set out to determine if the fluorine content of mono-fluorous phase tails affected the immobilisation densities of ODNs onto fluorinated supports. Our results suggest that increasing the fluorine content increases the hybridisation densities on fluorous microarrays. As such, mono-C_8F_{17}-fluorous phase tails allowed for the highest sensitivity and hybridisation capability. These fluorous phase tails also had an increased stability in methanol: a 40 % MeOH wash was required to remove the duplex from the surface compared to a 30 % MeOH wash for the mono-C_6F_{13}-tagged ODN and a 20 % MeOH wash for the mono-C_4F_9-tagged ODN. Future work should include an examination into the density of the fluorous-tagged ODN on the surface. This would allow the initial immobilisation density of the probe strand on the surface to be taken into account when determining the effect of the methanol content of the wash on the removal capabilities.

Examining the effect of the linker molecule between the fluorous-tag and the ODN also showed interesting results. It was found that the inclusion of a HEG linker between the ODN and the fluorous tag was vital for the hybridisation of the fluorous-tagged ODN, immobilised on the solid support, with its complementary strand in solution. This was deemed to be due to the flexibility the HEG linker imparted on the ODN allowing it to be less sterically hindered compared to a fluorous-tagged ODN without a HEG linker. Nevertheless, this observation could be due to a reduced amount of fluorous-tagged ODN immobilised on the surface. Without fluorescently tagging the fluorous-tagged ODN, or carrying out another method for quantification of the ODN immobilised on the surface, it is difficult to differentiate between these two hypotheses. Therefore, determining the amount of fluorous-tagged ODN on the surface would allow for more sound conclusions to be drawn. This could be carried out using SPR.

Branched fluorous-tags, based on the C_8F_{17} motif, were also investigated as a means to immobilise ODNs onto fluorinated-solid supports for hybridisation reactions. It was observed that the hybridisation densities on the surface following the immobilisation of bis-C_8F_{17}-tagged ODNs and tetra-C_8F_{17}-tagged ODNs were comparable to that of the mono-C_8F_{17}-tagged ODN containing a HEG group. As such, it was postulated that for this series, the maximum coverage of the ODNs was

achieved and therefore the surface was saturated with probe strands. However, without determining the initial immobilisation densities of the ODNs on the surface, it difficult to add weight this conclusion. Nevertheless, the hybridisation densities were the same and, therefore, in the context of fabricating DNA microarrays, using branched fluorous-tagged ODNs did not increase the sensitivity of the microarray. However, enhanced stability in methanol washes was observed when using the branched ODNs compared to the mono-tagged ODNs. It was then shown that the fluorous effect could be tuned to allow for the specific removal of ODNs based on their fluorine content, and the concentration of MeOH used in the wash buffer, from fluorous microarrays. This could have potential application in the purification of immobilised ODNs via their fluorous tag.

5 Deposition of DNA Nanostructures Directed by the Fluorous Effect

5.1 Introduction

The technique known as DNA origami allows for the construction of arbitrary nanoscale objects in two or three dimensions. The importance of these structures lies in their ability to spatially organize functional materials. This would have significant impact on nanoscale electronics and optical device fabrication. However, in order to fully harness the potential of DNA as a universal nanoscale template, assembly defects must be controlled.(143) These include defects in the alignment, relative orientation, and in the up/down orientation of nanostructures.(144)

5.1.1 The Two-Sided Nature of DNA Nanostructures

Adsorption of DNA nanostructures onto solid supports can occur on either side. This can render binding groups present on one side of the nanostructure inaccessible.(145) This has been cited as one of the most critical issues that this technology must overcome in order to realise its potential applications.(144) As a result only 50 %, and sometimes less, of the DNA nanostructures are still functional following their immobilisation onto surfaces: although the reason why some designs show less than 50 % in the correct orientation is still not understood.

Therefore, many studies have been conducted on retaining the functionality of the groups incorporated into the nanostructures independent of the face that the structure is immobilised on. One method used to retain the functionality of these groups following immobilisation is known as molecular threading. This relies on holes within the structure allowing the functional groups, with spacers of sufficient length, to pass through onto the solution facing side. However, this is known to result in lower binding efficiencies between streptavidin and biotin functionalised ODNs within the structure when the ODNs, present on the nanostructures, are pointing towards the surface compared to when they are pointing towards the solution.(145)

Design methods can also be used to control the relative orientation and alignment of DNA nanostructures. This includes the introduction of single stranded linkers in conjunction with the elimination of staple strands from the edge of the structure leading to structures either in an "up-up" or "down-down" relative orientation.(144) Decoration of DNA origami with proteins, specifically streptavidin, can also aid in the immobilisation of nanostructures with the same relative orientations.(146)

Streptavidin-biotin interactions are amongst the strongest known non-covalent interactions with a dissociation constant of 10^{-14} -10^{-15} M. Due to its size (~5 nm) and the ability to modify ODNs with biotin groups, streptavidin is widely employed as a means to visualize individual binding sites on DNA nanostructures using AFM. Furthermore, it has been found that by decorating nanostructures with biotin, and binding streptavidin to the structures before immobilisation, nanostructures can be deposited onto surfaces in solely "up" orientations, that is the face decorated with streptavidin molecules points towards the solution. This is due to the isoelectric point of streptavidin (pI ~ 6) and therefore the nanostructures have a higher affinity for mica compared to the streptavidin molecules. However, the number of streptavidin molecules bound to the structure is important, with less than 3 modifications showing no preference for the immobilisation side.(144)

5.1.2 Context & Aim of Result Chapter

The work carried out in this chapter hopes to overcome the issues resulting from the two-sided nature of DNA nanostructures by forcing them into an "up"

orientation using the fluorous effect. We reason that due to the avoidance of unfavourable interactions of fluorine atoms with other atoms, the nanostructures will deposit onto mica whereby the fluorous-tags point towards the solution. This work builds on the effect seen in Chapter 3 where the fluorous-tagged ODNs were assumed to immobilise on non-functionalised QCM chips with the tag pointing away from the surface. As such, the aims addressed in this chapter are:

1. Determine if fluorous tags can be incorporated into DNA nanostructures without distorting their structure.
2. Determine if the fluorous effect can be used as a means to facially direct the deposition of DNA nanostructures onto mica and SiO_2.
3. Determine if the fluorous tags are able to take part in fluorous-fluorous interactions in order to capture fluorous-tagged biotin from solution.
4. Determine if the fluorous tags present on the DNA nanostructures could be used to capture fluorous-encapsulated Au Nanoparticles.

5.2 Results & Discussion

5.2.1 Proposed Strategy to Control the Facial Immobilisation of DNA Nanostructures onto Mica

The proposed strategy to facially direct the immobilisation of DNA nanostructures, modified to contain both fluorous and biotin groups, onto mica can be seen in Figure 5.1. Divalent cations, particularly Mg^{2+} and Ni^{2+}, are used to bind DNA nanostructures onto mica. This is because the original surface charge of mica is the same as that of DNA: they are both negatively charged. As such, divalent ions are required to form a bridge between the mica and the DNA, thus weakly binding it to the substrate.(147) The origami is then deposited onto mica with no preference as to the face on which the origami is adsorbed. This can limit the applications, as building up on the structures is impaired if the functional groups are no longer available. As such, it was postulated that introducing fluorous "ponytails" into the nanostructures, by modifying staple strands with a mono-C_8F_{17}-tag, would result in directed adsorption of said nanostructures onto mica. This hypothesis is based on the work conducted in Chapter 3 (Figure 3.7) whereby ODNs, modified with a mono-C_8F_{17}-tag, were immobilised onto silicon dioxide coated QCM chips. It was noticed that there was a decrease in the frequency (relating to an increase in mass) in the QCM chamber following the introduction of the fluorous-tagged ODN. However, when the complementary sequence was introduced, there was no further binding. As such, it was proposed that the ODNs were immobilised in an orthogonal arrangement on the surface where the fluorous "ponytails" pointed away from the surface and towards the solution. This would reduce unfavourable interactions between the fluorine atoms and the surface and create a hydrophobic barrier preventing the complementary sequence from either binding to the ODN or non-specifically adsorbing onto the surface. Therefore, the introduction of fluorous modifications into the DNA nanostructures, on one face, could see the nanostructures immobilised on the opposite face. This directed immobilisation was then visualised using the biotin-streptavidin interaction. Hence, the nanostructures were modified to contain both fluorous and biotin motifs (Figure 5.3, Table 5.1).

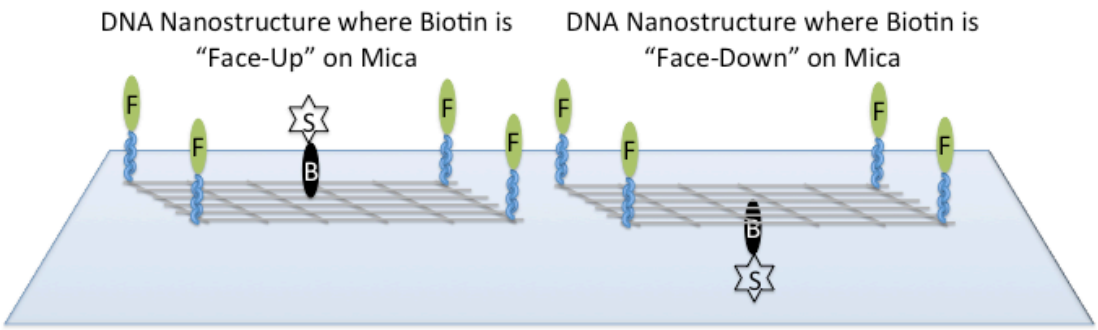

Figure 5-1 Schematic of Proposed Method of Deposition of DNA nanostructures onto Mica directed by the Fluorous Effect. Due to the fluorous effect, the fluorous tags should force the nanostructures to adsorb onto mica via the unmodified face so that the fluorous tags will not be in contact with the surface. In order to test this hypothesis, the streptavidin-biotin interaction was used to distinguish the "face" that the origami was adsorbed onto the surface.

5.2.2 Synthesis and Characterisation of Modified DNA Nanostructures

Several combinations of modifications, shown in Figure 5.3, were used in the work to determine if the fluorous-modified nanostructures showed a preference for which side they were deposited on. Biotin groups were always present in the "centre" of the structure, in either an "up" or "down" position. The "up"/"down" nomenclature refers to the positions of the fluorous-tags, i.e. "up" is on the same face as the fluorous-tags whereas "down" is on the opposite side to the fluorous-groups. The nanostructures were also modified to contain fluorous groups ranging in number and position, Table 5.1, where the modification is described by a coordinate system outlined in Figure 5.2. This was carried out to determine how many fluorous tags were required to specifically orientate the nanostructures and to allow binding to fluorous-tagged biotin. Several of the synthesised structures can be seen in Figure 5.3.

The DNA nanostructures were synthesised by a technique known as DNA origami, developed by Paul Rothemund. This method takes a long single strand, known as a scaffold strand, and folds it via shorter strands, known as staple strands.(148) The wireframe design used for this structure was taken from Reference 64.(64) This

structure uses 7,100 nucleotides of the M13mp18 single-stranded DNA (scaffold strand) and 223 staple strands, ranging in length from 20-52 bases. This leaves 138 nucleotides left over from the scaffold strand, which is present as an unpaired loop on the outer edge of the structure. Dr Sarah Henry, University of Glasgow, then designed this structure to contain both biotin and fluorous groups.

AFM scans of the synthesised structures can be seen in Figure 5.4. The wireframe template, before inclusion of any modifications, can be seen in Figure 5.4 (a). This was used as a reference to determine if the inclusion of any modifications distorted the structure. To determine the effect of missing staples during the synthesis, a mixture containing the scaffold strand and 210 staples was used, Figure 5.4 (b). This structure lacks the staples that were modified with fluorous and biotin groups in order to determine if the structure could still form without them. From this, it was determined that the modified staple strands were essential for the formation of the nanostructures, as without them the structure did not form correctly. Comparison of both the control structures with nanostructures modified to contain a biotin group in the C3 "up" position (Figure 5.4 (c)) and 12 fluorous and one biotin in the C3 "up" position (Figure 5.4 (d)) shows that these modifications were correctly inserted into the structure and did not distort the geometry of the nanostructure. Furthermore, throughout the experiments bright spots can seen on the AFM scans. These were attributed to salt crystals forming on the surfaces during the drying stage.

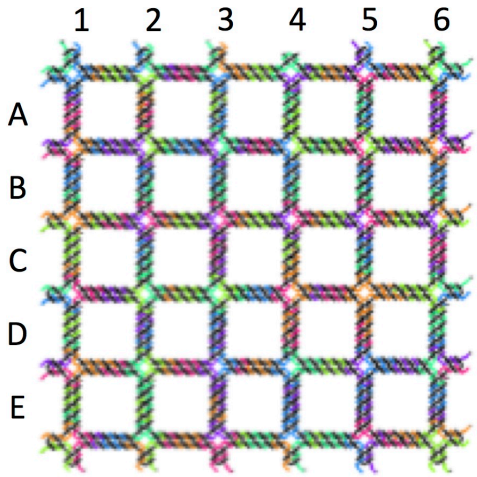

Figure 5-2 **Diagram of DNA Nanostructure Template used in Experimental Work. The placement of the modification is described in the text by a**

coordinate system where the x- position is denoted by a letter and the y-position a number.

Table 5.1 Names Given to the Different Nanostructures Designed and Synthesised. Table shows the names of the nanostructures used in the text and their modifications.

Name of Nanostructure	Biotin Modification	Number and position of Fluorous Modifications
DNS1	**C3 Up**	**0**
DNS2	**C3 Down**	**0**
DNS3	**C3 Up**	**1 (A1)**
DNS4	**C3 Down**	**1 (A1)**
DNS5	**C3 Up**	**2 (A1, E5)**
DNS6	**C3 Up**	**4 (A1,E1,A5,E5)**
DNS7	**C3 Up**	**8 (A1, A3, A5, E1, E3, E5)**
DNS8	**C3 Up**	**12 (A1, A3, A5, B2, B4, D2, D4, E1, E3, E5)**
DNS9	**C3 Down**	**12 (A1, A3, A5, B2, B4, D2, D4, E1, E3, E5)**
DNS10	**-**	**1 (C3)**
DNS11	**-**	**1 (A1)**
DNS12	**-**	**-**
DNS13	**-**	**13 (A1, A3, A5, B2, B4,**

C3, D2, D4, E1, E3, E5)

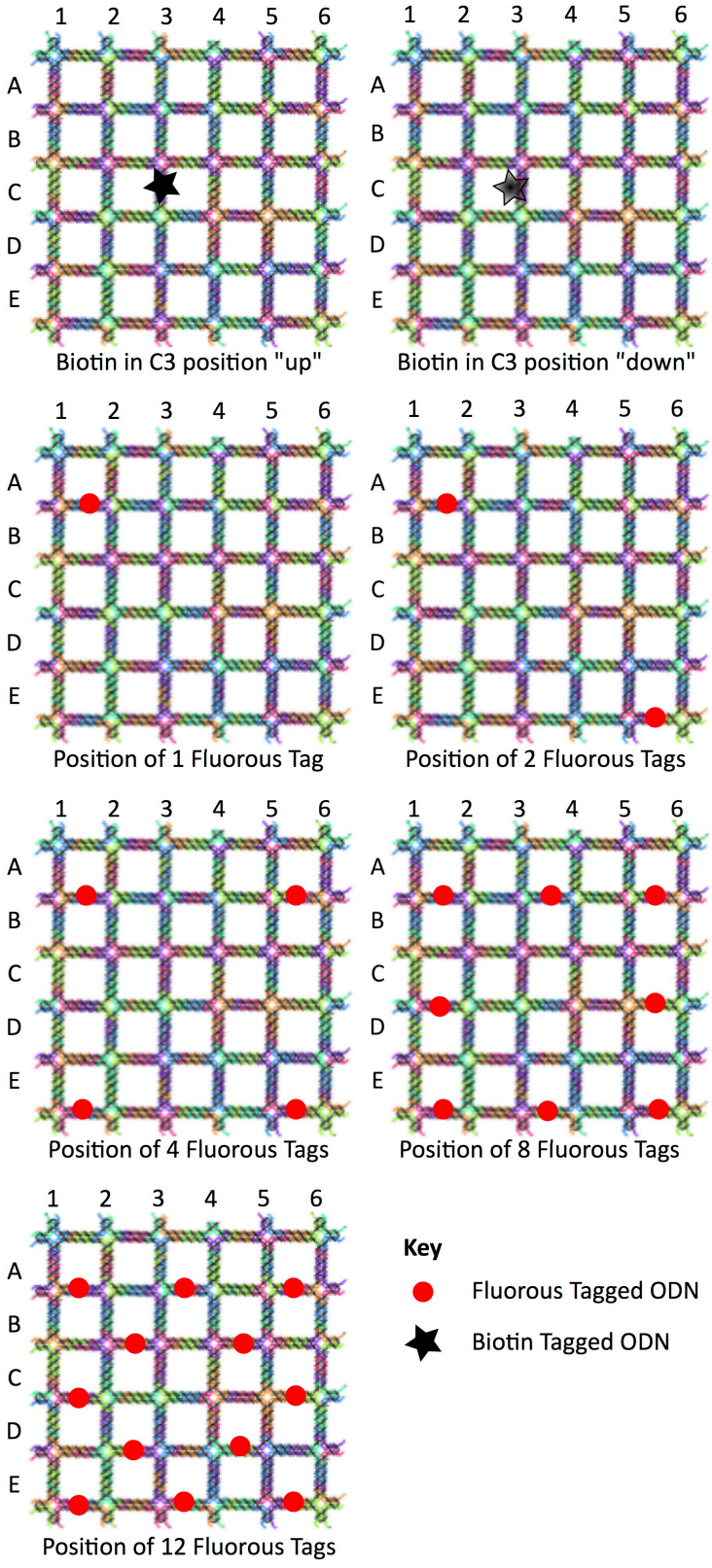

Figure 5-3 Schematic of DNA Nanostructures used in Work. DNA nanostructures were designed to contain a combination of fluorous tags and biotin tags in order to determine the effect of increasing the fluorous content on the immobilisation of said nanostructures onto the surfaces. The combinations of fluorous tags and biotin modifications used in the work, and their given name can be found in Table 5.1.

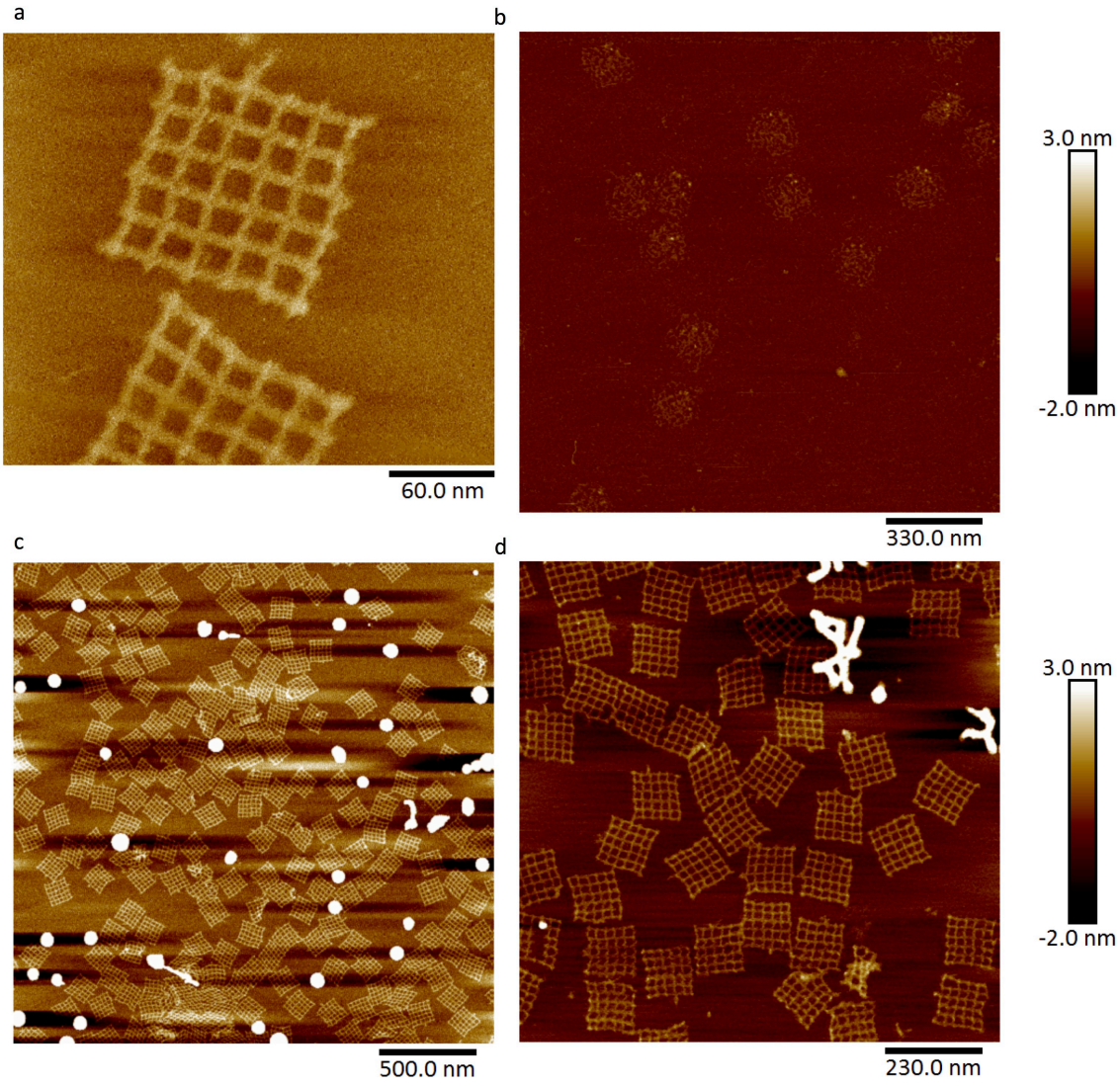

Figure 5-4 Examples of Synthesised DNA Nanostructures. (a) DNA nanostructure wireframe template with no modifications; (b) DNA nanostructure with staple strands removed from mixture; (c) DNA nanostructure with biotin modification in "up" position (DNA1); and (d) DNA nanostructure with 12 fluorous modifications and 1 biotin modification (DNS5).

5.2.3 Analysis of Nanostructures in order to determine "up"/"down" Orientations

As already mentioned, the biotin-streptavidin interaction was used to determine the "face-up"/"face-down" orientation of the nanostructures onto mica. Firstly, the structures were incubated with streptavidin in solution before being purified away from free streptavidin. They were then deposited onto mica. This method was used due to an inability to carry out liquid AFM, which would have permitted the immobilisation of the origami onto the mica first and then the observation of the binding events with streptavidin in real-time.(149, 150)

Following immobilisation of the nanostructures bound to streptavidin onto mica, it was imperative to decide an appropriate analysis technique to determine if said structures were in a "face-up"/"face-down" orientation. As can be seen in Figure 5.5 (a), two structures, one in a "face-up" orientation and one in a "face-down" orientation can be seen. They both have a streptavidin molecule bound, as can be seen from the height profiles (Figure 5.5 (b)). However, there is a marked difference in the height profile resulting from a streptavidin molecule pointing towards the solution ("face-up") compared to the streptavidin molecule pointing towards the mica ("face-down").

In order to analyse the data, a similar method was used to that found Reference 151. (151) In brief, 2.5 μm scans were flattened to the 1st order. This filter centres and removes the tilt on each line by calculating and removing the offset, a, and slope, b, so that the $z = a + bx$.(152) The height was then set from -2 nm to 3 nm and the scans were exported and opened in ImageJ, Figure 5.5 (c). The colour threshold was then changed for each image so that only the streptavidin molecules pointing towards the solution showed up in red. For each sample set, 3 biological repeats were carried out and 3 scans were taken of each sample set. The total number of structures, and the number of structures with a streptavidin "face-up", was counted. This was then used to give a percentage of structures in a "face-up" orientation which was averaged over the three biological repeats and the standard deviation was calculated.

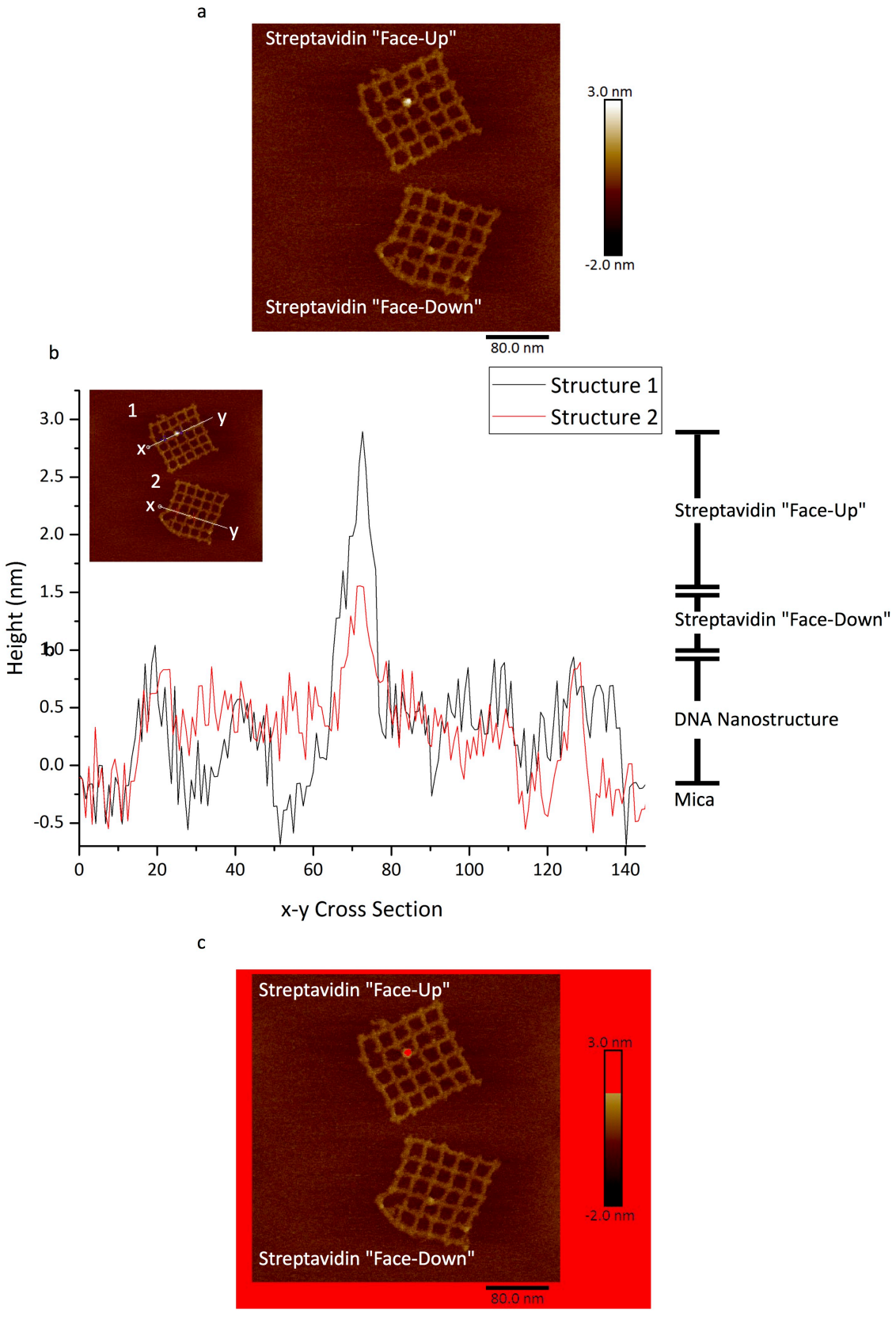

Figure 5-5 Explanation of Data Analysis Process used to Determine if Nanostructures were in "Face-Up" or "Face-Down" Orientation. (a) AFM Scan of DNA Nanostructures showing Streptavidin in both a "face-up" and "face-down" orientation; (b) Height profile obtained from AFM scan showing the

difference in height between a "face-up" nanostructure and "face-down" nanostructure; and (c) Colour Threshold was changed to 155-255 and if the streptavidin showed up in red it was counted as face-up.

5.2.4 Determination if the biotin-streptavidin conjugation influenced the Orientation of the Nanostructures

As previously mentioned, nanostructures that have been decorated with streptavidin molecules have shown a preference for the face on which they are adsorbed onto surfaces if the number of streptavidin molecules exceeds three. Therefore, before the influence of the fluorous "ponytails" on the immobilisation of nanostructures onto solid supports was investigated, a study into the influence of one streptavidin in the C3 position (on either the "up"/"down" face) was carried out. Again, the structures were synthesised, and incubated with streptavidin for 2 hours (in 10 X excess) at room temperature. Extensive purification steps were required to remove excess streptavidin from the solution, which was then dropped onto freshly cleaved mica. The surfaces were then imaged and large area scans (2.5 μm) were obtained for both the samples, allowing for a greater number of structures to be observed, (Figure 5.6 (a) & (c)). In order to fully observe the detail in the structures, smaller scans were also acquired (Figure 5.6 (b) & (d)). The scans were then subjected to the analysis described in Section 5.2.3 and the data obtained can be seen in Figure 5.6 (e).

It was found that around 50 % of the nanostructures, modified to contain a streptavidin molecule in either an "up" or "down" position, were deposited in a "face-up" orientation, that is the streptavidin molecule pointed towards the solution. Therefore the modified nanostructures showed no preference for the face on which they were adsorbed following binding to a streptavidin molecule. This confirmed the viability of the methodology used in this section to determine the effect of fluorous tags on the orientation of deposited nanostructures.

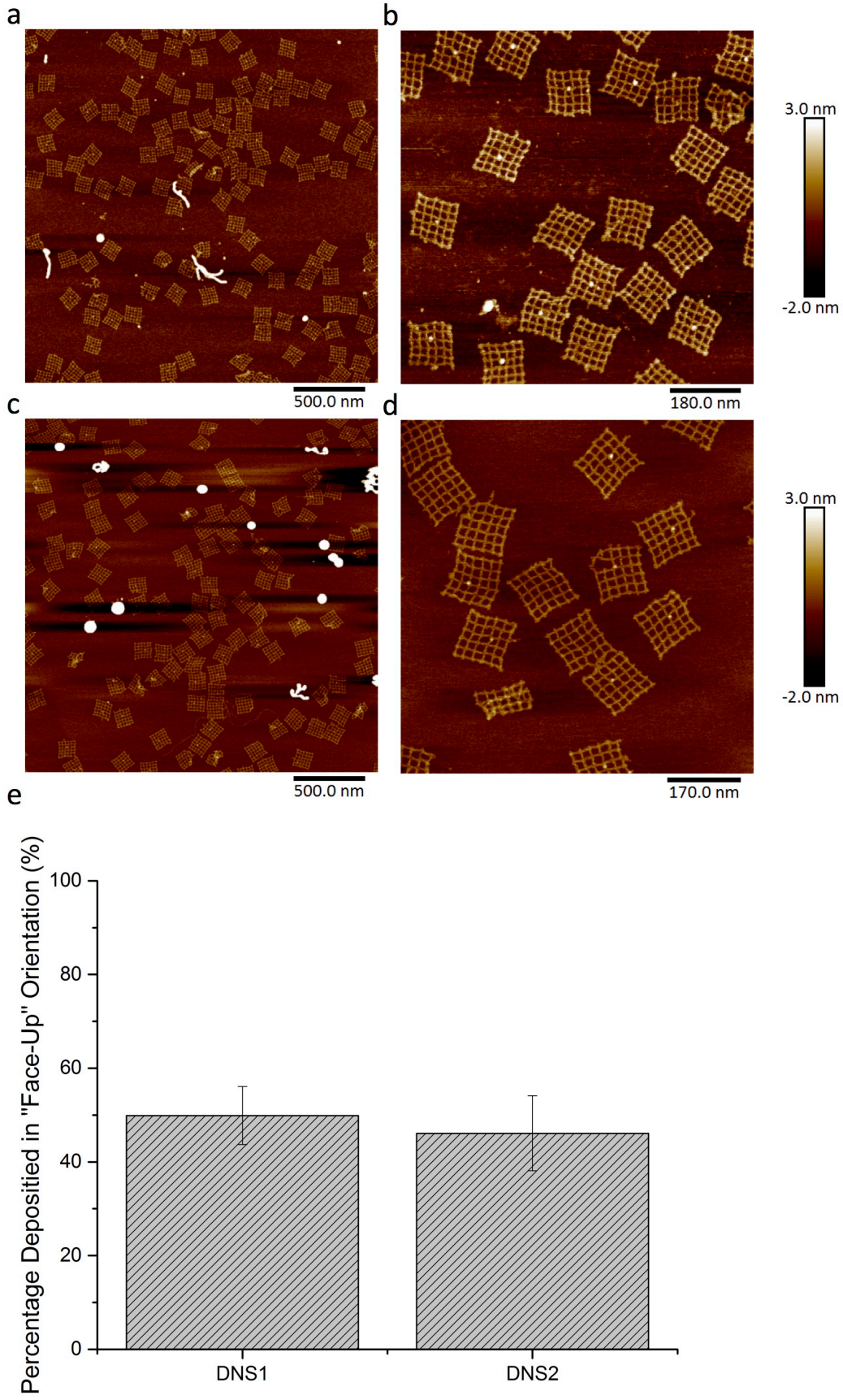

Figure 5-6 Effect of a Streptavidin Molecule on the Deposition of DNA Nanostructures from Solution onto Mica. Nanostructures, modified with

biotin motifs, were incubated with streptavidin and then deposited onto mica. (a) 2.5 µm AFM scan of DNS1; (b) Zoomed in AFM scan of DNS1; (c) 2.5 µm AFM scan of DNS2; (d) Zoomed in AFM scan of DNS2; and (e) Graph showing average percentage (and the standard deviation) of nanostructures in "face-up" orientation. Total number of nanostructures analysed for DNS1= 880: total number of nanostructures analysed for DNS2 = 638.

5.2.5 Determination if the Fluorous Effect could Specifically Orientate DNA Nanostructures on Mica.

DNA nanostructures (DNS8 & DNS9) were used to determine if the fluorous effect could be used to influence the face on which DNA nanostructures are deposited onto mica. These structures contained 12 fluorous groups evenly distributed throughout the structure, and a biotin motif either on the same face as the fluorous tags (DNS8) or on the opposite face to the fluorous tags (DNS9). Following the incubation of DNS8 and DNS9 with streptavidin and their deposition onto mica, AFM scans were taken of the surfaces (Figure 5.7 (a)-(h)). The total DNA nanostructures were counted and compared to the number of structures in the "face-up" orientation. The data was then analysed and can be seen in Figure 5.7 (i).

It was found in this study that the inclusion of fluorous modifications into the structure of DNS8 and DNS9 was found to force them to deposit in an orientation whereby the fluorous "ponytails" pointed away from the mica and into the solution. In the case where the biotin-streptavidin modification was on the same face as the fluorous "ponytails", around 85 % of the structures were found to be in a "face-up" orientation. Again, when the biotin-streptavidin modification was present on the opposite side to the fluorous "ponytails", around 15 % of the structures were in the "face-up" orientation, however this does not include the structures that were in a "face-up" orientation and did not have a streptavidin bound as they could not be distinguished. However, this result does suggest that the fluorous effect influenced the face on which the nanostructures were deposited onto mica, as the structures tended to be adsorbed onto the mica on the face opposite the face modified with fluorous groups regardless of the error associate with those structures without a streptavidin bound to them or synthesised without a biotin modification.

As the number of fluorous groups significantly exceeded that of the biotin-streptavidin modifications on the structures, an investigation into the number of fluorous groups required to relatively orientate the nanostructures was carried out, Figure 5.8.

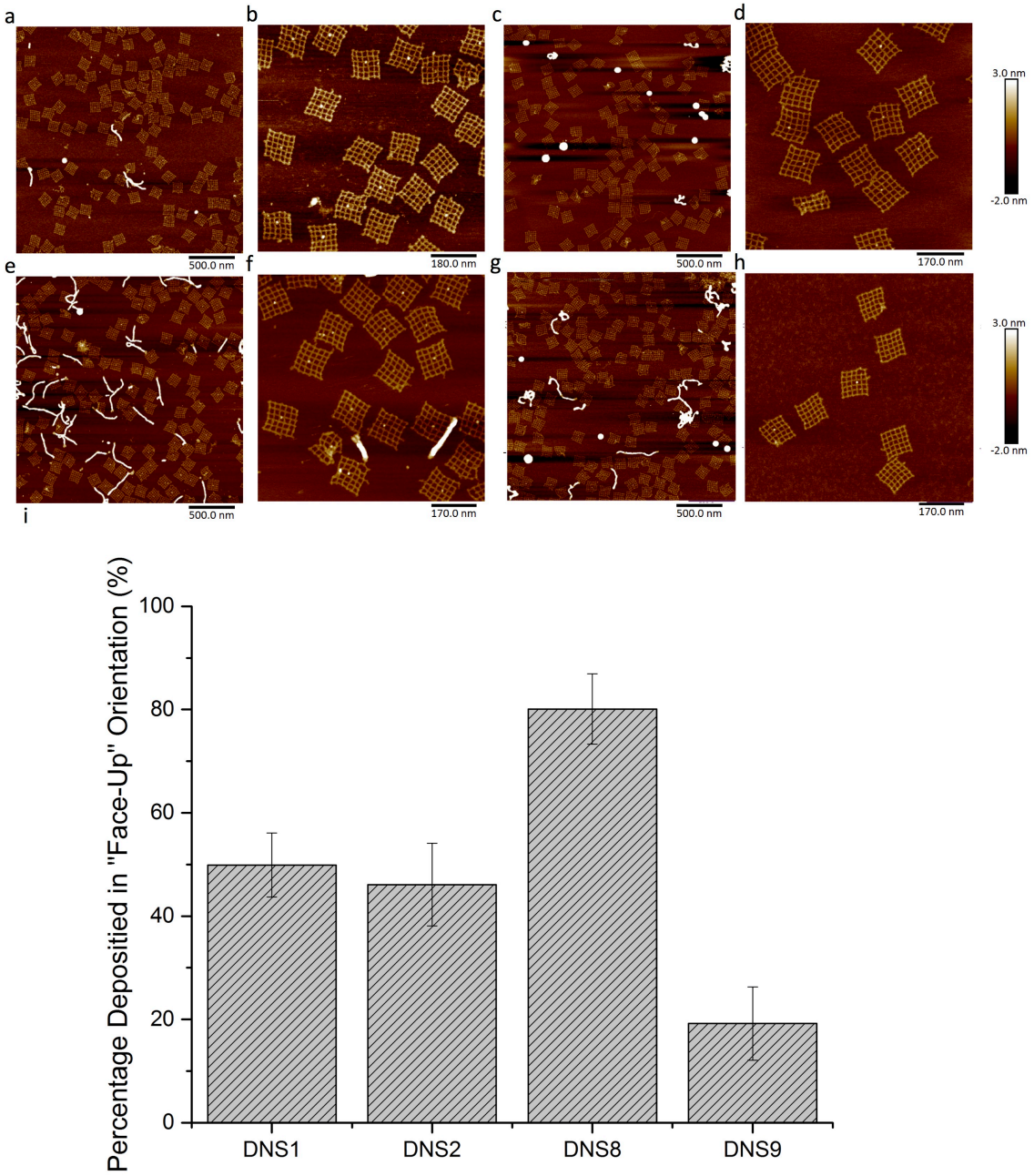

Figure 5-7 Effect of Fluorous Groups on the Deposition of DNA Nanostructures from Solution onto Mica. Nanostructures, modified to contain biotin groups and 12 fluorous tags were incubated with streptavidin and then deposited onto mica. (a) 2.5 µm AFM scan of DNS1; (b) Zoomed in AFM scan on DNS1; (c) 2.5 µm AFM scan of DNS2; (d) Zoomed in AFM scan of DNS2;

(e) 2.5 µm AFM scan of DNS8; (f) Zoomed in AFM scan on DNS8; (g) 2.5 µm AFM scan of DNS9; (h) Zoomed in AFM can of DNS9; and (i) Graph showing average percentage (and the standard deviation) of nanostructures in "up" orientation. Total number of structures analysed for DNS8 = 350: total number of structures analysed for DNS9 = 403.

DNA nanostructures were designed, and synthesised, to contain a biotin modification in the "up" orientation and various numbers of fluorous tags: 1, 2, 4, 8 and 12. Again the structures were incubated with streptavidin and deposited onto mica. Several representative scans from the experiment can be seen in Figure 5.8 (a)-(l) and the data from the analysis of the percentage nanostructures found to be deposited in the "face-up" orientation can be seen in Figure 5.8 (m).

It was determined from this study that only one fluorous tag was required to specifically orientate the nanostructures deposited onto mica. This is consistent with the data obtained in Chapter 3 where it was found that only one fluorous tag (mono-C_8F_{17}) was required to orientate the ODNs away from the unmodified QCM chip and point toward the solution. Again, in order to complete the analysis, the nanostructures were synthesised with 1 fluorous tag and a biotin modification on either the "up" or "down" position. The data from this analysis can be found in Figure 5.9.

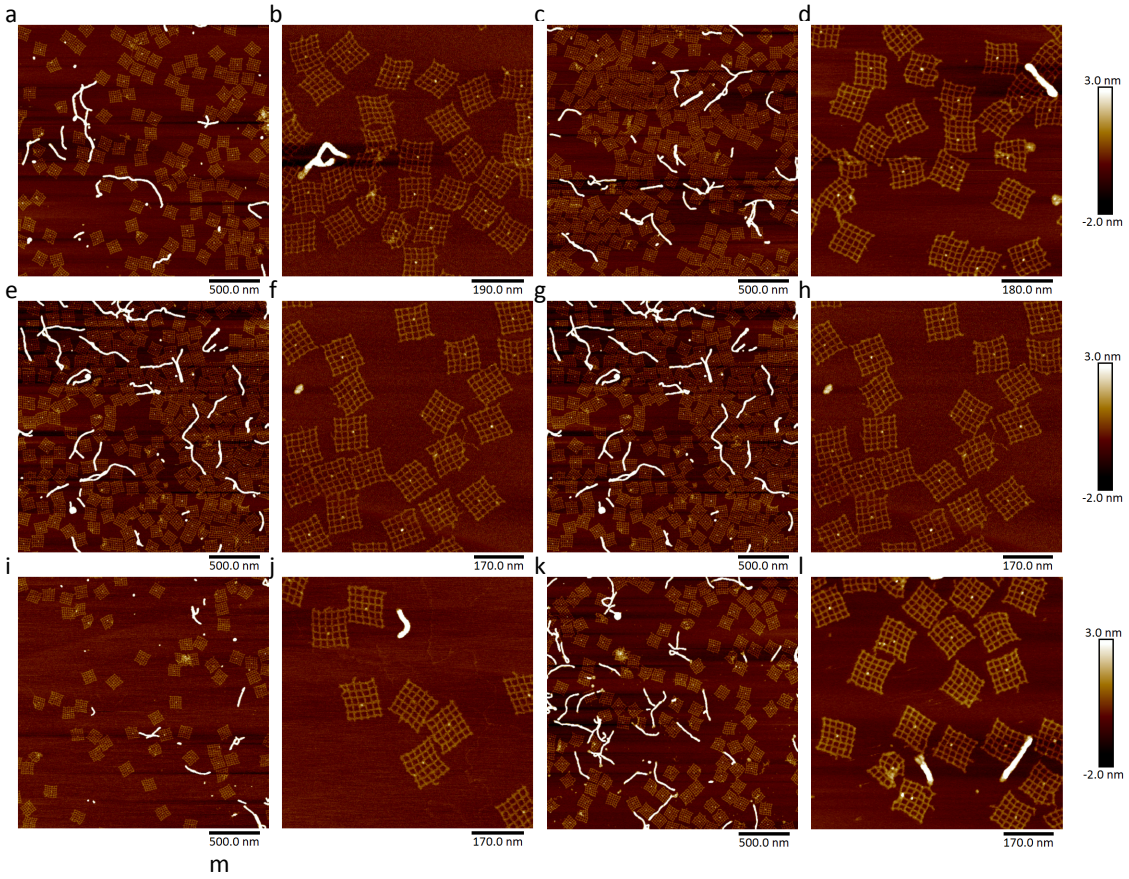

Figure 5-8 Effect of the Number of Fluorous Tags on Percentage of DNA Nanostructures Deposited onto Mica in "Face-Up" Orientation. Images a-l are AFM scans of: (a & b) DNS1- 0 fluorous tag; (c & d) DNS3- 1 fluorous tags; (e &

f) DNS5- 2 fluorous tags; (g & h) DNS6- 4 fluorous tags; (i & j) DNS7- 8 fluorous tags; and (k & l) DNS8- 12 fluorous tags. Graph (m) shows the average percentage (and the standard deviation) of DNA nanostructures in the "Face-Up" orientation. Total number of nanostructures analysed for DNS1= 880, DNS3 = 1165, DNS5 = 903, DNS6 = 1374, DNS7 = 750, and DNS8 = 350.

Similar results were found for the inclusion of just one fluorous modified staple strand on the relative orientations of the nanostructures. When the biotin group was on the same face as the fluorous tag, it was found that around 80 % of the structures were deposited onto the mica in the "face-up" orientation. This is lower than other methods for facially directing the immobilisation of nanostructures onto surfaces: up to 95 % of nanostructures have been deposited onto lipid-supporting bilayers in the "face-up" orientation.(153) However, when the biotin modification was present on the opposite side to the fluorous tag, only 15 % of the structures were in the "face-up" orientation. These relative percentages could suggest that around 15-20 % of the structures did not contain the fluorous modifications or were not bound to a streptavidin molecule. Therefore, by purifying the structures through a streptavidin column the percentage of structures found in a "face-up" orientation could increase when the fluorous and biotin modifications are on the same face as one another.

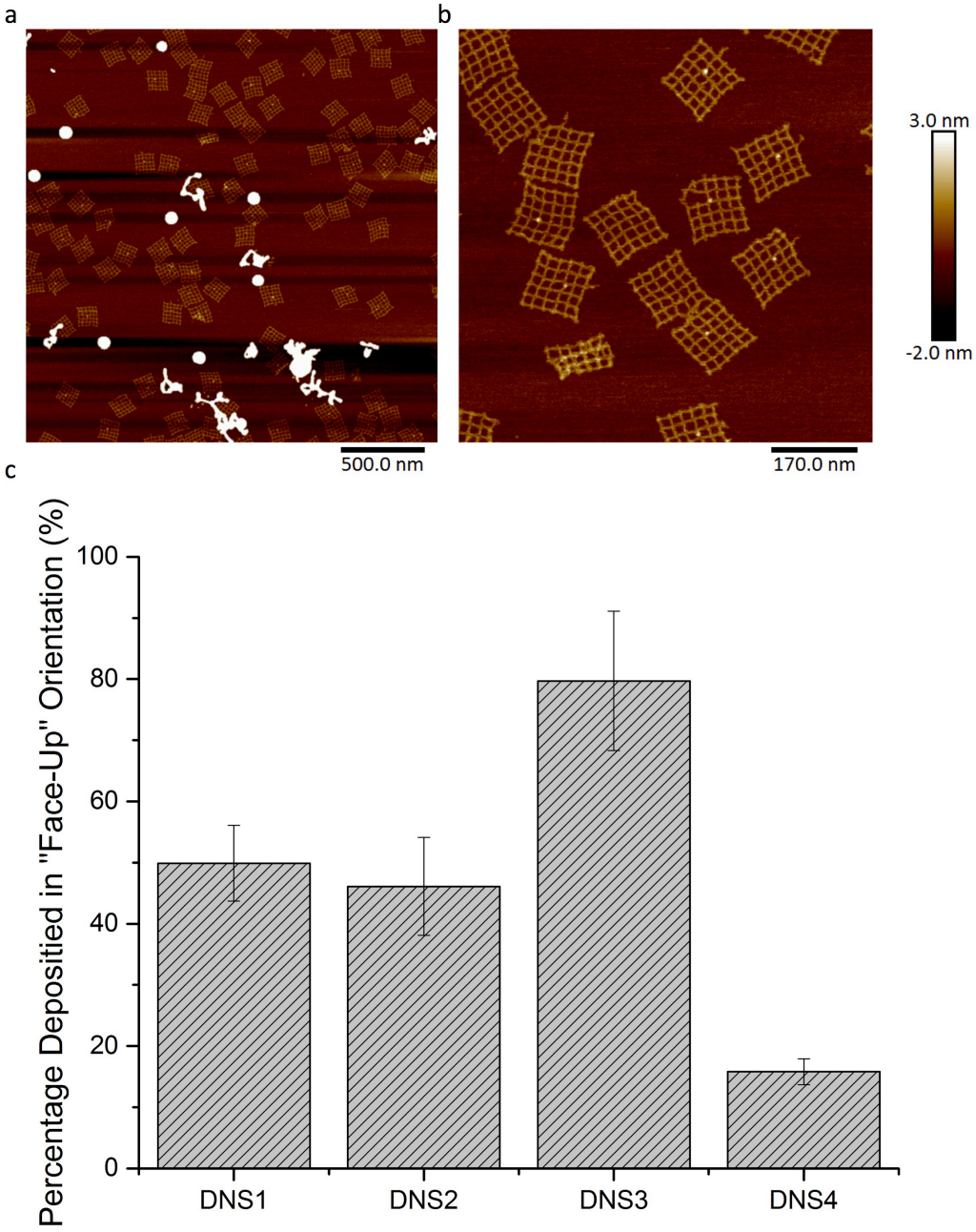

Figure 5-9 Determination of Lower Limit of Fluorous tags Required in order to Specifically Deposit Nanostructures in "Face-Up" position on Mica. Nanostructures, modified to contain 1 biotin group and 1 fluorous group, were incubated with streptavidin, and then deposited onto mica. (a) 2.5 µm AFM scan of DNS4 which is the negative control i.e. the biotin group is in the "down" orientation; (b) Zoomed in AFM scan of DNS4; (c) Graph showing average percentage of nanostructures in "face-up" orientation. Total number of nanostructures analysed for DNS1= 880, DNS2 = 638, DNS3 = 1165 and, DNS4 = 1161.

5.2.6 Determination if the Fluorous Effect could Specifically Orientate DNA Nanostructures on SiO_2.

The deposition of DNA nanostructures onto mica is ill suited for integration with micro- or nano- fabrication.(154) Therefore, an investigation was carried out to determine if the fluorous effect could be used to influence the face on which the DNA nanostructures were immobilised onto SiO_2, as this material can be easily integrated into fabrication processes. However, the method of deposition was modified: although SiO_2 would have a negative charge at the pH of the buffer (~pH 8.0), more Mg^{2+} ions are required to invert the charge on the surface compared to that required for mica (~125 mM compared to~12.5 mM). Therefore, the DNA nanostructures were concentrated in 10X TAE.Mg buffer, in order to obtain the required Mg^{2+} concentration, and were deposited onto SiO_2 in the same manner as carried out for mica.

As can be seen in Figure 5.10 (a), it was observed that the inclusion of 12 fluorous tags into the nanostructure, on one face, specifically orientated the DNA nanostructures so that around 68 % of them were in a "face-up" orientation. In order to make sure this observation was due to the fluorous tags, the control structure, no fluorous tags and only a biotin modification in the centre of the structure, was incubated with streptavidin and then deposited onto SiO_2, Figure 5.10 (b). This showed around 40 % of the structures in the "face-up" orientation and therefore the influence of the fluorous effect was confirmed for the structures on SiO_2. However, the observed decrease in the percentage of nanostructures in a "face-up" orientation compared to that observed for mica is not fully understood as there are several factors that may have had an effect including the roughness of the substrate making the designation of the structures in a "face-up" orientation difficult, and the increase in the Mg^{2+} concentration may have caused the streptavidin to aggregate.(67)

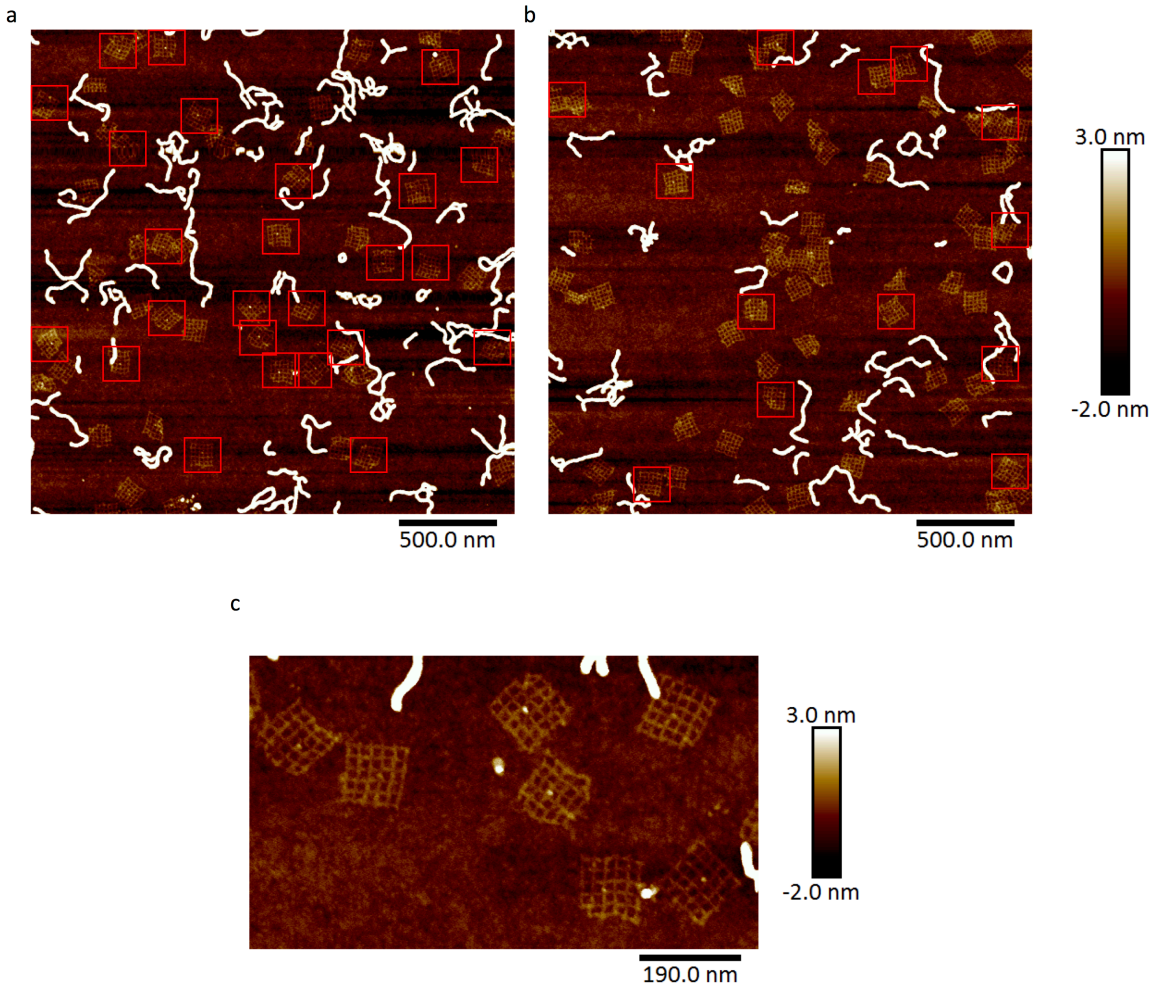

Figure 5-10 Effect of the Inclusion of Fluorous "Ponytails" into DNA nanostructures on their Deposition from Solution onto SiO_2. (a) 2.5 µm AFM scan of DNS 8; (b) 2.5 µm AFM scan of DNS1, the negative control; and (c) Zoomed in AFM scan of DNS8.

5.2.7 Determination if the Fluorous Tags could Take Part in Fluorous-Fluorous Interactions

5.2.7.1 Fluorous-Tagged Biotin

In order to determine if the fluorous-tags present on the DNA nanostructures could also be used to capture fluorous-tagged molecules from solution, the structures were incubated with fluorous-tagged biotinylated DNA, as shown in Figure 5.11.

Briefly, both the DNA nanostructures and the fluorous-tagged biotinylated DNA were incubated with streptavidin separately (Fig 5.11 (a) & (b)). Following this, the streptavidin-DNA nanostructures and streptavidin-fluorous-tagged biotinylated DNA were incubated together (Fig 5.11 (c)). The resulting structures were then purified away from free streptavidin and deposited onto mica. As can be seen in Figure 5.11, three types of biotinylated DNA were investigated. These differed in the fluorous-tag coupled to the DNA strand: ATS51 (mono-C_8F_{17} tag); ATS52 (bis-C_8F_{17} tag); and ATS53 (tetra-C_8F_{17} tag).

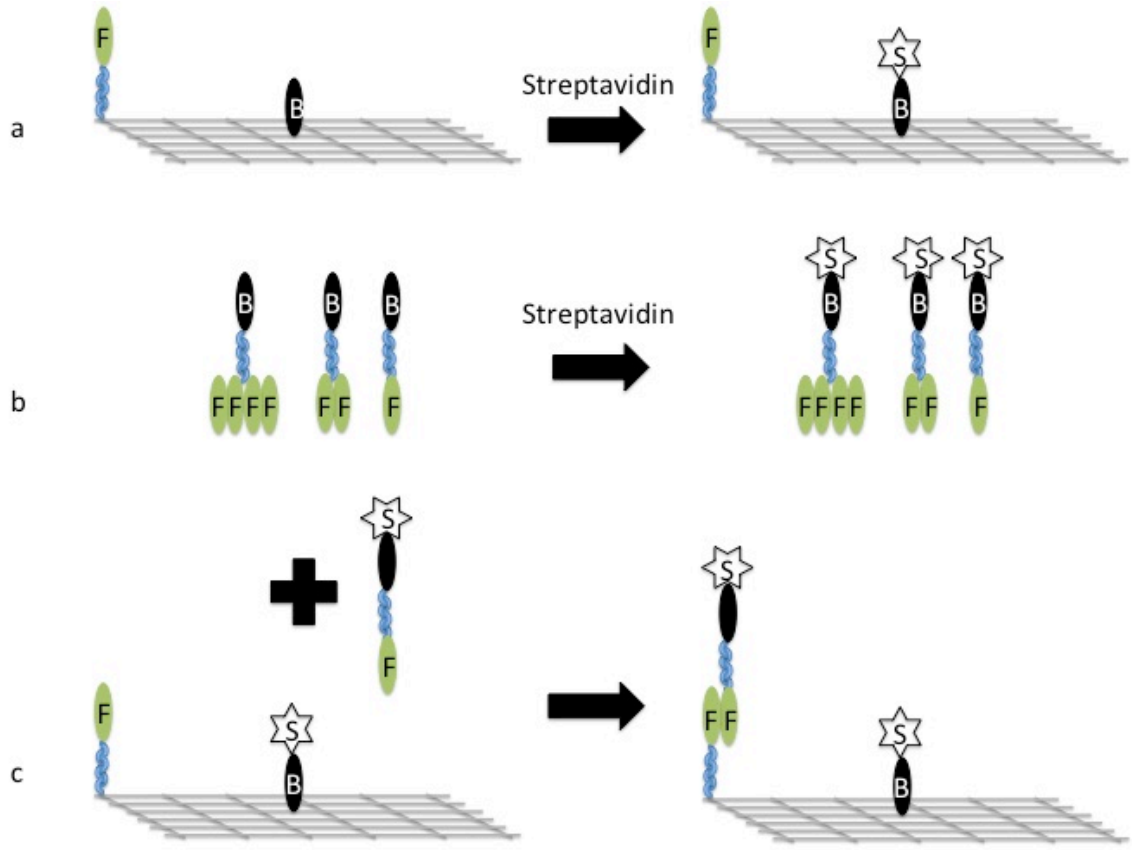

Figure 5-11 Schematic of the Proposed Method to Determine if the Fluorous Effect could be used to Capture Fluorous-Tagged Molecules on a DNA Nanostructure. (a) Incubation of DNS3 with streptavidin; (b) Incubation of fluorous-tagged biotinylated DNA with streptavidin; and (c) Incubation of streptavidin bound biotinylated DNA (ATS51) with DNS3 bound to streptavidin.

Results from the experiments can be seen in Figure 5.12. Only the use of ATS51, mono-C_8F_{17}-tagged biotinylated DNA, resulted in the capture of fluorous-tagged biotin from solution (Figure 5.12 (c)). Closer scans of DNA nanostructures appearing to have captured a fluorous-tagged biotinylated DNA bound to a streptavidin molecule were obtained and a representative image can be seen in Figure 5.12 (d). The DNA nanostructures were designed to have a biotin modification in the centre, as a control for streptavidin binding, and two fluorous tags. Only one of the fluorous-tags present on the structure was ever observed to have captured a fluorous-tagged biotinylated DNA bound to a streptavidin molecule. A control sample, a representative scan of which can be seen in Figure 5.12 (d), which had no fluorous tags incorporated into the structure and therefore

shouldn't have captured any fluorous-tagged molecules from solution, was also incubated with streptavidin and streptavidin-fluorous-tagged biotinylated DNA. These scans also showed the presence of DNA nanostructures with bright spots in close proximity to where the fluorous-tags were on the actual sample. Therefore, a comparison of the total number of DNA nanostructures investigated and the number of structures with bright spots in the regions where the fluorous-tags were, or were supposed to be, can be seen in Table 5.2. This shows that it is unlikely that the fluorous-tagged biotin was captured from solution and that the presence of bright spots on said structures were due to random chance.

However, the presence of bright spots on the mica for the sample incubated with ATS53, tetra-C_8F_{17}-tagged biotinylated DNA, was very interesting, Figure 5.12 (a). These bright spots, not present in any other sample, were attributed to the formation of micelles with a fluorous interior and biotin corona bound to streptavidin molecules.(106) As such, it is postulated that the incorporation of tetra-C_8F_{17}-tags into the DNA nanostructures could lead to the capture of tetra-C_8F_{17}-tagged molecules from solution due to the enhanced fluorous effect these tags show.

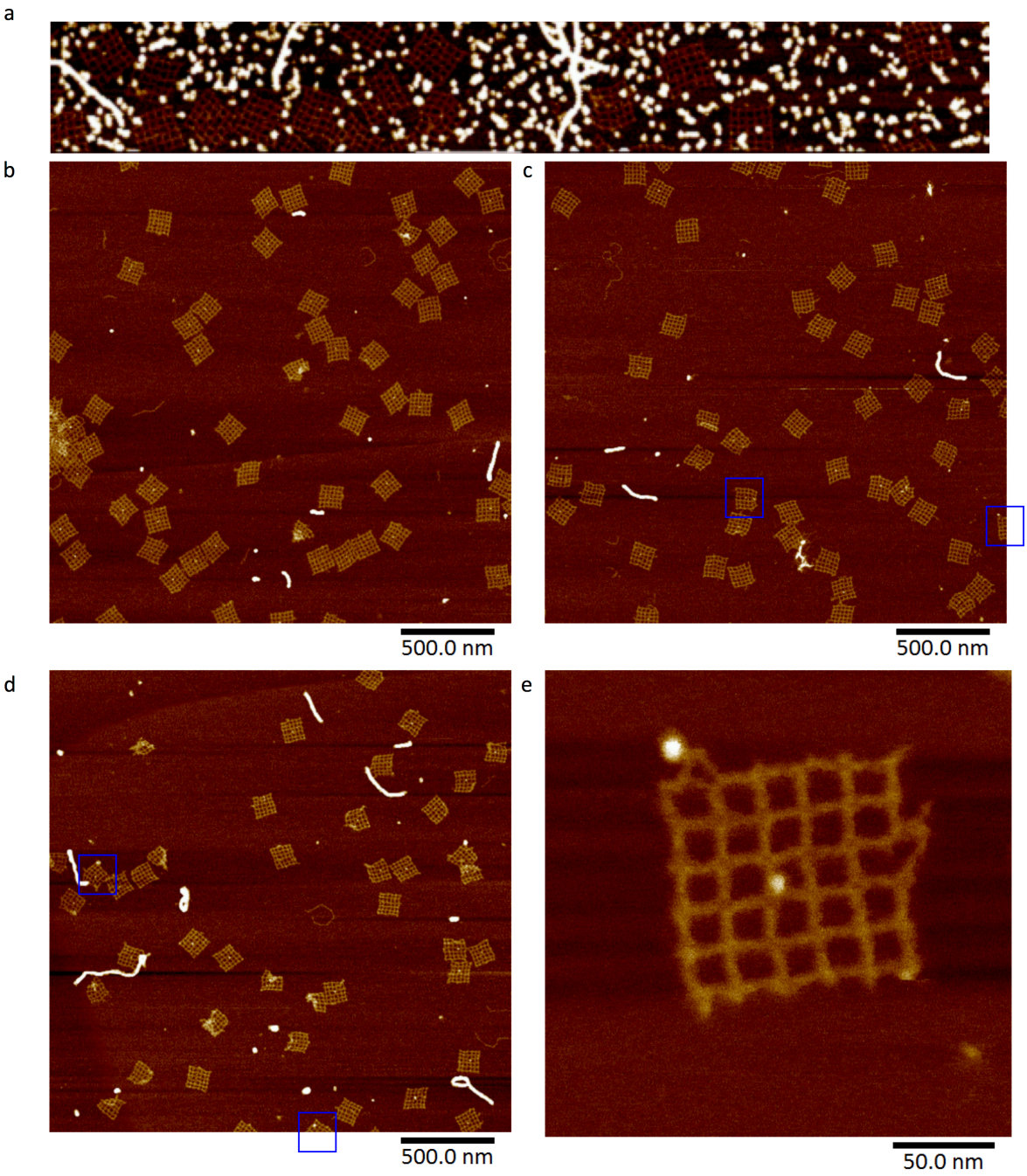

Figure 5-12 Investigation into the Feasibility of Capturing Fluorous-Tagged Molecules from Solution using the Fluorous-Tags Present on the DNA Nanostructure. (a) Incubation of DNS3-streptavidin with ATS53-streptavidin; (b) Incubation of DNS3-streptavidin with ATS52-streptavidin; (c) Incubation of DNS3-streptavidin with ATS51-streptavidin; (d) Control sample showing incubation of DNS1-streptavidin with ATS51-streptavidin; and (e) closer scan of DNS3-streptavidin with potentially captured ATS51-streptavidin. Blue squares represent DNA nanostructures with potentially capture fluorous-tagged molecules.

Table 5.2 Investigation into Feasibility of using the Fluorous Effect to Capture Fluorous-Tagged Molecules onto a DNA Nanostructure. Table shows the total number of nanostructures counted for each sample and the total number of structures with a bright spot where the fluorous-tag was and therefore potential captured fluorous-tagged molecule.

Nanostructure and fluorous-biotinylated DNA	Number of Nanostructures	Number of Nanostructures with captured fluorous-biotinylated DNA
DNS3 & ATS53	**42**	**Unknown**
DNS3 & ATS52	**102**	**0**
DNS3 & ATS51	**107**	**6**
DNS1 & ATS51 (control)	**60**	**3**

5.2.7.2 Fluorous-Tagged DNA & Hybridisation to DNA conjugated to a Nanoparticle.

Due to the inability of the fluorous modified DNA nanostructures to capture fluorous-tagged molecules from solution, an investigation was carried out as to whether fluorous-tagged DNA nanostructures could be captured onto the surface of a fluorinated nanoparticle, Figure 5.13 (a). It was postulated that the presence of multiple fluorous "ponytails" on the surface of the nanoparticle would act similar to that of a fluorinated solid support and therefore capture the DNA nanostructures. As such, Au nanoparticles were modified to have a fluorous surface by reacting them with a fluorinated thiol, synthesised in Dr Glenn Burleys group. However, this resulted in the nanoparticles aggregating in solution. Therefore, in order to circumvent this, DNA strands were modified to contain a thiol group at the 3' end and a fluorous tag at the 5' end, Figure 5.13 (b). However, again the nanoparticles were found to aggregate on the sides of Eppendorf tubes

and therefore incubation of the nanoparticles with fluorous modified DNA nanostructures could not be carried out.

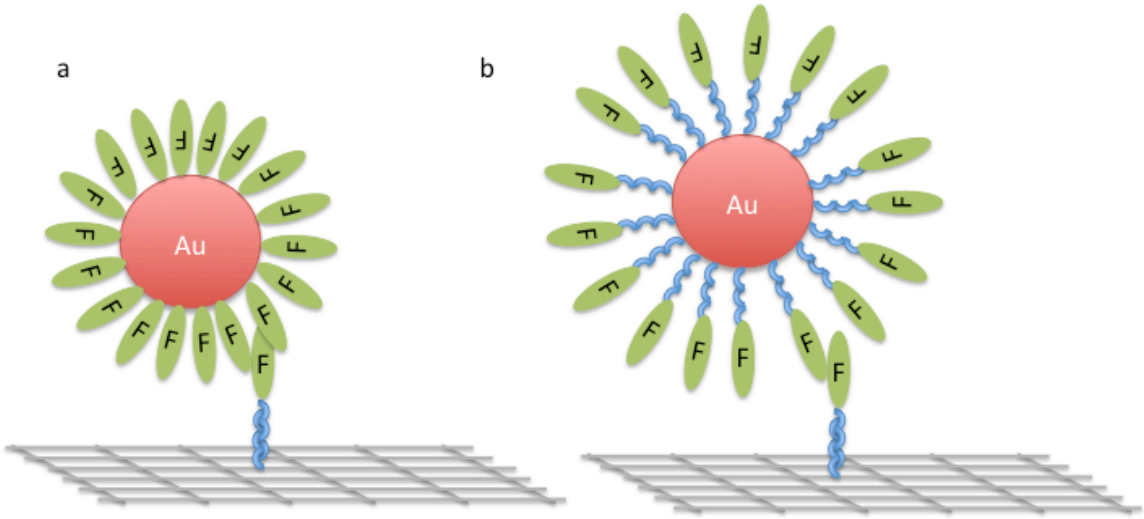

Figure 5-13 Schematic of the Proposed Method to Determine if the Fluorous Effect could be used to Capture Fluorous Modified DNA Nanostructures on Fluorous Modified Nanoparticles. Two methods were investigated (a) capture of nanoparticles modified with fluorous thiol; and (b) capture of nanoparticles modified with fluorous-modified thiolated DNA. Both methods resulted in the aggregation of the nanopartciles on the sides of the Eppendorf tube.

5.3 Conclusions & Future Work

In order to realise the many potential applications of DNA nanostructures, there needs to be control over the orientation of their immobilisation onto solid supports. Due to the results found in Chapter 3, it was postulated that the fluorous effect could be used to control the adsorption of fluorous modified DNA nanostructures on mica and silicon dioxide. Therefore, DNA nanostructures were successfully synthesised to contain a range of fluorous (mono-C_8F_{17}) tags and biotin motifs. The DNA nanostructures were then deposited onto both mica and SiO_2 surfaces where they were found to specifically adsorb onto the surface via the face opposite to the fluorous tags. It was found that only one fluorous tag on the structure was sufficient to influence the facial adsorption of the nanostructures onto the surfaces, with around 80 % of the structures being adsorbed via the face opposite to that modified with a fluorous tag. However, lower efficiencies were found on SiO_2 surfaces. This was attributed to the change in the buffer composition causing the streptavidin molecules to aggregate.

This work was then built on by testing the ability of the fluorous tags to capture fluorous-tagged molecules from solution. Unfortunately, it was found that the tags could not capture fluorous-tagged biotinylated DNA from solution. However, attachment of a tetra-C_8F_{17} ponytail resulted in the aggregation of the fluorous-tagged biotinylated DNA bound to a streptavidin molecule. Therefore, it is postulated that the incorporation of tetra-C_8F_{17} ponytails into the DNA nanostructures will allow it to capture fluorous molecules from solution.

Again, in order to determine if the fluorous effect could be used to capture fluorous modified particles onto the surface of fluorous modified DNA nanostructures, fluorous encapsulated Au nanoparticles were synthesised. However, the nanoparticles were found to aggregate in solution. In order to circumvent this, an ODN modified with a thiol group at the 3' end and a fluorous tag at the 5' end was synthesised. However, this also resulted in the aggregation of the nanoparticles in solution due to their hydrophobicity.

As stated, the fluorous effect resulting from one mono-C_8F_{17}-tag was insufficient to capture fluorous-tagged molecules from solution. However, it is postulated from the results found in this chapter that the use of a tetra-C_8F_{17}-tag could have a strong enough fluorous effect to capture tetra-C_8F_{17}-tagged molecules from

solution. Therefore, future work should focus on the synthesis of DNA nanostructures containing tetra-C_8F_{17}-tags in order to capture said molecules from solution. Furthermore, an investigation into the strength of the fluorous interaction could be carried out using fluorous modified DNA nanostructures and a fluorous modified cantilever.(155) Furthermore, the use of the fluorous effect to capture fluorous modified DNA nanostructures onto fluorinated solid supports in a reversible fashion could be another avenue of research, combining the work carried out in this chapter and the work from previous chapters.

6 Conclusions & Future Work

By tagging oligonucleotides (ODNs) with fluorous "ponytails", it was shown in this work that said strands could be specifically immobilised onto fluorinated solid supports in an arrangement that permits hybridisation to its complementary sequence. This immobilisation technique occurs through fluorous-fluorous interactions, and is due to its non-covalent nature. It was then demonstrated that by using a simple washing procedure, the fluorous-tagged ODNs could be removed from the solid support. This immobilisation and removal strategy has potential for the fabrication of reusable sensing platforms, and future work would be to test the design for the fabrication of a multiplexed DNA microarray, and determine the detection limits that the immobilisation chemistry permits.

Building on this work, it was found that by varying the fluorine content of the fluorous "ponytail" the fluorous-fluorous interaction could be tuned, with the higher the fluorine content, the stronger the interaction. This in turn required a more stringent washing procedure to remove the ODN via the fluorous tag. Using this, it was demonstrated in a preliminary study, that by immobilising two distinct ODN strands, with different fluorous tags, we could specifically remove one strand, leaving the other intact on the surface, depending on the methanol content of the wash. It was also apparent that the linker molecule, present between the fluorous "ponytail" and the ODN, had a strong effect on the hybridisation densities: it was

found that the longer the linker, and therefore the further the ODN was from the surface, the better the hybridisation capabilities. This work has the potential for the design of platforms that can allow for the separation and purification of, for example, PCR products on solid supports.

Finally, fluorous-tagged ODNs were incorporated into DNA nanostructures. This allowed for the immobilisation of the nanostructures, onto both mica and SiO_2, in a facially directed manner: the fluorous "ponytails" orientated the nanostructures so that they immobilised on the face opposite to the tags. This has the potential to be used as a means to specifically orientate DNA nanostructures onto solid supports. This would then permit bottom up self-assembly by providing a means to control the facial immobilisation of the nanostructures by ensuring that the functional groups are present on the solution facing side on the nanostructure.

An investigation into the capture of fluorous-tagged biotin onto the DNA nanostructures with incorporated fluorous "ponytails" was then carried out. Unfortunately, it was found that neither the mono-C_8F_{17} tag nor bis-C_8F_{17} tag was sufficient to capture the fluorous-tagged biotin from solution. This was attributed to the accumulative effect of fluorous-fluorous interactions, and as such there was not enough attraction between two single tags. It was also found the tetra-C_8F_{17} tagged biotin formed micelles in solution which could not be purified away from the nanostructures and therefore the AMF images obtained were not clear enough to determine if the fluorous-biotin had been captured onto the DNA nanostructures. Nevertheless, due to the formation of fluorous micelles, it is postulated that by incorporating tetra-C_8F_{17} tags into the DNA nanostructures themselves, and subsequently tagging the biotin with a tetra-C_8F_{17} tag, said biotin could be captured onto the nanostructures. Finally, due to the non-covalent nature of the fluorous-fluorous interaction, it is postulated that by tuning the concentration of the ions, specifically magnesium, in the buffer, a completely reversible system could be designed, allowing for the capture and release of molecules on DNA nanostructures. This would have potential applications as a means for drug delivery.

As the use of the fluorous effect as a means for attaching molecules to surfaces is still in its infancy, there are many other avenues of research that could be perused. For example, the fluorous effect could be used as a means to reversibly immobilise

DNA nanostructures onto fluorinated solid supports. The immobilisation of DNA nanostructures onto fluorinated supports has been carried out elsewhere.(156) However, this method utilised hydrophobic porphyrins to facilitate immobilisation onto the fluorinated solid support. Furthermore detailed AFM scans of the DNA nanostructures following immobilisation onto the solid support were not provided. Therefore following the immobilization of the structures onto the solid support, the structural integrity of the structures was not probed. A preliminary study carried out in this work showed that there was a change in the morphology of the DNA nanostructures following the immobilization of DNA nanostructures, with 13 fluorous tags incorporated into the structure, onto a fluorinated solid support, Figure 6.1. As such, more work needs to be carried out to determine why this occurred, and explore possible methods to stabilise the structures following their immobilisation onto solid supports.

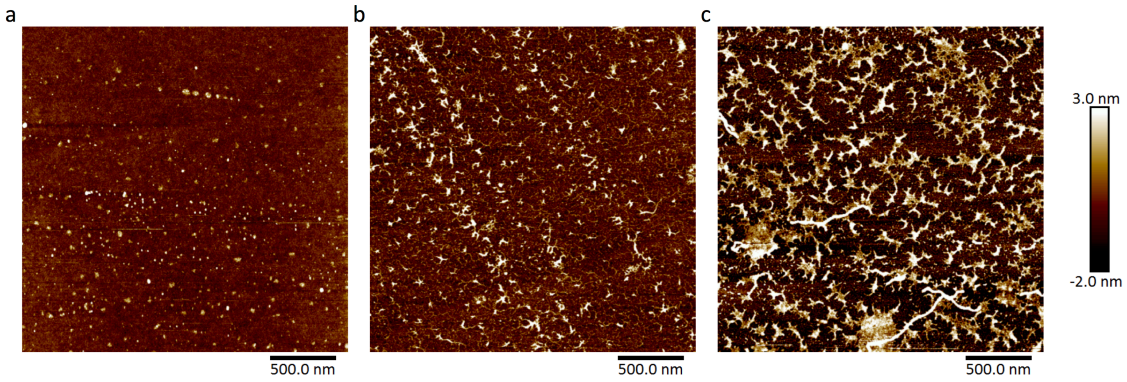

Figure 6-1 Immobilisation of Fluorous Tagged DNA nanostructures onto Fluorinated Solid Supports. (a) AFM image of fluorinated solid support before immobilisation of DNA nanostructures; (b) AFM image of fluorinated solid support following the immobilisation of DNS12 (no fluorous ponytails); and (c) AFM image of fluorinated solid support following the immobilisation of DNS13 (13 fluorous ponytails).

7 Appendices

APPENDIX 1 MODIFIED ODN STRANDS USED FOR THE SYNTHESIS OF DNA NANOSTRUCTURES

Attachment	Name	Sequence 5' to 3'
Fluorous 5'	A1 107F	TTTTATCGAGAACCAATTACCTGAGCAAAAGAAGAGTACCGCACTC
	C1 132F	TTTTACAAAAGGTTGAGAAGAGTCAATAGTGAATTATAAAGTACCG
	E1 47F	TTTTAAATAAGAACCGTGTGATAAATATAGCAAACG
	B2 158F	TTTTTTTTCATAACCAGAATGGAAAGCGCAGTCTGCGTTTGCCATC
	D2 146F	TTTTCACCGACTTGGATTAGGATTAGCGGGGTTTAATTATCACCGT
	C3 178F	TTTTTTGAGGATTTTCACCAGTCACACGACCAGTTAGATAATACAT
	A3 185F	TTTTTTCTGAATAAGTCTGTCCATCACGCAAATTTTTGGATTATAC
	E3 170F	TTTTGTCACCAGATGTACCGTAACACTACCGCCTG
	D4 32F	TTTTTTCACGTTGATATTCATTACCCAAATCAACAATAATAATTTT
	B4 84F	TTTTCCTCAGCAGAAAGTACAACGGAGATTTGTACGGGATCGTCAC
	A5 64F	TTTTGCGCGTAACGTGCCAAGCTTGCATGCCTGCAGCGGTCACGCT

	C5 123F	TTTTAACCGTCTAGAGTGAGCTAACTCACATTAACAAAGGGC GAAA
	E5 73F	TTTTACATTATTAATAAAACGAACTAACCTTCACC
	E1 48 new:	TAGAAAATTATTACGCAGTATGTAGGCGTT
5'Biotin	C3 178F Biotin	TTTTTTGAGGATTTTCACCAGTCACACGACCAGTTAGATAAT ACAT
5'Biotin	C3 Biotin 152	TTTTGCAGCACCGTAATCCCTTGAGTAACAGTGCCCGTAATC GATA
5' Fluorous	Fluorou s oligo	ATTATTATTATTATTATT
5'thiol	NP cDNA	AATAATAATAATAATAAT

8 REFERENCES

1. Watson JD, Crick FHC. Molecular Structure of Nucleic Acids: A Structure for Deoxyribose Nucleic Acid. Nature. 1953;171:737.

2. Alberts B JA, Lewis J, et al. The Structure and Function of DNA. Molecular Biology of the Cell. 4th ed. New York: Garland Science; 2002.

3. Seeman NC. DNA in a material world. Nature. 2003;421(6921):427-31.

4. Ito Y, Fukusaki E. DNA as a 'Nanomaterial'. Journal of Molecular Catalysis B: Enzymatic. 2004;28(4–6):155-66.

5. Arber W. Host-Controlled Modification of Bacteriophage. Annual Review of Microbiology. 1965;19(1):365-78.

6. Broker TR, Lehman IR. Branched DNA molecules: Intermediates in T4 recombination. Journal of Molecular Biology. 1971;60(1):131-49.

7. Seeman NC. Nucleic acid junctions and lattices. Journal of Theoretical Biology. 1982;99(2):237-47.

8. Williams S, Lund K, Lin C, Wonka P, Lindsay S, Yan H. Tiamat: A Three-Dimensional Editing Tool for Complex DNA Structures. In: Goel A, Simmel FC, Sosík P, editors. DNA Computing: 14th International Meeting on DNA Computing, DNA 14, Prague, Czech Republic, June 2-9, 2008 Revised Selected Papers. Berlin, Heidelberg: Springer Berlin Heidelberg; 2009. p. 90-101.

9. Rothemund PWK. Folding DNA to create nanoscale shapes and patterns. Nature. 2006;440:297.

10. Zhang X, Hu H. DNA molecules site-specific immobilization and their applications. Central European Journal of Chemistry. 2014;12(10):977-93.

11. Wittmann C, Alegret S, SpringerLink. Immobilisation of DNA on chips. New York;Berlin;: Springer; 2005.

12. Taylor S, Smith S, Windle B, Guiseppi-Elie A. Impact of surface chemistry and blocking strategies on DNA microarrays. Nucleic Acids Research. 2003;31(16):e87-e.

13. Zhang X, Xu W, Tan J, Zeng Y. Stripping custom microRNA microarrays and the lessons learned about probe:slide interactions. Analytical biochemistry. 2009;386(2):222-7.

14. Tjong V, Tang L, Zauscher S, Chilkoti A. "Smart" DNA interfaces. Chemical Society Reviews. 2014;43(5):1612-26.

15. Wittmann C, Marquette C. DNA Immobilization. Encyclopedia of Analytical Chemistry: John Wiley & Sons, Ltd; 2006.

16. Niemeyer CM, Boldt L, Ceyhan B, Blohm D. DNA-Directed Immobilization: Efficient, Reversible, and Site-Selective Surface Binding of Proteins by Means of Covalent DNA–Streptavidin Conjugates. Analytical Biochemistry. 1999;268(1):54-63.

17. Huang F, Xu H, Tan W, Liang H. Multicolor and Erasable DNA Photolithography. ACS Nano. 2014;8(7):6849-55.

18. Shin D-S, Hyun Seo J, Sutcliffe JL, Revzin A. Photolabile micropatterned surfaces for cell capture and release. Chemical Communications. 2011;47(43):11942-4.

19. Kim J, Hayward RC. Mimicking dynamic in vivo environments with stimuli-responsive materials for cell culture. Trends in Biotechnology.30(8):426-39.

20. Kim D, Herr AE. Protein immobilization techniques for microfluidic assays. Biomicrofluidics. 2013;7(4):041501.

21. Cui J, Miguel VS, del Campo A. Light-Triggered Multifunctionality at Surfaces Mediated by Photolabile Protecting Groups. Macromolecular Rapid Communications. 2013;34(4):310-29.

22. Yamaguchi S, Yamahira S, Kikuchi K, Sumaru K, Kanamori T, Nagamune T. Photocontrollable Dynamic Micropatterning of Non-adherent Mammalian Cells Using a Photocleavable Poly(ethylene glycol) Lipid. Angewandte Chemie International Edition. 2012;51(1):128-31.

23. Nakanishi J, Kikuchi Y, Takarada T, Nakayama H, Yamaguchi K, Maeda M. Photoactivation of a Substrate for Cell Adhesion under Standard Fluorescence Microscopes. Journal of the American Chemical Society. 2004;126(50):16314-5.

24. Agasti SS, Chompoosor A, You C-C, Ghosh P, Kim CK, Rotello VM. Photoregulated Release of Caged Anticancer Drugs from Gold Nanoparticles. Journal of the American Chemical Society. 2009;131(16):5728-9.

25. Brieke C, Rohrbach F, Gottschalk A, Mayer G, Heckel A. Light-Controlled Tools. Angewandte Chemie International Edition. 2012;51(34):8446-76.

26. Klán P, Šolomek T, Bochet CG, Blanc A, Givens R, Rubina M, et al. Photoremovable Protecting Groups in Chemistry and Biology: Reaction Mechanisms and Efficacy. Chemical Reviews. 2013;113(1):119-91.

27. He M, Herr AE. Automated microfluidic protein immunoblotting. Nature Protocols. 2010;5:1844.

28. Ovsejevi K, Manta C, Batista-Viera F. Reversible Covalent Immobilization of Enzymes via Disulfide Bonds. In: Guisan JM, editor. Immobilization of Enzymes and Cells: Third Edition. Totowa, NJ: Humana Press; 2013. p. 89-116.

29. Arumugam S, Popik VV. Attach, Remove, or Replace: Reversible Surface Functionalization Using Thiol–Quinone Methide Photoclick Chemistry. Journal of the American Chemical Society. 2012;134(20):8408-11.

30. Gandavarapu NR, Azagarsamy MA, Anseth KS. Photo-Click Living Strategy for Controlled, Reversible Exchange of Biochemical Ligands. Advanced Materials. 2014;26(16):2521-6.

31. Du X, Li J, Welle A, Li L, Feng W, Levkin PA. Reversible and Rewritable Surface Functionalization and Patterning via Photodynamic Disulfide Exchange. Advanced Materials. 2015;27(34):4997-5001.

32. Choi I, Bae SW, Yeo W-S. Recyclable Surfaces for Amine Conjugation Chemistry via Redox Reaction. Bulletin of the Korean Chemical Society. 2017;38(2):296-9.

33. Yakovleva J, Davidsson R, Bengtsson M, Laurell T, Emnéus J. Microfluidic enzyme immunosensors with immobilised protein A and G using chemiluminescence detection. Biosensors and Bioelectronics. 2003;19(1):21-34.

34. Liébana S, Drago Guido A. Bioconjugation and stabilisation of biomolecules in biosensors. Essays in Biochemistry. 2016;60(1):59-68.

35. Bhattacharyya A, Klapperich CM. Design and testing of a disposable microfluidic chemiluminescent immunoassay for disease biomarkers in human serum samples. Biomedical Microdevices. 2006;9(2):245.

36. Ko K-S, Jaipuri FA, Pohl NL. Fluorous-Based Carbohydrate Microarrays. Journal of the American Chemical Society. 2005;127(38):13162-3.

37. Nicholson RL, Ladlow ML, Spring DR. Fluorous tagged small molecule microarrays. Chemical Communications. 2007(38):3906-8.

38. Horváth IT, Rábai J. Facile Catalyst Separation Without Water: Fluorous Biphase Hydroformylation of Olefins. Science. 1994;266(5182):72-5.

39. Gladysz JA, Curran DP. Fluorous chemistry: from biphasic catalysis to a parallel chemical universe and beyond. Tetrahedron. 2002;58(20):3823-5.

40. Gladysz JA, Jurisch M. Structural, Physical, and Chemical Properties of Fluorous Compounds. In: Horváth IT, editor. Fluorous Chemistry. Berlin, Heidelberg: Springer Berlin Heidelberg; 2012. p. 1-23.

41. Studer A, Hadida S, Ferritto R, Kim S-Y, Jeger P, Wipf P, et al. Fluorous Synthesis: A Fluorous-Phase Strategy for Improving Separation Efficiency in Organic Synthesis. Science. 1997;275(5301):823-6.

42. Studer A, Curran DP. A strategic alternative to solid phase synthesis: Preparation of a small isoxazoline library by “fluorous synthesis”. Tetrahedron. 1997;53(19):6681-96.

43. Studer A, Jeger P, Wipf P, Curran DP. Fluorous Synthesis: Fluorous Protocols for the Ugi and Biginelli Multicomponent Condensations. The Journal of Organic Chemistry. 1997;62(9):2917-24.

44. Curran DP, Ferritto R, Hua Y. Preparation of a fluorous benzyl protecting group and its use in fluorous synthesis approach to a disaccharide. Tetrahedron Letters. 1998;39(28):4937-40.

45. Curran DP, Hadida S, He M. Thermal Allylations of Aldehydes with a Fluorous Allylstannane. Separation of Organic and Fluorous Products by Solid Phase Extraction with Fluorous Reverse Phase Silica Gel. The Journal of Organic Chemistry. 1997;62(20):6714-5.

46. Curran DP, Luo Z. Fluorous Synthesis with Fewer Fluorines (Light Fluorous Synthesis): Separation of Tagged from Untagged Products by Solid-Phase Extraction with Fluorous Reverse-Phase Silica Gel. Journal of the American Chemical Society. 1999;121(39):9069-72.

47. Brittain SM, Ficarro SB, Brock A, Peters EC. Enrichment and analysis of peptide subsets using fluorous affinity tags and mass spectrometry. Nat Biotech. 2005;23(4):463-8.

48. Nakamura Y, Takeuchi S, Ohgo Y, Curran DP. Asymmetric alkylation of aromatic aldehydes with diethylzinc catalyzed by a fluorous BINOL–Ti complex in an organic and fluorous biphase system. Tetrahedron Letters. 2000;41(1):57-60.

49. Luo Z, Zhang Q, Oderaotoshi Y, Curran DP. Fluorous Mixture Synthesis: A Fluorous-Tagging Strategy for the Synthesis and Separation of Mixtures of Organic Compounds. Science. 2001;291(5509):1766-9.

50. Trevino V, Falciani F, Barrera-Saldaña HA. DNA microarrays: a powerful genomic tool for biomedical and clinical research. Molecular Medicine. 2007;13(9-10):527-41.

51. Cutler DJ, Zwick ME, Carrasquillo MM, Yohn CT, Tobin KP, Kashuk C, et al. High-Throughput Variation Detection and Genotyping Using Microarrays. Genome Research. 2001;11(11):1913-25.

52. Wang D, Coscoy L, Zylberberg M, Avila PC, Boushey HA, Ganem D, et al. Microarray-based detection and genotyping of viral pathogens. Proceedings of the National Academy of Sciences of the United States of America. 2002;99(24):15687-92.

53. Sedighi A, Li PCH. Chapter 2 - Challenges and Future Trends in DNA Microarray Analysis. In: Simó C, Cifuentes A, García-Cañas V, editors. Comprehensive Analytical Chemistry. 63: Elsevier; 2014. p. 25-46.

54. Bumgarner R. DNA microarrays: Types, Applications and their future. Current protocols in molecular biology / edited by Frederick M Ausubel [et al]. 2013;0 22:Unit-22.1.

55. Tong X, Smith L. Solid-phase method for the purification of DNA sequencing reactions. Analytical Chemistry. 1992;64(22):2672-7.

56. Claridge SA, Goh SL, Fréchet JMJ, Williams SC, Micheel CM, Alivisatos AP. Directed Assembly of Discrete Gold Nanoparticle Groupings Using Branched DNA Scaffolds. Chemistry of Materials. 2005;17(7):1628-35.

57. Mirkin CA, Letsinger RL, Mucic RC, Storhoff JJ. A DNA-based method for rationally assembling nanoparticles into macroscopic materials. Nature. 1996;382(6592):607-9.

58. Qin WJ, Yung LYL. Efficient Manipulation of Nanoparticle-Bound DNA via Restriction Endonuclease. Biomacromolecules. 2006;7(11):3047-51.

59. Sterman S, Marsden JG. Silane Coupling Agents. Industrial & Engineering Chemistry. 1966;58(3):33-7.

60. Britt DW, Hlady V. Protonation, Hydrolysis, and Condensation of Mono- and Trifunctional Silanes at the Air/Water Interface. Langmuir. 1999;15(5):1770-6.

61. Krasnoslobodtsev AV, Smirnov SN. Effect of Water on Silanization of Silica by Trimethoxysilanes. Langmuir. 2002;18(8):3181-4.

62. Levinson HJ, Society of Photo-optical Instrumentation E. Principles of lithography. 3rd ed. Bellingham, Wash. (1000 20th St. Bellingham WA 98225-6705 USA): SPIE; 2010.

63. Cui Z. Nanofabrication by Electron Beam. Nanofabrication: Principles, Capabilities and Limits. Cham: Springer International Publishing; 2017. p. 91-148.

64. Zhang F, Jiang S, Wu S, Li Y, Mao C, Liu Y, et al. Complex wireframe DNA origami nanostructures with multi-arm junction vertices. Nat Nano. 2015;10(9):779-84.

65. Hansma HG, Vesenka J, Siegerist C, Kelderman G, Morrett H, Sinsheimer RL, et al. Reproducible Imaging and Dissection of Plasmid DNA Under Liquid with the Atomic Force Microscope. Science. 1992;256(5060):1180-4.

66. Yang J, Takeyasu K, Shao Z. Atomic force microscopy of DNA molecules. FEBS Letters. 1992;301(2):173-6.

67. Gopinath A, Rothemund PWK. Optimized Assembly and Covalent Coupling of Single-Molecule DNA Origami Nanoarrays. ACS Nano. 2014;8(12):12030-40.

68. Harwood AJ. Native Polyacrylamide Gel Electrophoresis. In: Harwood AJ, editor. Basic DNA and RNA Protocols. Totowa, NJ: Humana Press; 1996. p. 93-6.

69. Summer H, Grämer R, Dröge P. Denaturing Urea Polyacrylamide Gel Electrophoresis (Urea PAGE). Journal of Visualized Experiments : JoVE. 2009(32):1485.

70. Ryan J, Gerhold AR, Boudreau V, Smith L, Maddox PS. Introduction to Modern Methods in Light Microscopy. In: Markaki Y, Harz H, editors. Light Microscopy: Methods and Protocols. New York, NY: Springer New York; 2017. p. 1-15.

71. Tkaczyk TS, Society of Photo-optical Instrumentation E. Field guide to microscopy. Bellingham, Wash. (1000 20th St. Bellingham WA 98225-6705 USA): SPIE; 2010.

72. Waters JC. Accuracy and precision in quantitative fluorescence microscopy. The Journal of Cell Biology. 2009;185(7):1135-48.

73. Sauerbrey G. Verwendung von Schwingquarzen zur Wägung dünner Schichten und zur Mikrowägung. Zeitschrift für Physik. 1959;155(2):206-22.

74. Binning G, Rohrer H, Gerber C, Weibel E. Surface Studies by Scanning Tunneling Microscopy. In: Neddermeyer H, editor. Scanning Tunneling Microscopy. Dordrecht: Springer Netherlands; 1993. p. 31-5.

75. Jaggi N, Vij DR. Fouier Transform Infrared Spectroscopy. In: Vij DR, editor. Handbook of Applied Solid State Spectroscopy. Boston, MA: Springer US; 2006. p. 411-50.

76. Law K-Y, Zhao H. Contact Angle Measurements and Surface Characterization Techniques. Surface Wetting: Characterization, Contact Angle, and Fundamentals. Cham: Springer International Publishing; 2016. p. 7-34.

77. Scanning Electron Microscopy for the Life Sciences. Cambridge: Cambridge University Press; 2012.

78. Nimse SB, Song K, Sonawane MD, Sayyed DR, Kim T. Immobilization Techniques for Microarray: Challenges and Applications. Sensors (Basel, Switzerland). 2014;14(12):22208-29.

79. Fustero S, Aceña JL, Catalán S. Synthetic and Biological Applications of Fluorous Reagents as Phase Tags. In: Horváth IT, editor. Fluorous Chemistry. Berlin, Heidelberg: Springer Berlin Heidelberg; 2012. p. 45-67.

80. Wang D, Liu S, Trummer BJ, Deng C, Wang A. Carbohydrate microarrays for the recognition of cross-reactive molecular markers of microbes and host cells. Nat Biotech. 2002;20(3):275-81.

81. Fukui S, Feizi T, Galustian C, Lawson AM, Chai W. Oligosaccharide microarrays for high-throughput detection and specificity assignments of carbohydrate-protein interactions. Nat Biotech. 2002;20(10):1011-7.

82. Mamidyala SK, Ko K-S, Jaipuri FA, Park G, Pohl NL. Noncovalent fluorous interactions for the synthesis of carbohydrate microarrays. Journal of Fluorine Chemistry. 2006;127(4):571-9.

83. Vegas AJ, Bradner JE, Tang W, McPherson OM, Greenberg EF, Koehler AN, et al. Fluorous-Based Small-Molecule Microarrays for the Discovery of Histone Deacetylase Inhibitors. Angewandte Chemie International Edition. 2007;46(42):7960-4.

84. Collet BYM, Nagashima T, Yu MS, Pohl NLB. Fluorous-based peptide microarrays for protease screening. Journal of Fluorine Chemistry. 2009;130(11):1042-8.

85. Li B-Y, Juang DS, Adak AK, Hwang K-C, Lin C-C. Fabrication of a protein microarray by fluorous-fluorous interactions. Scientific Reports. 2017;7(1):7053.

86. Horváth IT, Curran DP, Gladysz JA. Fluorous Chemistry: Scope and Definition. Handbook of Fluorous Chemistry: Wiley-VCH Verlag GmbH & Co. KGaA; 2005. p. 1-4.

87. Kobrin B, Zhang T, Grimes MT, Chong K, Wanebo M, Chinn J, et al. An Improved Chemical Resistance and Mechanical Durability of Hydrophobic FDTS Coatings. Journal of Physics: Conference Series. 2006;34(1):454.

88. Hsu SL, Reynolds N, Bohan SP, Strauss HL, Snyder RG. Structure, crystallization, and infrared spectra of amorphous perfluoro-n-alkane films prepared by vapor condensation. Macromolecules. 1990;23(21):4565-75.

89. Gonzalez-Benito J, Cabanelas JC, Aznar AJ, Vigil MR, Bravo J, Baselga J. Surface characterization of silanized glass fibers by labeling with environmentally sensitive fluorophores. Journal of Applied Polymer Science. 1996;62(2):375-84.

90. Xu D, Sun L, Li H, Zhang L, Guo G, Zhao X, et al. Hydrolysis and silanization of the hydrosilicon surface of freshly prepared porous silicon by an amine catalytic reaction. New Journal of Chemistry. 2003;27(2):300-6.

91. Rabolt JF, Fanconi B. Raman Scattering from Finite Polytetrafluoroethylene Chains and a Highly Oriented TFE-HFP Copolymer Monofilament. Macromolecules. 1978;11(4):740-5.

92. Pan Z, Zhang W, Kowalski A, Zhao B. Oleophobicity of Biomimetic Micropatterned Surface and Its Effect on the Adhesion of Frozen Oil. Langmuir. 2015;31(36):9901-10.

93. Devaprakasam D, Sampath S, Biswas SK. Thermal Stability of Perfluoroalkyl Silane Self-Assembled on a Polycrystalline Aluminum Surface. Langmuir. 2004;20(4):1329-34.

94. Caruso F, Rodda E, Furlong DN, Niikura K, Okahata Y. Quartz Crystal Microbalance Study of DNA Immobilization and Hybridization for Nucleic Acid Sensor Development. Analytical Chemistry. 1997;69(11):2043-9.

95. Okahata Y, Matsunobu Y, Ijiro K, Mukae M, Murakami A, Makino K. Hybridization of nucleic acids immobilized on a quartz crystal microbalance. Journal of the American Chemical Society. 1992;114(21):8299-300.

96. Caruso F, Furlong DN, Niikura K, Okahata Y. In-situ measurement of DNA immobilization and hybridization using a 27MHz quartz crystal microbalance. Colloids and Surfaces B: Biointerfaces. 1998;10(4):199-204.

97. Zhou XC, Huang LQ, Li SFY. Microgravimetric DNA sensor based on quartz crystal microbalance: comparison of oligonucleotide immobilization methods and the application in genetic diagnosis. Biosensors and Bioelectronics. 2001;16(1):85-95.

98. Dixon MC. Quartz Crystal Microbalance with Dissipation Monitoring: Enabling Real-Time Characterization of Biological Materials and Their Interactions. Journal of Biomolecular Techniques : JBT. 2008;19(3):151-8.

99. Papadakis G, Tsortos A, Gizeli E. Acoustic Characterization of Nanoswitch Structures: Application to the DNA Holliday Junction. Nano Letters. 2010;10(12):5093-7.

100. Papadakis G, Tsortos A, Bender F, Ferapontova EE, Gizeli E. Direct Detection of DNA Conformation in Hybridization Processes. Analytical Chemistry. 2012;84(4):1854-61.

101. Dunn KE, Trefzer MA, Johnson S, Tyrrell AM. Investigating the dynamics of surface-immobilized DNA nanomachines. 2016;6:29581.

102. Keiji Kanazawa K, Gordon JG. The oscillation frequency of a quartz resonator in contact with liquid. Analytica Chimica Acta. 1985;175:99-105.

103. Smith SB, Cui Y, Bustamante C. Overstretching B-DNA: The Elastic Response of Individual Double-Stranded and Single-Stranded DNA Molecules. Science. 1996;271(5250):795-9.

104. Rodahl M, Hook F, Fredriksson C, A. Keller C, Krozer A, Brzezinski P, et al. Simultaneous frequency and dissipation factor QCM measurements of biomolecular adsorption and cell adhesion. Faraday Discussions. 1997;107(0):229-46.

105. Sundh M, Svedhem S, Sutherland DS. Influence of phase separating lipids on supported lipid bilayer formation at SiO2 surfaces. Physical Chemistry Chemical Physics. 2010;12(2):453-60.

106. de Rochambeau D, Barlog M, Edwardson TGW, Fakhoury JJ, Stein RS, Bazzi HS, et al. "DNA-Teflon" sequence-controlled polymers. Polymer Chemistry. 2016;7(31):4998-5003.

107. Slavin S, Soeriyadi AH, Voorhaar L, Whittaker MR, Becer CR, Boyer C, et al. Adsorption behaviour of sulfur containing polymers to gold surfaces using QCM-D. Soft Matter. 2012;8(1):118-28.

108. Cho N-J, Frank CW, Kasemo B, Hook F. Quartz crystal microbalance with dissipation monitoring of supported lipid bilayers on various substrates. Nat Protocols. 2010;5(6):1096-106.

109. Rozkiewicz DI, Gierlich J, Burley GA, Gutsmiedl K, Carell T, Ravoo BJ, et al. Transfer Printing of DNA by "Click" Chemistry. ChemBioChem. 2007;8(16):1997-2002.

110. Singh I, Wendeln C, Clark AW, Cooper JM, Ravoo BJ, Burley GA. Sequence-Selective Detection of Double-Stranded DNA Sequences Using Pyrrole–Imidazole Polyamide Microarrays. Journal of the American Chemical Society. 2013;135(9):3449-57.

111. Höök F, Rodahl M, Brzezinski P, Kasemo B. Energy Dissipation Kinetics for Protein and Antibody−Antigen Adsorption under Shear Oscillation on a Quartz Crystal Microbalance. Langmuir. 1998;14(4):729-34.

112. Castronovo M, Radovic S, Grunwald C, Casalis L, Morgante M, Scoles G. Control of Steric Hindrance on Restriction Enzyme Reactions with Surface-Bound DNA Nanostructures. Nano Letters. 2008;8(12):4140-5.

113. Hyun J, Kim J, Craig SL, Chilkoti A. Enzymatic Nanolithography of a Self-Assembled Oligonucleotide Monolayer on Gold. Journal of the American Chemical Society. 2004;126(15):4770-1.

114. Kaufmann R, Peled D, Naaman R, Daube SS. Three-Dimensional Surface Patterning by DNA-Modifying Enzymes. ACS Applied Materials & Interfaces. 2009;1(10):2320-4.

115. Schroeder MM, Wang Q, Badieyan S, Chen Z, Marsh ENG. Effect of Surface Crowding and Surface Hydrophilicity on the Activity, Stability and Molecular Orientation of a Covalently Tethered Enzyme. Langmuir. 2017;33(28):7152-9.

116. Lubin AA, Lai RY, Baker BR, Heeger AJ, Plaxco KW. Sequence-Specific, Electronic Detection of Oligonucleotides in Blood, Soil, and Foodstuffs with the Reagentless, Reusable E-DNA Sensor. Analytical Chemistry. 2006;78(16):5671-7.

117. Pohl NL. Fluorous Tags Catching on Microarrays. Angewandte Chemie International Edition. 2008;47(21):3868-70.

118. Xue Y, Li X, Li H, Zhang W. Quantifying thiol–gold interactions towards the efficient strength control. 2014;5:4348.

119. Edwards HD, Nagappayya SK, Pohl NLB. Probing the limitations of the fluorous content for tag-mediated microarray formation. Chemical Communications. 2012;48(4):510-2.

120. Ravishankara AR, Solomon S, Turnipseed AA, Warren RF. Atmospheric Lifetimes of Long-Lived Halogenated Species. Science. 1993;259(5092):194-9.

121. Lopez-Espinosa M-J, Fletcher T, Armstrong B, Genser B, Dhatariya K, Mondal D, et al. Association of Perfluorooctanoic Acid (PFOA) and Perfluorooctane Sulfonate (PFOS) with Age of Puberty among Children Living near a Chemical Plant. Environmental Science & Technology. 2011;45(19):8160-6.

122. Loi EIH, Yeung LWY, Taniyasu S, Lam PKS, Kannan K, Yamashita N. Trophic Magnification of Poly- and Perfluorinated Compounds in a Subtropical Food Web. Environmental Science & Technology. 2011;45(13):5506-13.

123. Yu MS. Chemical Applications of Fluorous Reagents and Scavengers. In: Horváth IT, editor. Fluorous Chemistry. Berlin, Heidelberg: Springer Berlin Heidelberg; 2012. p. 69-104.

124. Zhang W, Luo Z, Chen CH-T, Curran DP. Solution-Phase Preparation of a 560-Compound Library of Individual Pure Mappicine Analogues by Fluorous Mixture Synthesis. Journal of the American Chemical Society. 2002;124(35):10443-50.

125. Curran DP, Furukawa T. Simultaneous Preparation of Four Truncated Analogues of Discodermolide by Fluorous Mixture Synthesis. Organic Letters. 2002;4(13):2233-5.

126. Henry SL, Withers JM, Singh I, Cooper JM, Clark AW, Burley GA, et al. DNA-directed spatial assembly of photosynthetic light-harvesting proteins. Organic & Biomolecular Chemistry. 2016;14(4):1359-62.

127. Kwak M, Herrmann A. Nucleic acid amphiphiles: synthesis and self-assembled nanostructures. Chemical Society Reviews. 2011;40(12):5745-55.

128. Beller C, Bannwarth W. Noncovalent Attachment of Nucleotides by Fluorous-Fluorous Interactions: Application to a Simple Purification Principle for Synthetic DNA Fragments. Helvetica Chimica Acta. 2005;88(1):171-9.

129. Oka N, Murakami R, Kondo T, Wada T. Stereocontrolled synthesis of dinucleoside phosphorothioates using a fluorous tag. Journal of Fluorine Chemistry. 2013;150(Supplement C):85-91.

130. Hong M, Zhou X, Lu Z, Zhu J. Nanoparticle-Based, Fluorous-Tag-Driven DNA Detection. Angewandte Chemie International Edition. 2009;48(50):9503-6.

131. Bondi A. van der Waals Volumes and Radii. The Journal of Physical Chemistry. 1964;68(3):441-51.

132. Williams DE. Fluorine nonbonded potential parameters derived from crystalline perfluorocarbons. Acta Crystallographica Section B. 1986;3(42):286-95.

133. Lockhart DJ, Dong H, Byrne MC, Follettie MT, Gallo MV, Chee MS, et al. Expression monitoring by hybridization to high-density oligonucleotide arrays. Nat Biotech. 1996;14(13):1675-80.

134. Peterson AW, Heaton RJ, Georgiadis RM. The effect of surface probe density on DNA hybridization. Nucleic Acids Research. 2001;29(24):5163-8.

135. Southern E, Mir K, Shchepinov M. Molecular interactions on microarrays. Nat Genet.

136. Mir KU, Southern EM. Determining the influence of structure on hybridization using oligonucleotide arrays. Nat Biotech. 1999;17(8):788-92.

137. Koltai H, Weingarten-Baror C. Specificity of DNA microarray hybridization: characterization, effectors and approaches for data correction. Nucleic Acids Research. 2008;36(7):2395-405.

138. Glatz H, Blay C, Engelhardt H, Bannwarth W. New Fluorous Reversed Phase Silica Gels for HPLC Separations of Perfluorinated Compounds. Chromatographia. 2004;59(9):567-70.

139. Jian H, Tour JM. Preparative Fluorous Mixture Synthesis of Diazonium-Functionalized Oligo(phenylene vinylene)s. The Journal of Organic Chemistry. 2005;70(9):3396-424.

140. de Miguel I, Exbrayat S, Samain D. Study of the selective retention of fluorinated compounds on perfluorinated stationary phases. Chromatographia. 1987;24(1):849-53.

141. Hatanaka K. Incorporation of Fluorous Glycosides to Cell Membrane and Saccharide Chain Elongation by Cellular Enzymes. In: Horváth IT, editor. Fluorous Chemistry. Berlin, Heidelberg: Springer Berlin Heidelberg; 2012. p. 291-306.

142. Musumeci D, Montesarchio D. Synthesis of a cholesteryl-HEG phosphoramidite derivative and its application to lipid-conjugates of the anti-HIV 5'TGGGAG³' Hotoda's sequence. Molecules. 2012;17(10):12378.

143. Gerdon AE, Oh SS, Hsieh K, Ke Y, Yan H, Soh HT. Controlled Delivery of DNA Origami on Patterned Surfaces. Small. 2009;5(17):1942-6.

144. Kim KN, Sarveswaran K, Mark L, Lieberman M. Comparison of methods for orienting and aligning DNA origami. Soft Matter. 2011;7(10):4636-43.

145. Wu N, Czajkowsky DM, Zhang J, Qu J, Ye M, Zeng D, et al. Molecular Threading and Tunable Molecular Recognition on DNA Origami Nanostructures. Journal of the American Chemical Society. 2013;135(33):12172-5.

146. Saccà B, Meyer R, Erkelenz M, Kiko K, Arndt A, Schroeder H, et al. Orthogonal Protein Decoration of DNA Origami. Angewandte Chemie International Edition. 2010;49(49):9378-83.

147. Horňáková V, Přibyl J, Skládal P. Study of DNA immobilization on mica surface by atomic force microscopy. Monatshefte für Chemie - Chemical Monthly. 2016;147(5):865-71.

148. Rothemund PWK. Folding DNA to create nanoscale shapes and patterns. Nature. 2006;440(7082):297-302.

149. Bezanilla M, Drake B, Nudler E, Kashlev M, Hansma PK, Hansma HG. Motion and enzymatic degradation of DNA in the atomic force microscope. Biophysical Journal. 1994;67(6):2454-9.

150. Wu N, Zhou X, Czajkowsky DM, Ye M, Zeng D, Fu Y, et al. In situ monitoring of single molecule binding reactions with time-lapse atomic force microscopy on functionalized DNA origami. Nanoscale. 2011;3(6):2481-4.

151. Lund K, Manzo AJ, Dabby N, Michelotti N, Johnson-Buck A, Nangreave J, et al. Molecular robots guided by prescriptive landscapes. Nature. 2010;465(7295):206-10.

152. Schönherr H, Vancso GJ. Atomic Force Microscopy in Practice. Scanning Force Microscopy of Polymers. Berlin, Heidelberg: Springer Berlin Heidelberg; 2010. p. 25-75.

153. Suzuki Y, Endo M, Sugiyama H. Lipid-bilayer-assisted two-dimensional self-assembly of DNA origami nanostructures. Nature Communications. 2015;6:8052.

154. Kershner RJ, Bozano LD, Micheel CM, Hung AM, Fornof AR, Cha JN, et al. Placement and orientation of individual DNA shapes on lithographically patterned surfaces. Nature Nanotechnology. 2009;4:557.

155. Xue Y, Li X, Li H, Zhang W. Quantifying thiol–gold interactions towards the efficient strength control. Nature Communications. 2014;5:4348.

156. Shaali M, Woller JG, Johansson PG, Hannestad JK, de Battice L, Aissaoui N, et al. Site-selective immobilization of functionalized DNA origami on nanopatterned Teflon AF. Journal of Materials Chemistry C. 2017;5(30):7637-43.

9 PAPERS & PRESENTATIONS

G.E. Flynn, J.M. Withers, A. Sender, J.M. Cooper, A.W. Clark and G.A. Burley, Effect of the Fluorine Content of Fluorous Phase Tags on the Immobilisation/Removal Properties of ODNs on Microarrays (In preparation).

S.L. Henry, **G.E. Flynn**, J.M. Withers, A. Sender, N. Chaher, G.A. Burley and A.W. Clark, Fluorous Directed Facial Deposition of DNA Nanostructures onto Mica (In Preparation).

G.E. Flynn, J.M. Withers, G. Macias, J.R. Sperling, S.L. Henry, J.M. Cooper, G.A. Burley and A.W. Clark, Reversible DNA Micro-patterning using the Fluorous Effect, Chemical Communications, 2017, 53, 3094-3097 (Journal).

G.E. Flynn, J.M. Cooper and A.W. Clark, Reversible DNA Micro-patterning using the Fluorous Effect, 14th Annual Conference on Foundations of Nanoscience, Snowbird, Utah (USA), April 2017 (Invited Speaker).

A.W. Clark, **G.E. Flynn**, and S.L. Henry, Assembling Nanoplasmonic Metastructures using DNA Origami Tiles, 14th Annual Conference on Foundations of Nanoscience, Snowbird, Utah (USA), April 2017 (Poster).

G.E. Flynn, J.M. Cooper and A.W. Clark, Site-Specific Recombination on Substrate Bound DNA as a means to Develop "Switchable" Nanopatterns on Surfaces, 22nd International Conference on DNA Computing and Molecular Programming, LMU, Munich (Germany), September 2016 (Poster).